The University of Nottingham

UNITED KINGDOM · CHINA · MALAYSIA

# Multibody Dynamic Analysis of Lightning Protection Systems for Modern Wind Turbines

Ikhazuangbe Ivbuobe Godson, B.Eng., M.Eng.

*A thesis submitted for the degree of Doctor of Philosophy in the Faculty of Engineering*

*The University of Nottingham*

OCTOBER 2018

# DECLARATION

I hereby declare that this thesis is the result of the author's original research. No portion of the work has been submitted in support of an application for examination which has led to the award of a degree. Referencing and citations were done in accordance with academic rules and ethical conduct.

# ACKNOWLEDGEMENTS

Firstly, I would like to express my sincere gratitude to my supervisors; Associate Prof Mumtaj Bagam, Prof. Chandima Gomes, Asst.Prof. Anandan Shanmugam, for their guidance, support and continual encouragement during the period of this research and throughout my studies. I would also like to thank my assessors; Assistant Prof Grace Lim Soo Young and Dr Mahendra Chilukuri for painstakingly reading through my work during examination. My previous supervisor Associate Prof. Shahram Mohanna also contributed immensely.

I also appreciate the support of the numerous people in and outside The University of Nottingham who have helped me in various capacities. A special thanks to Associate Prof Mohammadi Amin Malek and Professor Almurib Haider Abbas.

I would like to thank my friends, my Siblings, my spouse and every member of my family for every support.

Finally, I would like to thank GOD for given me this opportunity; the resources and the ability to start and finish, to him alone be all the glory.

This thesis is dedicated to my parents

Mr Godfrey Agbi Udubor Ikhazuangbe

and

Mrs Okhen Airujuan

## ABSTRACT

Modern wind turbines are increasing in size due to higher megawatt, reaching height of about 220 m with blade as long as 80 m moving with a tip velocity of 60-80 m/s. They are sometimes located offshore for better wind condition, bringing them closer to lightning, and the blade is mostly affected when hit. When lightning attaches to the blade surface instead of the air-terminal, the blade and sometimes the entire wind turbine may be destroyed resulting in downtimes, loss of wind turbine, expensive cost of repair and can cause some power companies to shut down and dismantle. Damage incidences has been recorded as well as increased insurance claims. In the past decades, lightning protection issues were well addressed for static objects and Lightning Protection Systems (LPS) are usually installed on modern wind turbines by applying the Electro Geometric Model (EGM) methods. Recently, these methods are invalidated and according to IEC 61400-24, the EGMs are no longer appropriate for large wind turbine blades. Lightning can either be downward initiated or upward initiated. In the presence of a thundercloud, tall wind turbines are increasingly subjected to upward lightning attachment triggered by the wind turbine itself. Lightning strike frequency, point of lightning attachment and lightning protection systems has been evaluated based on downward initiated lightning. However, these might not be effective for upward lightning. Research has shown that the maximum electric field strength distributed on the surface of the wind turbine and the surrounding air is very important in determining the point of inception of upward leader and would help in improving lightning protection systems. In contrast to static objects, maximum electric field strength required for the inception of upward leader from wind turbine changes majorly due to blade rotation and certain blade conditions such as; polluted blade condition, varying receptor sizes, receptor positions and type of protection method.

Maximum electric field variations due to these blade conditions has not been considered in literature. Analyzing the maximum electric field strength and conducting experimental test on full scale wind turbine is presently very difficult due to height constraint and lack of suitable equipment.

The work presented in this thesis aims at investigating the variations in maximum electric field strength required for the inception of upward leader from wind turbine due to varying blade conditions. The work extends the vertical tri-pole cloud charge distribution model made from two positive charges and a negative charge representing the idealized gross charge structure of a thundercloud to create an ambient field representing uniform electric field due to cloud charge distribution at 200 m above ground. The numerical model is developed with finite element analysis; COMSOL Multiphysics. The extended model is applied to a 3D electrostatics model of a full-scale wind turbine; Vestas V100 with 2 MW rated power, 164 m rotor diameter and 49 m long blade, and a model of a 19.1 m blade length of 600 kW wind turbine. As the blade is rotated, the variations in maximum electric field strength required for the initiation of upward leader is obtained. The results obtained for the point of initiation of upward leader is in agreement with high voltage strike attachment test experiment.

Initially, the model is utilized to evaluate and compare various receptor sizes. The receptor size is evaluated by comparing the electric field strength as the receptor size is changed and the blade is rotated.

Secondly, the model is utilized to evaluate and compare discrete receptor position from the blade tip. A more proficient receptor size and position is proposed

Again, the model is used to evaluate the effect of pollution on lightning protection systems. It is found that pollution dampens the performance of the receptor by 93% and on average, the general performance of the receptor in a polluted blade condition is found to be less than 10%.

Finally, two lightning protection systems (metallic cap and receptor methods) commonly in use are applied on a full scale polluted offshore wind turbine and evaluated. A new protection system with higher lightning protection efficiency is developed. This is found to influence the electric field distribution immensely.

This work forms a platform for further investigation on modern wind turbines with regard to protecting long blades from lightning. Manufacturers may look at the finding of this work when dealing with the design aspects of very large future wind turbine blades of practical importance.

# Table of contents

ABSTRACT ..... v
Publications ..... xv
1 Chapter 1 Introduction ..... 1
1.1 Research Scope and Background ..... 1
1.2 Problem statement ..... 8
1.3 Contribution of The Current Work ..... 11
1.4 Research Aims and Objectives ..... 12
1.5 Thesis Outline ..... 14
2 Chapter 2 Literature Review ..... 15
2.1 Introduction ..... 15
2.2 Overview ..... 16
2.2.1 Lightning Properties ..... 16
2.2.2 Lightning discharges and Strike Formation ..... 17
2.2.3 Types of lightning flashes ..... 18
2.2.4 Cloud-to-ground flashes ..... 19
2.3 Downward and Upward Initiated Lightning Flashes ..... 19
2.3.1 Downward Initiated Flashes ..... 19
2.3.2 Upward Initiated Flashes ..... 20
2.4 Risk Assessment ..... 21
2.4.1 Lightning Exposure Assessment ..... 21
2.4.2 Assessing the Frequency of Lightning Affecting a Wind Turbine ..... 21
2.4.3 Collection Area ..... 22
2.5 Air-Termination System Positioning Methods ..... 23
2.5.1 The Fixed Angle Method ..... 24
2.5.2 The Mesh Method ..... 25
2.5.3 The Rolling Sphere Method ..... 26
2.6 Blade Damage ..... 29
2.7 Rotation Effect ..... 30
2.8 Wind Turbine Lightning Protection ..... 31
2.8.1 Wind Turbine Blade ..... 31
2.8.2 Blade Lightning Protection ..... 32
2.8.3 Functions of Wind Turbine Lightning Protection System. ..... 33

2.8.4 Components of Lightning Protection System LPS ..... 34
2.8.5 Lightning Air-Termination Systems ..... 34
2.8.6 Air-Termination Systems (Non-Conventional) ..... 34
2.8.7 Protection Methods for Blades ..... 35
2.9 Numerical Evaluations ..... 41
2.10 Verification of Lightning Protection Systems ..... 43
2.11 Lightning Protection Zones (LPZ) ..... 44
2.12 Air-Termination Interception Efficiency ..... 46
2.13 Experimental Test ..... 47
2.14 Laboratory Test in IEC 61400-24 ..... 48
2.14.1 High-Voltage Strike Attachment Tests ..... 49
2.14.2 Initial Leader Attachment Test: ..... 49
2.14.3 Initial Leader Attachment Test Voltage Waveform ..... 51
2.15 Protecting Wind Turbine from Upward Lightning Flashes ..... 51
2.16 Estimating the Incidence of Upward Lightning to Wind Turbine ..... 53
2.17 Electric Fields ..... 54
2.17.1 Electric Fields Generated by Thunderclouds ..... 54
2.17.2 Electric Fields Generated by Stepped Leaders ..... 56
2.18 Leader Inception Modelling ..... 58
2.18.1 Models Assumptions Used in Lightning Inception Studies ..... 58
2.19 Conclusion ..... 62
3 Chapter 3 Modeling Maximum Electric Field Strength Required for The Inception of Upward Leader from Wind Turbine ..... 63
3.1 Introduction ..... 63
3.2 Simulation Method ..... 64
3.2.1 Thundercloud ..... 65
3.2.2 Gross Charge Distribution in a Thundercloud ..... 65
3.2.3 The Cloud Model ..... 65
3.2.4 Electric Field Intensity ..... 66
3.2.5 Computation of Electric Field on Ground Surface ..... 67
3.3 Ambient Field Representing Uniform Electric Field Due to Cloud Charge Distribution at 200m Above Ground ..... 70
3.4 Wind Turbine Model ..... 72
3.5 Full Scale Blade and 3 m blade tip section model ..... 72

3.6 3 m blade tip section model ..... 73
3.7 Lightning Protection Air-Terminal ..... 74
3.8 Material Content for The Design ..... 75
3.9 Theory for Electric Field Interface ..... 76
3.9.1 Charge Relaxation Theory. ..... 77
3.9.2 Electrostatics Interface ..... 77
3.10 Procedure for Evaluation ..... 78
3.10.1 Unprotected Wind Turbine ..... 79
3.10.2 Protected Wind Turbine. ..... 80
3.10.3 Rotated Wind Turbine ..... 81
3.11 Conclusion ..... 85
4 Chapter 4 Effect of Receptor Size and Receptor Position on Wind Turbine Lightning Protection Systems ..... 86
4.1 Introduction ..... 86
4.2 Receptor Sizes ..... 86
4.2.1 Receptor 10mm diameter ..... 90
4.2.2 Receptor 15mm diameter ..... 91
4.2.3 Receptor 20mm diameter ..... 92
4.2.4 Receptor 25mm diameter ..... 93
4.2.5 Receptor 30mm diameter ..... 94
4.2.6 Receptor 35mm diameter ..... 95
4.2.7 Comparison ..... 95
4.3 Optimum Receptor Position on The Blade ..... 99
4.3.1 Receptor 2 m Away from Blade Tip. ..... 102
4.3.2 Receptor 1.5 m Away from Blade Tip. ..... 105
4.3.3 Receptor 1 m Away from Blade Tip. ..... 108
4.3.4 Receptor 0.6 m Away from Blade Tip. ..... 111
4.3.5 Comparison ..... 113
4.4 Conclusion ..... 117
5 Chapter 5 Pollution and Offshore Wind Turbine Lightning Protection ..... 119
5.1 Introduction ..... 119
5.2 The Effect of Pollution on Offshore Wind Turbine Blade Lightning Protection System's Performance ..... 119
5.2.1 Unpolluted Wind Turbine Blades ..... 123

5.2.2 Polluted Wind Turbine Blades ..... 124
5.3 Performance Enhancement for Offshore Wind Turbine Blade Lightning Protection Systems ..... 128
5.3.1 Lightning Protection Systems on the Blade ..... 129
5.3.2 Evaluation Conditions ..... 130
5.3.3 Receptor Method ..... 131
5.3.4 Metallic Cap Method ..... 133
5.3.5 Performance Enhancement method ..... 135
5.4 Conclusion ..... 147
6 Chapter 6 Experimental Validation ..... 149
6.1 Introduction ..... 149
6.2 Experimental setup and Procedure for high voltage strike attachment test ..... 149
6.2.1 Test Specimen ..... 151
6.2.2 Test Setup ..... 153
6.2.3 Test Procedure ..... 154
6.2.4 experimental conditions ..... 156
6.3 Results and Discussion ..... 157
6.3.1 Experiments with and without receptor on the model blade ..... 158
6.4 Conclusion ..... 168
7 Chapter 7 Conclusions and Future Work ..... 170
7.1 Introduction ..... 170
7.2 Conclusions ..... 170
7.3 Future Work ..... 173
8 REFERENCES ..... 175

# List of Figures

Figure 1-1: V164-80m blade wind turbine [5]. 2
Figure 1-2: (a) Distribution of wind power capacity produced by top 10 countries in 2015; and (b) development of wind turbine with large rotor diameter and higher power capacity since 1980 [7]. 3
Figure 1-3: Market forecast for 2016-2020 [8] 4
Figure 1-4: Blade damage due to lightning [27]. 6
Figure 1-5: Tip receptor 8
Figure 2-1: Wind turbine collection area 22
Figure 2-2: Effective height of a wind turbine on a hill 23
Figure 2-3: volume protected by a vertical rod 25
Figure 2-4: volume protected by a horizontal wire 25
Figure 2-5: Rolling sphere method (courtesy Dehn.co.uk) 27
Figure 2-6: Lightning protection methods for modern large wind turbine blades IEC 61400-24 . 35
Figure 2-7: Multiple receptors on blade 36
Figure 2-8 Lightning protection system by Ring-Shaped Electrodes [14] 38
Figure 2-9 Lightning discharge on wind turbine blade [17]. 39
Figure 2-10: Zoning concept for wind turbine blade [120] 45
Figure 2-11: Initial leader attachment test setup in IEC 61400-24 50
Figure 2-12: Switching impulse voltage (IEC 61400-24) 51
Figure 3-1: A vertical tri-pole made from two positive charges and a negative charge representing the idealized gross charge structure of a thundercloud. 66
Figure 3-2: The method of images 67
Figure 3-3: simulation model 71
Figure 3-4: Model meshing 71
Figure 3-5: Wind turbine model 72
Figure 3-6: V164-80m long wind turbine blade [5] 73
Figure 3-7 Full scale blade model 73
Figure 3-8: Tip receptor design 75
Figure 3-9: Unprotected wind turbine 80
Figure 3-10: Protected wind turbine 81
Figure 3-11: Rotation model 82
Figure 3-12: Rotated state 82
Figure 3-13: Activities around the receptor preceding leader initiation 83
Figure 3-14: Maximum electric field distribution as blade A is rotated from -60 to +60 degrees from the vertical position: (a) 30; (b) vertical position; (c) -30; (d) 60; and (e) -60. 84
Figure 4-1. Different receptor sizes: (a) No receptor (b) 10 mm; (c) 15 mm; (d) 20 mm; (e) 25 mm; (f) 30 mm and (g) 35 mm diameters 88
Figure 4-2. Receptor sizes and their various maximum electric field strength distribution: (a) 10mm; (b) 15 mm; (c) 20 mm; (d) 25 mm; (e) 30 mm and (f) 35 mm diameters respectively .... 88
Figure 4-3. Maximum electric field strength distributions due to 10mm diameter receptor as blade A is rotated. 90

Figure 4-4. Maximum electric field strength distributions due to 15mm diameter receptor as blade A is rotated. 91
Figure 4-5. Maximum electric field strength distributions due to 20mm diameter receptor as blade A is rotated. 92
Figure 4-6. Maximum electric field strength distributions due to 25mm diameter receptor as blade A is rotated. 93
Figure 4-7. Maximum electric field strength distributions due to 30mm diameter receptor as blade A is rotated. 94
Figure 4-8. Maximum electric field strength distributions due to 35 mm diameter receptor as blade A is rotated. 95
Figure 4-9. Comparison for various receptor sizes at the blade tip 96
Figure 4-10. Comparison for various receptor sizes at the leading edge 96
Figure 4-11. Comparison for various receptor sizes at the trailing edge 97
Figure 4-12. Comparison for various receptor sizes at the receptor tip 98
Figure 4-13: Discrete receptor position model 100
Figure 4-14: Different configurations of receptor positions from the blade tip used in the study: (a) No receptor; (b) 0.6 m; (c) 1 m; (d) 1.5 m; and (e) 2 m. 101
Figure 4-15: Wind Turbine 103
Figure 4-16: Blade 103
Figure 4-17: Blade 104
Figure 4-22: Comparing Blade Tip, Leading and Trailing Edge without considering Receptor. 104
Figure 4-23: Comparison with the receptor inclusive 105
Figure 4-24: Wind Turbine 106
Figure 4-25: Blade 106
Figure 4-30: Comparing Blade Tip, Leading and Trailing Edge without considering Receptor. 107
Figure 4-31: Comparison with the receptor inclusive 107
Figure 4-32: wind Turbine 108
Figure 4-33: Rotated wind Turbine 109
Figure 4-34: Blade 109
Figure 4-39: Comparing Blade Tip, Leading and Trailing Edge without considering Receptor. 110
Figure 4-40: Comparison with the receptor inclusive 110
Figure 4-41: Wind Turbine 111
Figure 4-42: Blade 112
Figure 4-47: Comparing Blade Tip, Leading and Trailing Edge without considering Receptor. 112
Figure 4-48: Comparison with the receptor inclusive 113
Figure 4-49: Blade Tip Comparison 114
Figure 4-50: Leading Edge Comparison 114
Figure 4-51: Trailing Edge Comparison 115
Figure 4-52: Receptor Tip Comparison 116
Figure 5-1. unpolluted wind turbine 123
Figure 5-2. unpolluted wind turbine blade 124
Figure 5-3. Polluted wind turbine 125
Figure 5-4. Polluted wind turbine blade 125
Figure 5-5. Pollution effect on the receptor 127

Figure 5-6. Tip receptor design ..... 129
Figure 5-7. The metallic cap design ..... 130
Figure 5-8. (a) Model for rotation mode, (b, c, d, e and f) Arrangement of blade sample ..... 131
Figure 5-9. Unpolluted blade with receptor method ..... 132
Figure 5-10. Polluted blade arrangement for the receptor method ..... 132
Figure 5-11. Unpolluted bade with metallic cap method ..... 134
Figure 5-12. Polluted blade arrangement for the metallic cap method ..... 134
Figure 5-13. Enhanced method ..... 135
Figure 5-14. Polluted blade arrangement for enhanced method ..... 136
Figure 5-15. Maximum electric field strength distributions on the protection system for vertical position ..... 137
Figure 5-16. Maximum electric field strength distributions on the blade surface for vertical position ..... 138
Figure 5-17. Maximum electric field strength distributions on the protection system for $45^0$ (TEFC) position ..... 139
Figure 5-18. Maximum electric field strength distributions on the blade surface for $45^0$ (TEFC) position ..... 140
Figure 5-19. Maximum electric field strength distributions on the protection system for horizontal (TEFC) position ..... 141
Figure 5-20. Maximum electric field strength distributions on the blade surface for horizontal (TEFC) position ..... 142
Figure 5-21. Maximum electric field strength distributions on the protection system for $45^0$ (LEFC) position ..... 143
Figure 5-22. Maximum electric field strength distributions on the blade surface for $45^0$ (LEFC) position ..... 144
Figure 5-23. Maximum electric field strength distributions on the protection system for horizontal (LEFC) position ..... 145
Figure 5-24 Maximum electric field strength distributions on the blade surface for horizontal (LEFC) position ..... 146
Figure 6-1 Different receptor sizes: (a) No receptor (b) 10mm; (c) 15mm; (d) 20mm; (e) 25mm; (f) 30mm and (g) 35mm diameters ..... 145
Figure 6-2. A receptor fixed in a blade tip ..... 146
Figure 6-3 Initial leader attachment test setup ..... 146
Figure 6-4 (a) Model for rotation mode, (b, c, d, e and f) Arrangement of blade sample ..... 148
Figure 6-5. A 3m GFRP blade tip elevated above the ground electrode ..... 149
Figure 6-6 discharge from the blade tip towards the ground plane ..... 157

# List of Tables

Table 1 Material used for a perfectly conducting ground (an ideal ground) design ..... 69
Table 2 Material used for Turbine blade design ..... 75
Table 3 Materials used for thunder cloud and lightning protection systems designs ..... 76
Table 4 Materials used for Air as the environment. ..... 76
Table 5 . Maximum electric field strength distribution (kV/m) ..... 89
Table 6 Values of maximum electric field strength (kV/m) obtained from the blade tip, leading edge, trailing edge and the receptor tip, as blade A is rotated for various configurations. ..... 102
Table 7 Relative efficiencies on the blade surface due to the positions of the receptor from the blade tip ..... 116
Table 8 Relative efficiencies of the receptor Tip due to its positions from the blade tip ..... 117
Table 9. Maximum electric field strength distribution (kV/m) at the receptor tip on blade A for various blade condition ..... 126
Table 10 Maximum electric field strength Kv/m with the Receptor method ..... 136
Table 11 Maximum electric field strength Kv/m with the Metallic cap method ..... 136
Table 12 Maximum electric field strength Kv/m with the Enhanced Method ..... 137
Table 13.No of discharge initiation for a blade-to-ground gap ..... 164

# Publications

The following is a list of the papers published or submitted during the project.

1. Optimum Receptor Location for Efficient Lightning Protection of Modern Wind Turbines. PUBLISHED IN; *International Journal of Simulation Systems, Science & Technology*, vol. 18, 2017.
2. Receptor Sizes and its Effect on Lightning Protection of Modern Wind Turbines. PUBLISHED IN; *Journal of Green Engineering*, vol. 7, 2017.
3. Effect of Pollution on Offshore Wind Turbine Blade's Lightning Protection System's Performance; PUBLISHED IN; *Journal of Multidisciplinary Engineering Science and Technology*, vol. 6, 2019
4. Performance Enhancement for Offshore Wind Turbine Blade Lightning Protection Systems; IEEE Transaction: UNDER REVIEW.
5. Testing of Wind Turbine Lightning Protection Systems - A Comparison of the Influence of a full-scale blade Length and a small blade Tip section on the Performance of the Receptor; IEEE Transaction: UNDER REVIEW.

# Chapter 1

# Introduction

## 1.1 Research Scope and Background

In the 21st century, global warming and the accompanying changes in the world climate pattern has been accepted worldwide as the most severe threat to humanity. Unlike other source of energy, such as coal, gas, and petroleum-based fuel, energy produced using wind turbines does not produce pollutants.

Due to higher generated power and better wind conditions, wind turbines are getting taller, the swept area and the blade length are increased, and they are also moving offshore bringing them closer to lightning. The blades are at the highest risk of lightning attachment with the tip more exposed than other parts [1]. According to field studies [2, 3], they experience a substantial amount of lightning strikes in their life-time. They have become very high that the tips of the rotating blades now reach altitudes as in rocket triggered lightning [4]. Presently, the largest wind turbine in the world (Figure 1-1), has 8 MW rated capacity, 164 m rotor diameter, 80 m blade length and a total height of 220 m [5]. It signifies a quantum leap forward in rotor size and energy capture with a swept area of 21,124 $m^2$


Figure 1-1: V164-80m blade wind turbine [5].

Winds at higher altitudes becomes more persistent, steadier and of higher velocity. Wind turbines are commonly placed on high ground because power available in wind increases as the cube of velocity as shown in equation 1.1 below.

The basic wind power equation: for 3-blade turbine

$$\textbf{Power} = \frac{1}{2}\rho A U^3 \textbf{ Watts} \qquad \textbf{(1.1)}$$

Where ρ is the air density (1.23kg/m$^3$); A is, the blade swept area (m$^2$); and U is the wind speed (m/s)

As shown in equation (1.1) above, wind turbine power output is directly related to the area swept by the blades. The larger the blade's diameter, the more power it can extract from the wind, also, higher power capacity requires higher height but with subsequent nearness to lightning and the most affected part are the blades. NASA maps shows that in most areas where wind density is high, the thunderstorm days per year are 30 or more [6]. Figure 1-2 shows (a) Distribution of wind power capacity produced by top 10 countries in 2015, and (b) development of wind turbine with large rotor diameter and higher power capacity since 1980.

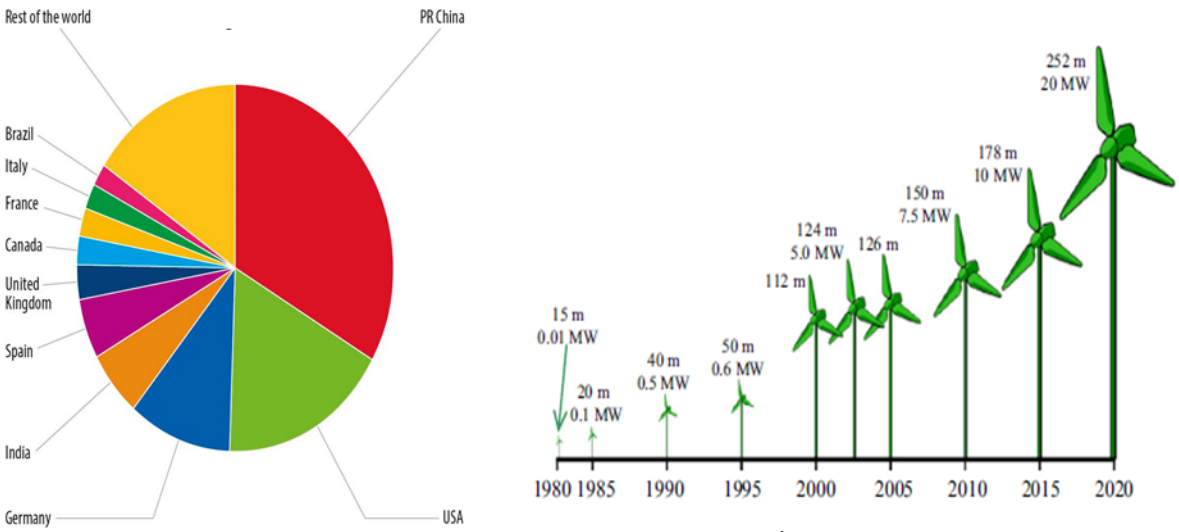


Figure 1-2: (a) Distribution of wind power capacity produced by top 10 countries in 2015; and (b) development of wind turbine with large rotor diameter and higher power capacity since 1980 [7].

Wind turbines as a source of electrical energy, are the fastest growing. Production of electricity by wind turbines has developed to become a major renewable energy resource. During the past three decade, the use of wind energy has greatly increased, and its generation capacity installed around the world as of the end of 2017, according to Global Wind Energy Council (GWEC), was 564.9 GW with market forecast of 792.1 GW in 2020 [8]. It has experienced an overwhelming rapid growth as shown in Figure 1-3 and currently represents approximately $70-$80 billion in annual capital investment [9]. Asia with continued dominance and having surpassed Europe in terms of cumulative installed capacity as shown in Figure 1-2 above.

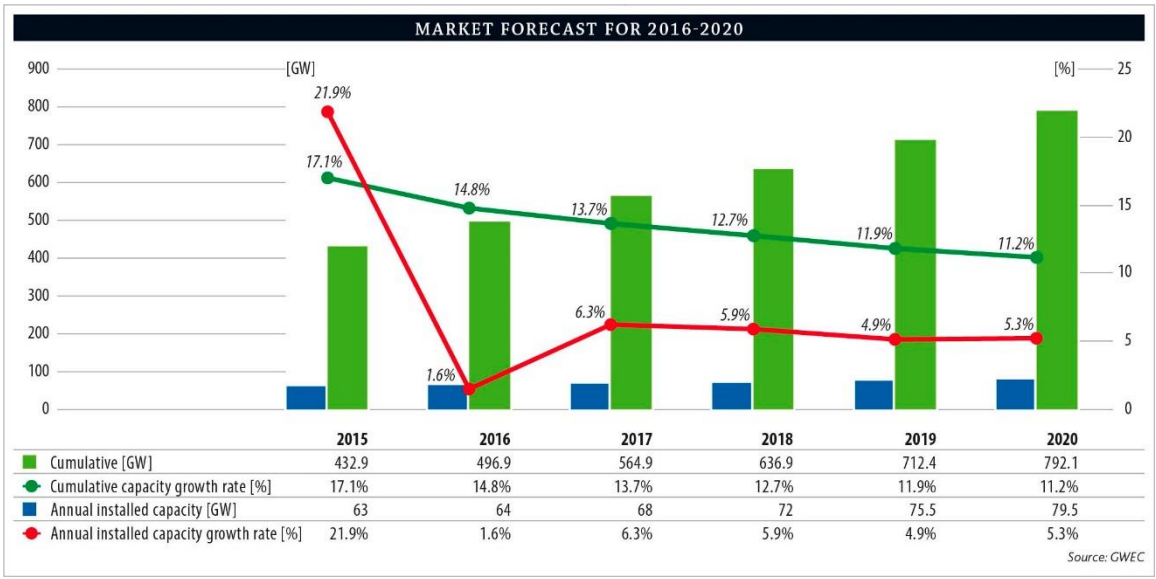


Figure 1-3: Market forecast for 2016-2020 [8]

As far as wind power generation is concerned, the size of the wind turbine blade is very pertinent to the capacity generated. Over the last 3 decades, blades have grown in length and continue to harvest more energy. There is a relationship between generated power and blade length, for instance, V100 model of vestas wind turbine can generate 2.0 MW power with 49 m blade length, V136 model of vestas wind turbine can generate 3.45 MW power with 66.7 m blade length and V164 model of vestas wind turbine can generate 8.0 MW power with 80 m blade length [5]. As wind turbine size and blade length continue to increase, they become more vulnerable with increasing probability of lightning strike.

Lightning protection systems (LPS) are usually installed on modern wind turbines [10-12]. It encompasses; a network of air terminals, bonding conductors, and ground electrodes, designed to provide a low impedance path to ground for potential lightning strikes [13]. Protection methods such as Receptors, Metallic Cap, Metallic Conductor on the Blade Tip, Mesh, Ring Electrode [10, 14], and the Backside Electrode [11] methods are all referred to as air-terminal. Knitted soldered meshes with nanostructured carbon particles used for

protection was presented in [15]. Lightning protection was suggested by some researchers to be as a natural part of wind turbine designs. Danoon et al. [16], are of the opinion that stealth coated wind turbine blades can be integrated with lightning protection. Air terminations such as the receptor are placed in such a way as to evade lightning puncturing a non-conducting blade surface, but laboratory experiments [17], and field observations [18], have shown that it is also possible for lightning attachment on the blade surface and inboard the blade tip instead of the air terminal, with the risk of substantial damages in the composite structure [6, 19-21]. The damages are quite serious, the cost of replacement is high compared to other components [20]. Existing design methods for air-termination placements is the Electro Geometric Model (EGM) methods which relate the striking distance to the prospective peak stroke current, have been used to design protection methods but recently invalidated and according to IEC 61400-24, the EGM are no longer appropriate for large wind turbine blades [22, 23]. In other words, air terminals are used in accordance with the EGM but blade failures are still highly recorded. It is required by internationally recognized standards that the LPS should intercept and conduct the majority of strikes to ground without damage to the wind turbine [9]; however, according to a German study, lightning strikes accounted for 80% of wind turbine insurance claims [24], and even caused some power company to shut down and dismantle.

Wind turbines damaged by lightning is shown in Figure 1-4. Just as lightning can cause serious damage to wind turbines, it is also a threat to livestock and humans. Kalair et al. [25], discussed lightning interactions with lifelines and humans. Modern wind turbines with increasing height have become more vulnerable to increased number of lightning strikes, i.e. lightning threat increases with height. When lightning strikes a wind turbine,

the resultant damage could be by direct strike or by producing electric and magnetic fields that can induce voltages in local wiring. Damages vary in magnitude, more severe with unprotected blades and can be eliminated or reduced by efficient protection with air termination. Lightning is a worldwide problem, Germany alone reported 393 events of lightning damage to wind turbines between 1992 and 1995 [26]. The events are now higher recently.

Figure 1-4: Blade damage due to lightning [27].

Typical types of damage at the lightning attachment points are delamination and incineration of the surface composite material, and heating or melting of metallic components serving as the attachment point. The most severe damage to wind turbine blades occurs when lightning forms high energy arcs inside the blade due to attachment to an unprotected part of the blade skin. The phenomenon responsible for the severe structural damage to wind turbine blades is therefore the formation of a pressure shock wave around an arc of lightning inside the blade.

The receptor though effective [19], also failed in so many instances [28, 29]. The continuous failure of wind turbines due to lightning despite various advancement has

brought it to the front burner in research and a re-evaluation of lightning problems with wind turbine.

Lightning problems with wind turbine arise due to:

- The nonconductive nature of blade material
- Rotation of the blade
- Increase in size on account of higher power requirement on the order of megawatts.
- Recently, multiple discharge on the turbine associated with nearby cloud to ground lightning [30] and also strikes attaching inboard on the blade due to dart leader [31] are also mentioned as some possible causes of continued blade failures. Malcolm et.al [32], presented failure rate estimation of wind turbine electrical systems due to lightning strikes.

Proper positioning of the receptor ensures that upward leader is incepted from the receptor alone. When lightning attaches to the blade surface instead of the air-terminal, the blade and even the entire wind turbine can be destroyed resulting in downtimes, loss of wind turbine, and expensive cost of repair. Lightning attaching to the blade surface instead of the air-terminal is the major cause of damage because when lightning attaches to the air-terminal, it will be conducted to ground. Therefore, the efficient location of possible leader attachment points, optimization of the location of air termination systems and performance of protection devices is key to an improved lightning protection for modern wind turbines. A wind turbine blade with a receptor located at the tip is shown below in Figure 1-5

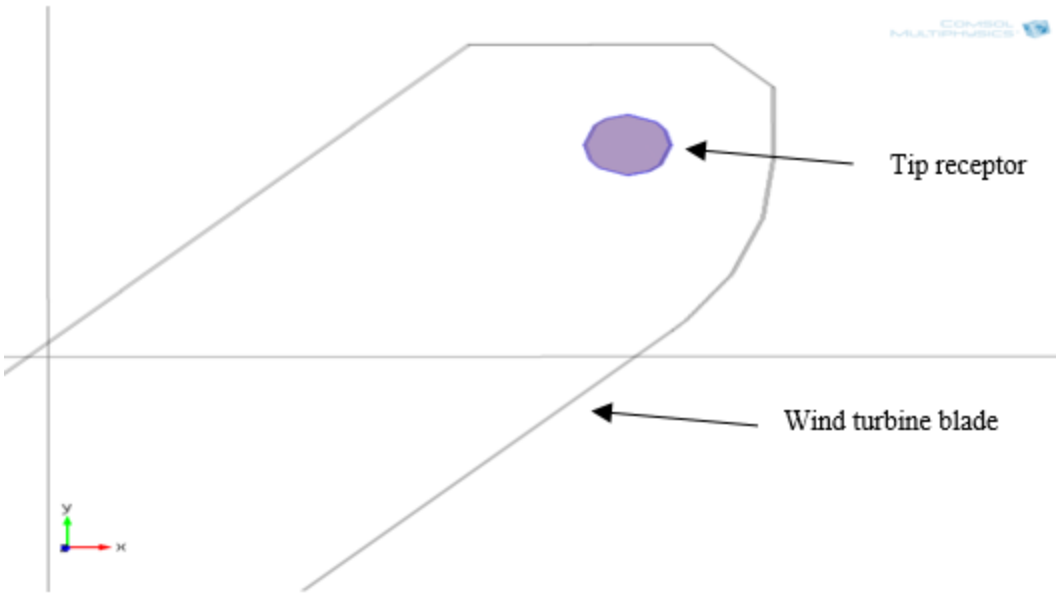


Figure 1-5: Tip receptor

Some progress has been made with wind turbine lightning protection [6, 22, 33-35] on finding protection measures and their locations [35], and has revealed that the lightning parameters found in probability distributions of standards are no longer appropriate for large wind turbines [1], and that lightning protection proficiency can depend on air termination location, numbers and sizes [36], and concluded that this field requires a detailed investigation.

## 1.2 Problem Statement

Lightning can either be downward initiated or upward initiated. In the presence of a thundercloud, tall wind turbines are increasingly subjected to upward lightning attachment triggered by the wind turbine itself. Some progress has been made in examining the role of upward lightning in increasing the number of lightning strikes to a wind turbine [37, 38]. However, lightning strike frequency, point of lightning attachment and lightning protection systems has been evaluated based on downward initiated lightning, these protection

methods have shown some effectiveness for downward lightning, but might not be effective for upward lightning. Air-terminal assessment based on upward propagating lightning is very necessary.

Research has shown that the maximum electric field strength around a structure is very important in determining the point of inception of upward leader. In contrast to static objects, the maximum electric field strength for the inception of upward leader from wind turbine changes due to conditions such as;

- ✓ Rotation
- ✓ Receptor sizes and position
- ✓ Blade pollution
- ✓ Type of protection method
- ✓ Blade size etc.

Analyzing the maximum electric field strength and conducting experimental test on full scale wind turbine is presently very difficult due to height and lack of equipment.

The vertical tri-pole cloud charge distribution model is very useful for lightning protection, however, it can be extended and used to create ambient field representing uniform electric field above ground. This can be a viable substitute for the invalidated EGM as well as existing protection methods that has not been able to address key issues in wind turbine lightning protection, such as receptor position on the blade, size of the receptor, the effect of pollution on the receptor's performance and evaluation of the performance of the protection systems.

With the invalidation of the EGM, laboratory experiment has been used to analyze protection methods, as prescribed by IEC 61400-24, however, the physics and properties of natural lightning are different from those in the laboratory. Also, the electric field present between a small test sample and the opposite electrode as it is currently the practice in the laboratory, is different than when the entire blade is present. Full scale analysis is presently lacking in the wind industries and it is very much desired.

The efficiency of the receptor is dependent on its interception proficiency which is its ability to intercept a lightning stroke. This strongly dependent on the size and position of the receptors [39]. The effect of receptor size and position has not been well considered in literature and standards. An attempt was made [40, 41], in evaluating the effect of receptor, however, only the shape (tip shape receptor, also referred to as metallic cap and disk shape receptor) were considered and not the various sizes and positions. Since there are no standard as well as detailed experimental and numerical research governing receptor sizes and positions, choices are made randomly by researchers. This is not healthy for an efficient lightning protection because the results are affected as the size and position of the receptor has been found to significantly affect its efficiency. It is therefore necessary to harmonize on the most efficient receptor size and receptor position for an efficient lightning protection of wind turbines.

GFRP blade model and its lightning protection systems such as a receptor and metallic cap has been experimentally evaluated in [17, 19, 42, 43]. However, some of these evaluations has been limited to downward initiated lightning, also, a 2m or 3m blade tip of an actual

blade length were used and not full-scale blade length since it is difficult to experiment or take a blade as long as 80 m into the laboratory.

When offshore wind turbines get in contact with salt water, they become polluted. This has been found to drastically affects the lightning protection systems. The effect of pollution has been experimentally evaluated in [44, 45], however, the performance of the receptor considering pollution has not been considered in literature and are not suggested in the current lightning protection standards. Up to date, the level of pollution influence on receptor performance has not been estimated and simulation studies associated to this topic have rarely been reported. The effect of pollution on offshore wind turbine receptor performance is very important to enable improvement on the protection systems.

The incident of upward flashes estimated using existing methods is undervalued and the maximum electric field strength around a wind turbine required for the initiation of upward lightning flashes has not been quantitatively analyzed in literature. The work presented in this thesis, focus on the interaction between wind turbine and the maximum electric field strength due to thunder cloud charge.

### 1.3 Contribution of The Current Work

As mentioned above, though lightning protection have been well addressed for static objects and lightning protection systems (LPS) are usually installed on wind turbines, but due to height and lack of equipment, the effect of changes in maximum electric field strength required for the inception of upward leader from wind turbine due to changes in blade conditions has not been discussed sufficiently yet. To protect modern wind turbines

from lightning strikes, the investigation of the maximum electric field strength required for the inception of upward leader from wind turbine due to varying blade conditions is carried out in this thesis. Major contributions to knowledge are summarized below.

1. Developed an extended vertical tri-pole model made from two positive charges and a negative charge representing the idealized gross charge structure of a thundercloud to create an ambient field representing uniform electric field due to cloud charge distribution at 200m above ground.
2. Proposed a receptor size with higher protection efficiency.
3. An optimum receptor location for modern wind turbine is identified. It is showed that locating the receptor 1.5 m away from the blade tip will allow the leader to be initiated from the receptor before any other part of the blade.
4. The effect of blade pollution on receptor performance is evaluated and estimated. It is found that pollution dampens the performance of the receptor by 93% and on average, the general performance of the receptor in a polluted blade condition is found to be less than 10%.
5. Existing protection methods are compared, and a new protection system with higher lightning protection efficiency is developed.
6. This work forms a platform for further investigation on modern wind turbines with regard to protecting long blades from lightning.

## 1.4 Research Aims and Objectives

The central aim of the research presented in this thesis can be stated as:

*Analyzing the maximum electric field strength required for the initiation of upward leader from wind turbine due to changes in blade conditions. This is intended for a more efficient lightning protection system.*

The work extends the vertical tri-pole cloud charge distribution model made from two positive charges and a negative charge representing the idealized gross charge structure of a thundercloud to create an ambient field representing uniform electric field due to cloud charge distribution at 200 m above ground. It is then applied to a full-scale wind turbine to study the variations in maximum electric field strength required for the initiation of upward leader as the blade condition is changed. The changed blade conditions are;

- Polluted blade condition (How does pollution affect the performance of the protection systems)
- Varying receptor sizes and positions (How does the size and position of the receptor affect the performance of the protection systems)
- Type of protection method (How does the type of protection systems affect the performance of the protection systems)

The research objectives of the work are:

- The development of the extended vertical tri-pole cloud charge model
  - Development of full-scale wind turbine blade model for analysis.
  - To investigate the effect of pollution on offshore wind turbine lightning protection systems.
  - Determine the effect of receptor size and position on upward leader inception.
  - To evaluate the performance of existing protection methods and to propose new effective protection scheme.

## 1.5 Thesis Outline

The thesis has been organized into 7 chapters.

Chapter 1: This chapter introduces the background of the research and defines the objective of thesis.

Chapter 2: This chapter gives an overview of the state of art in lightning protection of wind turbines. It also forms the basis of reason for research.

Chapter 3: A model is developed to simulate the vertical tri-pole cloud charge distribution model made from two positive charges and a negative charge representing the idealized gross charge structure of a thundercloud to create an ambient field representing uniform electric field due to cloud charge distribution at 200 m above ground.

Chapter 4: The analysis of receptor sizes and positioning is presented in this chapter and recommendation are made.

Chapter 5: In this chapter, the model is applied to study the maximum electric field strength distribution on polluted wind turbine.

Chapter 6: In this chapter, simulation results are experimentally validated.

Chapter 7: A summary of the work is presented and outlines some suggestions for further work.

# Chapter 2

# Literature Review

## 2.1 Introduction

This chapter's framework is premised on the effect of upward initiated lightning on wind turbine blade lightning protection systems due to varying blade conditions. It reviews previous research on lightning protection such as; air-termination systems, existing protection methods, numerical evaluations, upward lightning flashes, electric fields, leader inception models etc.

Benjamin Franklin first used a metal rod as a lightning receptor and it is still widely in use due to its effectiveness, though attempt has been made to improve its performance but proven to have no significant effect. Radioactive lightning rods were also considered, though they were also effective in attracting lightning strokes but were abandoned due to restrictions in the use of radioactive materials. Early Streamer Emission (ESE) air-terminals were recently explored. As compared to a simple Franklin Rod, the ESE rod were expected to reduce the time of streamer development, but field experiments show that the Franklin Rod can breakdown faster and therefore more effective. Hence, the principle of the franklin rod is still a general guide in modern lightning protection.

Firstly, a brief review of power systems lightning protection is presented.

As Franklin Rod is used in power substation, shielding wire is also used in power transmission lines and they both have similar design principle which aimed to arrest the lightning strokes before they reach the object that is protected. In evaluating the lightning

protection for power transmission and distribution system, information about Isokeraunic level, Ground flash density (GFD) and the relationship between the stroke current and the strike distance is very important.

*The isokeraunic level is the average number of days per year on which thunder will be heard during a 24-hour period.*

*Ground flash density (GFD) is the average number of strokes per unit area per year at any location of interest*

A number of methods such as Cone of Protection, Faraday Cage, Rolling Sphere and the collection volume methods have been proposed, some of which are in common use.

To allow for proper understanding of lightning protection, the properties of lightning are first discussed.

## 2.2 Overview

In this section, various topics leading to the problems in this thesis is reviewed, these include; the properties of lightning, downward and upward initiated lightning flashes, risk assessment, air-termination positioning methods, blade damage, rotation effect, wind turbine lightning protection systems, numerical evaluations, lightning protection zones, air-termination interception efficiency, protecting wind turbine from upward lightning flashes, estimating the incidence of upward lightning to wind turbine, electric fields and leader inception modelling.

### 2.2.1 *Lightning Properties*

Lightning, a common but spectacular natural phenomenon is an atmospheric discharge, and a lightning strike is regarded as a current source. In the design and dimensioning of

lightning protection, four lightning current parameters are relevant to the point of strike, and they determine the amount of damage that is done to a wind turbine, these are: the peak lightning current (*I*), the charge transferred (*Q*), the steepness of the lightning stroke current impulses (d*i*/d*t*) and the specific energy (*W/R*). Research has shown that 2 kA to 300 kA is the maximum recorded value of lightning current produced by one single stroke, while 350 C and 15 MJ/Ω are the maximum recorded values of charge transfer and specific energy respectively [46]. The point where lightning will attach to a structure is determined by the electric fields that instantaneously precede lightning attachments. The electric field and the point of upward leader inception on a blade are the major focus of this thesis.

When designing a lightning protection system, it is a good practice to have a detailed knowledge of different types of lightning strikes and their electrical characteristics. These are discussed below.

### 2.2.2 *Lightning discharges and Strike Formation*

The separation of charge in thunderstorm clouds produces Lightning strikes, the process is detailed in [47, 48]. When this charge is discharged, a lightning is observed. It could be discharged to the earth or to a region of opposite polarity charge of a neighboring cloud or within the same cloud.

**Various stages of lightning discharge:** The process of charge separation is complicated, but the important fact to the design engineer is that it does occur in thunderstorm clouds. Lightning discharge consists of the following steps.

1. Charge separation in a thunderstorm cloud
2. Ionization of the air surrounding the charge center

3. Step leader develops
4. Step leader approaches to ground and strike to ground
5. Return stroke occurs
6. The first discharge forms and more step leaders start in cloud
7. Dart leader approaches to ground and strike to ground
8. Second return stroke occurs

Usually there are several components that forms a lightning flash, it is the entire event following the same ionized path that lasts up to about 1s. The individual components of a lightning flash are called short strokes and long strokes respectively.

### 2.2.3 *Types of lightning flashes*

The various types of lightning flashes are;

1. A downward initiated flash. It is a lightning flash that begins at the thundercloud and heads towards the ground. This is also referred to as cloud to ground flash or downward flash
2. Upward initiated flash. It is a lightning flash that begins at an exposed location on the earth such as peak of mountain or at the highest point of tall grounded structure like wind turbine and heads towards a thundercloud. This is also referred to as ground to cloud flash or upward initiated flash.

The polarity of the charge removed from the thundercloud can further be used to sub-divide both types of lightning into;

1. A negative flash. This results in negative charge being transferred to the earth from the thundercloud. They are the dominant type of lightning flashes, around 90% of all cloud to ground, exhibiting the steepest current impulses (highest d*i*/d*t*).
2. A positive flash. This lowers positive charge from the thundercloud to the earth, around 10 % of all cloud to ground flashes, exhibiting the most powerful current parameters (higher *I*, *Q* and *W/R*). Current waveforms associated with positive flashes were recorded on the santis tower [49].

### 2.2.4 *Cloud-to-ground flashes*

A downward initiated discharge as mentioned above is also referred to as cloud to ground flash. It is primarily formed as a result of initial breakdown in the cloud. Cloud-to-ground can either be negative cloud-to-ground or positive cloud-to-ground.

## 2.3 Downward and Upward Initiated Lightning Flashes

Downward and upward initiated flashes are detailed further.

### 2.3.1 *Downward Initiated Flashes*

As mentioned above, this type of lightning begins from the cloud. As a step leader approaches the earth, its tip with respect to the earth, is at a potential in excess of 10 MV. The strength of the electric field on the earth surface is raised by this high potential and when the breakdown value of air is exceeded, upward moving leaders also called answering leaders or connecting leaders are emitted from the earth or from structures on the ground such as wind turbines. When the point of attachment of a lightning flash to an object is to

be determined, connecting leaders plays a vital role. A path that is continuous from cloud to ground is established when the descending stepped leader meets or get in contact with the upward moving connecting leader. At around 1/3 the speed of light, the charge that is deposited in the leader channel, by a process called the first return stroke is discharged to ground by a current wave propagating upward the ionized channel.

### 2.3.2 *Upward Initiated Flashes*

In contrast to downward initiated lightning, upward initiated lightning origins from the ground. The earth surface electric field rises due to the thundercloud charge, though usually not enough for an upward moving leader to be launched. However, at objects placed on high ground, at mountains, or at tall structures, the electric field may be well enhanced. The electric field strength at such locations, may become sufficient to initiate an upward moving leader towards the thundercloud from ground. Tall structures with heights more than 100 m over the encompassing terrain, are especially exposed to upward initiated flashes. Modern wind turbines due to their heights initiate upward propagating lightning. When the turbine is subjected to an elevated electric field, upward lightning can initiate at any points that has high stress. Answering leaders are most likely to form at these locations when downward lightning approaches. These locations are the vulnerable points.

Upward initiated flash parameters are measurements on tall objects. Information from observations as well as discussion of upward flashes by Rakov and Uman are in [50] and in recent years, upward flashes have also been measured on wind turbines [51]. Upward propagating lightning strikes are mostly of negative polarity, upward initiated positive flashes although observed, they are rare. The maximum peak current of the waveform of an upward negative flash is relatively low, about 10kA, the charge transfer related to the

first strike can reach high value as 300 C. Frequent upward lightning flashes may be experienced by tall objects placed at exposed locations particularly during winter thunderstorms, this is highly relevant for wind turbines because due to favorable wind conditions, high and exposed locations are preferred. Direct lightning strike on wind turbines in winter season was discussed in [52]. Considering information on the risk of upward lightning flashes and winter lightning conditions at prospected sites is therefore necessary.

## 2.4 Risk Assessment

### 2.4.1 *Lightning Exposure Assessment*

Designing lightning protection should consider the risk of lightning striking and damaging the structure. These damages could be any of the following; Blade damage, damage to the mechanical part, damage to electrical and control systems, personnel exposed to hazards from step/touch voltages [53], even fires and explosions due to lightning. The risk of lightning flashes attaching to a structure is a function of the following; height of the structure, the local topography and also, the local level of lightning activity. Sarajcev et al. [54], discussed assessment of lightning stroke occurrence to modern wind turbines. Wind turbines exposure to lightning was presented in [55], it was shown that, as turbines become larger, the risk of lightning damage increased.

### 2.4.2 *Assessing the Frequency of Lightning Affecting a Wind Turbine*

For lightning risk analysis of a wind turbine, the first stage is to estimate the frequency of lightning flashes to it and guidance on how this number can be estimated is given in IEC 62305-2. In assessing the frequency of lightning flashes to a structure such as wind

turbines, information about the local ground flash density (*N*g) is very important. This information can be provided by national organization such as weather bureau.

### 2.4.3 *Collection Area*

The collection area of a structure is defined as an area of ground surface which has the same annual frequency of lightning ground flashes as the structure. For isolated structures, the equivalent collection area is the area enclosed with a border line obtained from the intersection between the ground surface and a straight line with a 1:3 slope which passes from the upper parts of the structure (touching it there) and rotating around it.

Usually, wind turbines are modelled as a tall mast having a height equal to the hub height plus one rotor radius. Shown in Figure 2-1 is the collection area of a wind turbine placed on flat ground. Obviously, this is a circle having a radius three times the turbine height.

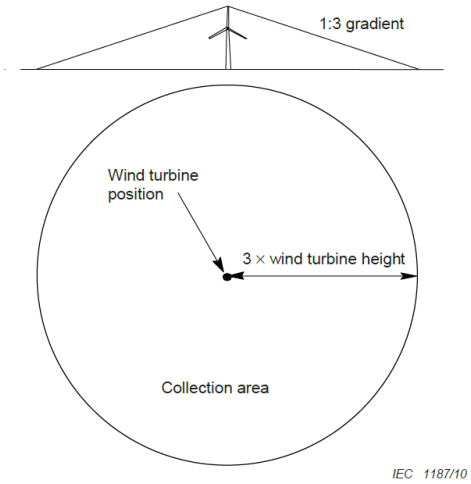


Figure 2-1: Wind turbine collection area

The following equation can be used to estimate the annual number of lightning flashes to a wind turbine located on flat ground.

$$N_d = N_g \,.\, A_d \,.\, 10^{-6} = N_g \,.\, 9\,\pi \,.\, H^2 \,.\, 10^{-6} \qquad (2.1)$$

where

$H$ [m] is the height of the wind turbine;

$A_d$ [$m^2$] is the collection area of lightning flashes to the structure;

$N_g$ [$km^{-2} \cdot year^{-1}$] is the annual average ground flash density.

In more complex terrain, it is appropriate to consider the effective height of the wind turbine including the height of the wind turbine position, e.g. if placed on exposed hills or ridges as shown in Figure 2-2.

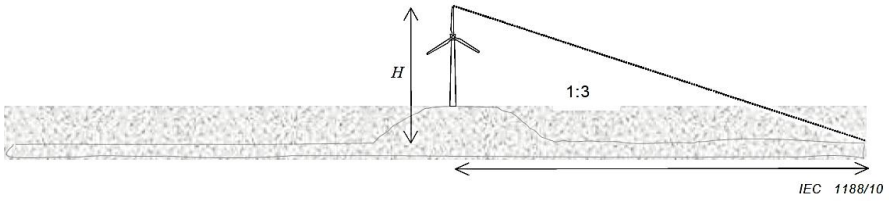


Figure 2-2: Effective height of a wind turbine on a hill

## 2.5 Air-Termination System Positioning Methods

The effectiveness of a lightning protection conductors or air-terminals are most important, and it depends on the position that it is placed on the object that is to be protected. Existing design methods for air-termination placements are (a) Empirical or Classical Design methods, (b) Electro Geometric methods (EGM)

These methods are briefly explained below.

(a) Empirical or Classical Design methods; this method assumes that the protection device (wire or mast) can intercept all the lightning strokes arriving over the subject area if the protection device maintains a certain geometrical relation to the protected

object. These methods include; the fixed angle method and the empirical curve method.

(b) Electro geometric methods (EGM's); these methods recognize that the attractive effect of the protection device i.e. wires, or mast depends on the amplitude of the lightning stroke current. In other words, the methods relate the striking distance to the prospective peak stroke current.

These methods are detailed below.

### 2.5.1 *The Fixed Angle Method*

Determining the volume protected by a vertical conductor has been subject of research Since the time of Benjamin Franklin. According to Gay-Lussac in 1823, a lightning rod effectively protects against a lightning strike in a circular space around it, with the radius of the space been twice the height of the rod [56]. Successive modifications to the definition of protection zone are shown in [57-59]. Except for few exceptions, the zone of protection of a vertical conductor is regarded as a cone. The top angle of the cone is called the protection angle of the vertical conductor. The protective ratio is the ratio of the base radius of the cone to the rod height, for a protective ratio of 1:1, the angle between the lateral surface of the cone and the vertical rod is $45^0$, it corresponds to an angle of $60^0$ for a protective ratio of 2:1. Until recently, lightning protection standards [60] has recommended the protection angle method. Locating lightning conductors on a building can be achieved with the concept of the cone of protection. The smaller the assumed angle of protection, the more reliable the protection provided by the lightning conductors. The volume protected by a vertical air-termination rod is shown in Figure 2-3. ***A*** is the air-termination

rod tip, ***OC*** is the radius of the protected area, ***B*** is the reference plane and $h_1$ is the height of the air-termination rod above the reference plane of protection. The angle $\alpha$ is determined by the class of lightning protection system.

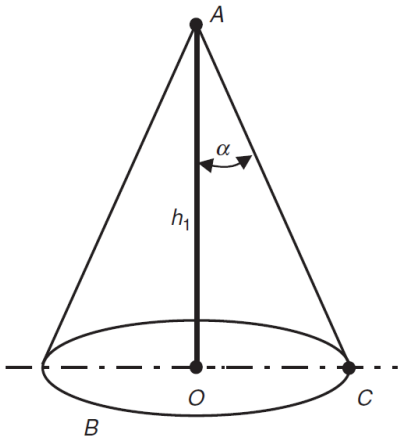


Figure 2-3: volume protected by a vertical rod

Figure 2-4. shows the volume protected by a horizontal wire

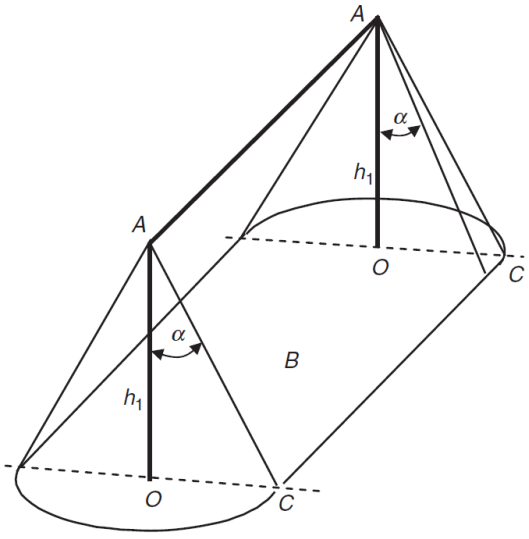


Figure 2-4: volume protected by a horizontal wire

### 2.5.2 *The Mesh Method*

The mesh method is suitable for the protection of plane surfaces e.g. flat roofs. It was suggested in 1838 by Maxwell that lightning protection system could increases incidence

of lightning strikes to a building and that encasing the building in a Faraday cage [58] could be the best procedure.

In lightning protection standards, such as the IEC standards, the four protection levels are defined as **I**, **II**, **III** and **IV**. A structure's lightning protection system based on level **I** would not allow a return stroke peak current larger than 2.9 kA to penetrate the lightning protection system. The corresponding currents for levels **II**, **III**, **IV** are 5.4, 10.1 and 15.7 kA, respectively. Maximum values of lightning current amplitudes are fixed to 200 kA at level **I**, 150 kA at level **II** and 100 kA at levels **III** and **IV** respectively.

### 2.5.3 *The Rolling Sphere Method*

Horvath [61], proposed positioning of lightning conductors on structures using fictitious sphere based on the idea of protected spaces boarded by circular arcs introduced by Schwaiger [62], in the early 1960s. Rolling sphere originates from the studies conducted by Lee [63, 64], in the United States. Rodrigues et al. [65], used the rolling sphere method to estimate the lightning vulnerability points on wind power plants.

The Rolling Sphere method is the most common (EGM) in Standards documents, and to apply it on a structure, an imaginary sphere, typically 45 m in radius, is rolled over the structure. All surface contact points are considered to require protection, whereas the unaffected volumes are assumed to be protected. Despite the widespread use of the rolling sphere method, its assumption that the radius is a function of the prospective return stroke peak current only and is independent of the geometry of the structure has led to serious errors in some situations. Rolling sphere method has been used on wind turbines as

presented in Figure 2-5, but according to IEC 61400-24 standard, the rolling sphere method must not be used for the rotor blades.

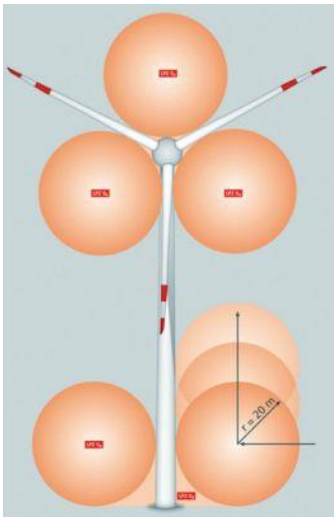

Figure 2-5: Rolling sphere method (courtesy Dehn.co.uk)

The point on a structure where lightning will attach as well as the positioning of air-terminal has been a subject of research. Existing methods for air-terminal placement has been very effective for wind turbines except for the rotating blades, also modern wind turbine with higher heights are found to be more vulnerable. The air-termination systems are placed on the surface of the blade at points where connecting leaders might originate and result in lightning flash attachments or punctures if no air terminations are present.

If air-terminal are not well positioned on the blade, lightning can attach on the blade surface instead of the air-terminal with a consequence of damage. The air-termination systems could be part of the blade structure itself or components added to the blade, and even combinations of both. There are a few air-termination positioning methods as mentioned above, and for a particular design, the lightning protection system designer may select.

The processes of downward initiated lightning which begins from the cloud and attaches in the vicinity of the grounded structure can be explained by the Electro Geometric Model

(EGM) and to link them to the peak current, the charge, striking distances, etc. but for upward initiated lightning which begins from the grounded structure and propagate upward towards the cloud, the grounded structure determines the attachment point and cannot be explained or described by the EGM, the rolling sphere and others.

Over time, research on various EGM models progressed. The result of the research on lightning protection for high voltage transmission lines was responsible for the emergence of the Electro Geometric Models (EGM). The Monte Carlo Method was developed in 1960 by J. G. Anderson [66], it is a computer program for evaluation of transmission line lightning performance. Young [67], developed the initial version of the (EGM) in 1963, and then, Whitehead model. Also of note is the Simulation of lightning performance using Monte Carlo by Sargent [68], who researched on lightning strokes to high structures. The application of the EGM was extended to substation facilities by Mousa [69], in 1976. There were certain apparent inconsistencies in the EGM that have a tendency to discredit it such as investigation by Eriksson [70], in 1978 and then, work by Anderson and Eriksson reported in 1980. However Mousa [71], proved that, explanations do exist for the apparent inconsistencies, and can be eliminated by the revised electro geometric model. Mousa and Srivastava [71, 72], developed the revised EGM.

These methods have been very effective and were extended to wind turbines as shown above. Up till 1994, according to a number of papers, since there were no information of lightning striking a wind turbine, the scale of the problem was not known [73].

Since the late 1970s when the first wind turbines were built in America, Lightning protection has been the subject of research, and the focus has changed over time with suggestions of different methods of lightning protection. Research has shown that lightning

is the major cause of wind turbine components damage and is actually the main sources of wind turbine insurance claims, downtimes and even caused some power company to shut down and dismantle. Notable research works are detailed in [73-81].

A fundamental aspect of wind turbine blade lightning protection is to identify vulnerable points on a blade and the most suitable location(s) for the air terminal(s) and also the type of air terminal and the area of protection it can afford. Its primary purpose is to capture the lightning stroke at a preferred point. Current protection systems and design methodology are prescribed in various Codes of Practice and are been improved employing computer modeling, theoretical, laboratory and field investigation techniques.

The continuous failure of wind turbines due to lightning in spite of various advancement has brought it to the front burner in research and a re-evaluation of lightning problem with wind turbine. Lightning problems with wind turbine arise due to: the nonconductive nature of blade material; rotation of the blade; and increase in size on account of higher power requirement on the order of megawatts. Recently, multiple discharge in the turbine associated with nearby cloud to ground lightning [30], and also strikes attaching inboard on the blade due to dart leader [31], are also mentioned as some possible causes of continued blade failures. Glushakow et al. [6], offered general guidelines for effective protection of wind turbines. Erichsen et al. [82], discussed safe locations in a wind turbine exposed to the first and subsequent return stroke during thunderstorms.

## 2.6 Blade Damage

When a wind turbine component is damaged, there is an associated repair costs, resulting loss in production and even downtime. These effects are worst with offshore wind turbines

because it requires to mobilize special floating cranes. Rukiye Canturk et al. [83], presented the computational acoustic interrogation inspection for wind turbine blade damage and Dongsheng et al. [84], gave a review of wind turbine blades damage detection methods. Protecting wind turbine against lightning damage was the focus in [85]. Wang et al. [86], evaluated the thermal damage associated with glass fiber Polymer matrix composites in blades due to lightning strike. A relationship exists between the risk of lightning damages and the number of thunderstorms in the area the wind turbines are located. Statistics have shown that the costs of repair increase with wind turbine size, and also that blade damages compared to other components, are the most expensive due to its relatively high costs, crane costs, repair costs and even production loss. Yasuda et al. [87-89], proposed a classification of wind turbine blade damage due to lightning by considering their possible causes.

## 2.7 Rotation Effect

Rockets reach an altitude of around 200 m before setting off a lightning in rocket triggered lightning, wind turbine blade tips now reach same altitudes with nacelle height of around 100 m and 80 m. Recent research and publications detailed the effect of rotation. Xishan et al. [90], experimentally studied effect of blade rotation on triggered lightning and suggested that rotation may be altering the charge distribution on the blade tip. Rachidi et al. [4, 91], suggest that large wind turbines might trigger their own lightning due to rotation of the blades and that a new set of problems are introduced by carbon reinforced plastics present in the blades. Mendez et al. [92], discussed blade electrostatic charging effect on lightning overvoltage. Montanyà et al. [93] , used a 3-D Lightning Mapping Array and

high-speed video to observe the initiation of lightning and showed that as compared to static objects having similar height, rotating wind turbines can easily produce electrical discharges and explained that an electric field growth rate required for the initiation of stable lightning leaders can be provided by the effect of rotation. Radicivic et al. [42, 94], studied the impact of wind turbine blade rotation with a reduced-size wind turbine model and observed a reduction in the number of direct lightning strikes in the air termination system zone and an increase of 50% flash over voltage (FOV) due to the blade rotation, but mentioned that the reduced-size model is not quite appropriate for analysis and comparison of blade lightning protection methods. Madsen et al. [43], discussed Interaction between materials for wind turbine blades electrical discharges. In [95], lightning discharge on the tip area of blade was discused regarding its dependency on material.

## 2.8 Wind Turbine Lightning Protection

A significant energy is conveyed by the high peak currents in a lightning strike which must be diverted to ground by the protection system, otherwise, substantial damage can result. Apart from resulting repair costs when a component of a wind turbine is damaged, the accompanying loss in production caused due to downtime is a serious concern particularly for offshore wind turbines. To avoid these problems, modern wind turbines are fitted with lightning protection systems.

### 2.8.1 *Wind Turbine Blade*

Normally, Wind turbine blades are made of composite materials such as wood-epoxy laminate, glass fibre reinforced plastic (GFRP) and carbon fibre reinforced plastic (CFRP).

CFRP is normally used for special components like the tip shaft or for reinforcement of the blade structure. Some parts and discrete components are made of metal, these are such as springs, fixtures, mounting flanges, electrical wiring, balancing weights, wires, hinges and bearings. Design of wind turbine blade is shown in [96]. The materials the blade is made of has been found to have significant effect on lightning interactions with wind turbines. Candela et al. [97], discussed tracking and breakdown properties of rubber materials used for wind turbine blades. Composite materials breakdown tests was conducted in [98], and for glass fibre reinforced polymers (GFRP) in [99]. Carbon nanotubes and polymer nanocomposites were discussed in [7], regarding wind blade materials.

### 2.8.2 *Blade Lightning Protection*

After the oil crises that happened in 1973 and 1979, which encouraged renewed interest in alternative energy sources, there was a renaissance for wind turbines. In the mid-1990s, lightning protection start to receive attention in the wind turbine industry when wind turbines with heights of around 50 m started to appear. At that time, lightning strikes each year caused damage to about 4–5 per cent of wind turbines operational in Denmark [100]. With larger wind turbines, it is a different situation, for instance, 2 MW rated power wind turbines exceed 100 m in height, and due to their height, they will most probably all be hit by lightning many times in their 20-year lifetime. Therefore, lightning has become an operational condition for large wind turbines and must be equipped with efficient lightning protection, mostly when situated offshore due to difficulty in access, and maintenance cost are very high.

In the mid-1990s, lightning protection system was developed for GFRP blades using tip air brakes. It comprises of lightning receptor and connected with a down-conductor. The blades are the utmost exposed component of wind turbine and would encounter the full effect from the electric fields related with the lightning attachment process, as well as lightning currents and its associated magnetic fields. As far as lightning protection is concerned, the blades are typically considered a very important part of wind turbine. They are at topmost part and therefore more vulnerable to lightning attachment. According to IEC 62305-1, blades of wind turbines are placed in lightning protection zone *0*A and are protected accordingly. The lightning protection should be sufficient to enable the blade to accept protection level LPL I lightning flashes without structural damage that would weaken the functioning of the blade.

### 2.8.3 *Functions of Wind Turbine Lightning Protection System.*

A lightning protection system LPS is a comprehensive system used to eliminate or lessen physical damage from lightning flashes to a structure such as wind turbine, and also to protect against injury to life owing to touch and step voltages. It comprises of both external and internal LPS.

An efficient wind turbine lightning protection system must carry out the following functions.

1 Allow leader incepting from and attaching to the protection device.

2 Ease the flow to ground of the lightning current from the protection device through the ground wire.

3 Reducing, in and around the wind turbine, the levels of voltages and voltage gradients.

### 2.8.4 *Components of Lightning Protection System LPS*

An efficient lightning protection system typically have the following components:

1 An air-termination system for forming upward and attracting downward propagating lightning leaders.

2 A down conductor for taking the lightning current to ground.

3 A transient suppressor to eliminate the effects of induced voltages.

4 Equipotential bonding to eliminate potential danger to equipment and human life.

5 An earthing system to minimize the local potential gradients.

### 2.8.5 *Lightning Air-Termination Systems*

The part of a lightning protection system LPS which intercept lightning flashes and uses metallic elements is called the air-termination system. The intercepted lightning flashes is sent to ground through a down conductor system and an earth termination system. The lightning air-termination system operates on the principle of faraday rod but with complexities when used on wind turbines. Therefore, efficient LPS design begins with proper positioning of the air-terminal system.

### 2.8.6 *Air-Termination Systems (Non-Conventional)*

Not so much improvement has been done to classical air-termination systems. Radioactive air-terminals were introduced in the past but are no longer allowed. They did not show better efficiency as compared to classical lightning rods of the same dimensions and shape. So far, as compared with simple Franklin rods, early streamer emission (ESE) devices, charge transfer systems, lightning repellers, ion plasma generators etc., when exposed to

natural lightning, does not show substantial difference in the distance of attraction or in the number of lightning strokes to the diverse types of air-terminals.

The air-termination system positioning tools such as protective angle, rolling sphere, etc. discussed above, according to IEC 61400-24, even though still useful for wind turbines, must not be used on wind turbine blades.

### 2.8.7 *Protection Methods for Blades*

In general, the major task of wind turbine lightning protection systems is to be able to conduct safely the lightning current from the attachment point to ground so as to avoid formation of a lightning arc inside the blade. To avoid damage and possible downtime resulting from lightning strikes, modern wind turbines are usually equipped with lightning protection systems. Various lightning protection methods are shown below in Figure 2-6.

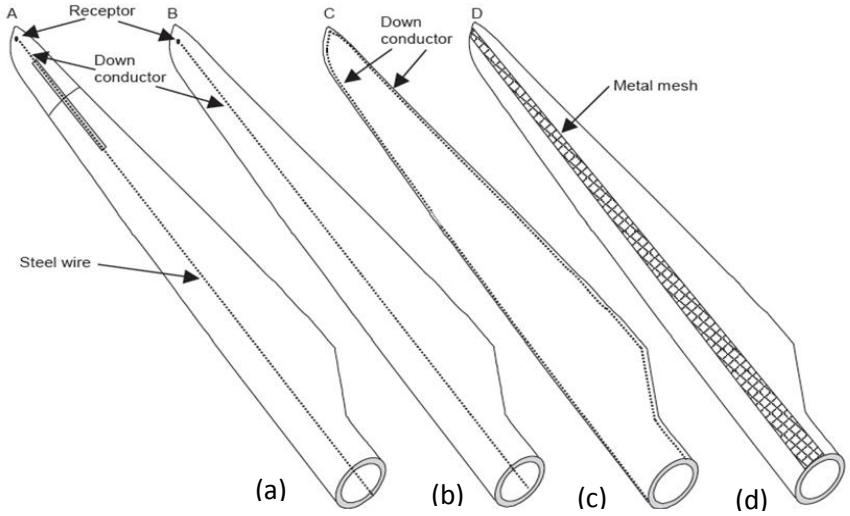


Figure 2-6: Lightning protection methods for modern large wind turbine blades IEC 61400-24

Figure 2-6 (a) and Figure 2-6 (b) are the receptor methods while Figure 2-6 (c) is the metallic conductor on the blade edges method and Figure 2-6 (d) is the metallic mesh method.

Figure 2-7. shows a large wind turbine blade with multiple receptors pairs.

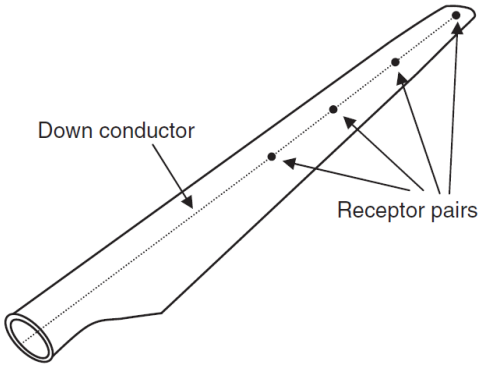


Figure 2-7: Multiple receptors on blade

Optimization of blade lightning protection air-terminal has also recently attracted research, this is as a result of continue damage to wind turbine blades due to lightning. Yasuda et al. [14], used two ring-shaped electrodes on the tower and the shaft (Figure 2-8) and Minowa et al. [11], studied creeping discharge characteristics and observed that by using the backside electrode, discharge on the test model blade was lead to the receptor. In June 2008, at the 29$^{th}$ international conference, held at Uppsala Sweden, on lightning protection, Sorensen et al. [23], presented the update of IEC 61400-24 on lightning protection of wind turbine and highlighted that the air termination system positioning tools such as the rolling sphere and protection angle method in IEC 62305-3 are not applicable to wind turbine blades. Damir et al. [101], presented an antenna model of a wind turbine struck by lightning. Yoh et al. [28], and Yokoyama et al. [29] , experimented with a high voltage impulse generator, and observed that without lightning receptors, Lightning discharges could penetrate into the blade cavity but blade with lightning receptors will be protected, though receptors are not adequate particularly when the blade change position and when polluted. Griffin et al. [27], compiled lessons learned from blade failures, primary causes and how to reduce risk. Kern et al. [102], presents the dynamic electro-geometrical model

method for evaluation of interception efficiencies for airterminations which is dissimilar to the classic rollingsphere in that instead of fixed radii, a varying radius is used. It was shown that the interception efficiencies of airterminations are higher than that documented in the standard series IEC 62305. Vidyadhar Peesapati and Ian Cotton compared lightning data with required protection level [103], and IEC 61400-24 [104], and found that the lightning parameters obtainable in probability distributions of IEC standard are not appropriate for large wind turbines. Also [1],compared measured lightning data with required protection levels. Conductive surface layer on wind turbine blade was suggested as lightning protection system in [105]. Zoro et al. [106], suggested that wind turbine structure can be used for lightning protection system. The methods enumerated above has been very useful however only downward lightning were considered. Modern wind turbines are usually very high and are mostly affected by upward initiated lightning.

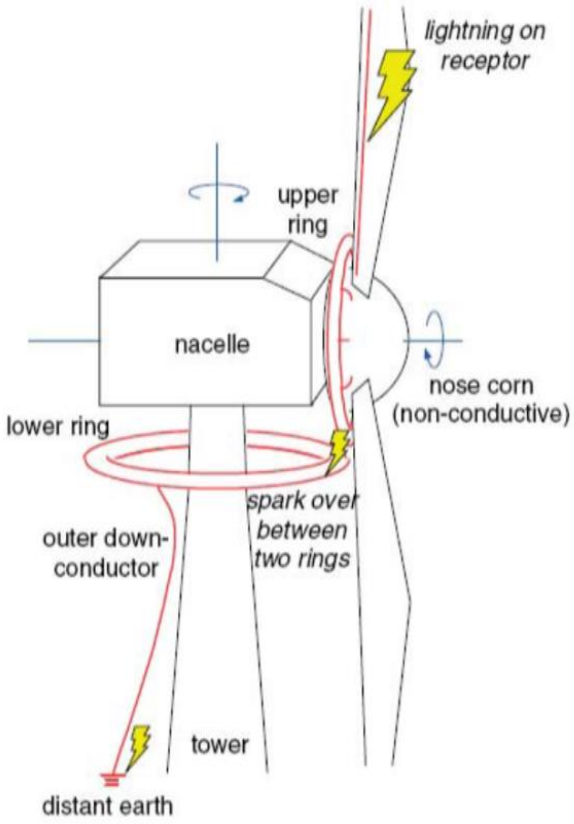


Figure 2-8 Lightning protection system by Ring-Shaped Electrodes [14]

The physics and properties of natural lightning as it affects wind turbine lightning protection systems have also attracted researchers, there are opinions that they are different from those in the laboratory[107, 108], for instance, the descending stepped leader's background electric field in the case of downward initiated lightning, increases continuously. Also, the electric field present between a small test sample and the opposite electrode as it is currently the practice in the laboratory, is different than when the entire blade is present. Other areas that have also been explored include air-terminal material and the blade surface conductivity. However, full blade length was not considered. Plumer et al. [20], compared natural lightning strike and laboratory test results and recommended longer blade lengths for test methods. Shindo et al. [19], experimentally studied the effects of receptor configuration on wind turbine blades with 3-m tip part of an actual blade length

and observed that the receptors effectiveness can depend on conditions such as the blade surface pollution. Abd-Elhady et al. [44], experimentally evaluated wind turbine blades air-termination systems by replicating the test in IEC-61400-24 standard with a 2 m blade tip section of a 19.1 m full blade length of 600 kW rated wind turbine and concluded that it is significant to use air-termination systems appropriate for all blade positions. Yokoyama et al. [17], experimented with a 3 m blade-sample with various configuration and different blade conditions and observed creeping discharge and penetrative destruction which occurred more frequently when the blade was polluted and concluded that the receptor lightning protection method effectiveness was not perfect. Instances of receptor failures have also been mention [28, 29]. Various test procedures and results can be found in literature [109, 110]. Lightning discharge on wind turbine blade using a small blade tip section is shown below in figure 2-9.

Figure 2-9 Lightning discharge on wind turbine blade [17].

The reduced-sized model has also been used for comparison [94], but according to [42],the reduced-size wind turbine model is not quite appropriate for analysis and comparison of lightning protection methods.

However, despite such advances in using experiments, the reduced size model, and computer simulations, there are still many challenges in trying to analyze full blade length particularly now that the blades are getting longer, and wind turbines are moving offshore. The increase in insurance claims due to lightning destroying wind turbine and wind farms, coupled with the fact that turbines are increasing in size and going offshore, and the invalidation of the EGM suggest the need for a more sophisticated method of analysis of full blade length of large wind turbine which is presently difficult. The key point is to know exactly the type of protection device and where to fix it at various orientation of the lightning source and also at different position of the blade when it is rotating.

Lightning attaching inboard area of blade have also raised concern. Candela et al. [30], in a paper, presented the analysis of events obtained in a wind farm in Kansas, USA, where simultaneous lightning discharges were noticed in different wind turbines. They suggested that multiple lightning discharges observed in wind turbines is associated with nearby cloud-to-ground lightning. Long et al. [31], proposes a mechanism to describe the lightning attachment in inboard area of blade owing to dart leaders. In the 23$^{rd}$ international lightning conference held in march 2014, in Tucson, Arizona, USA, Cummins, et al. [111], gave an overview of the field program of Kansas windfarm in 2013. Analysis of the CG lightning data by Cummins et al. [111], shows that wind turbines having rotating blade tip heights of about 120 m have a higher attractive radius (276 m) when compared to stationary towers of same height. According to IEC/TR 61400-24, “lightning protection of wind turbines

have problems that are not usually seen with other structures." It was suggested in [6], that Radom antenna towers and lighthouses are geometrically like wind turbines, and are also sited in high-lightning remote & exposed locations, however different from wind turbine due to lightning attachment to a rotating blade.

## 2.9 Numerical Evaluations

Here, previous simulations are mentioned; Recently, computer simulation has become very useful in analyzing wind turbine lightning protection. Madsen et al. [33], used COMSOL Multiphysics to analyze current distribution and magnetic fields within a wind turbine nacelle and presented numerical tools for wind turbines lightning protection [22]. Wind turbine blade lightning current distribution test and simulation are shown in [112]. Bagherian et al. [36], concluded that the voltage distribution on the surface of the blade has influence on lightning protection and that the receptor's position, number and size can modify voltage distribution. Simani et al. [34], discussed a fault diagnosis scheme of a wind turbine relying on identified fuzzy models. The simulation of Lightning caused delamination in unprotected laminates of CFRP was presented in [113]. Rodrigues et al. [35], used EMTP-RV software to analyze direct lightning surges in wind turbines and observe that it is helpful in finding adequate protection measures and their locations. Peesapati and Cotton [37], compared finite element lightning information with real lightning strike data and showed that the ambient electric fields which the wind turbine is exposed to, rises with a reduction in cloud height and that winter clouds at lower altitudes develop higher electric fields at ground than summer clouds. Compared to experimental evaluation, numerical simulation has become a very useful tool for analyzing lightning

protection of modern wind turbine. Nath et al. [114], used MATLAB to model and simulate wind energy based power system. Yamamoto et al. [115], presented a paper that describes the verifications of field tests of wind turbine grounding characteristics by using the FDTD (Finite Difference Time Domain) method. It concluded that the potential rise responses for all kinds of lightning currents can be simulated using the FDTD method. A FEM Model of wind turbine main shaft bearings for the development of specific lightning protection systems using FEMLAB software was shown in [116], it was used in reproducing electric field distribution between rollers. An electromagnetic compatibility (EMC) analysis of blade lightning protection system was presented in [117], it analyzed the electric properties of a 16 m blade tip sample taken from a 42 m wind turbine blade that is equipped with three lightning receptors using the commercial method-of-moments simulation tool FEKO. It gave insight into lightning interaction between wind turbine blade, the protection device and the maximum electric field strength. Bertelsen et al. [118], presented numerical models for wind turbine lightning attachment points, which was also implemented in [119], according to the revised IEC 61400-24. The model implemented in COMSOL Multiphysics and Matlab, was used to compute attachment distribution on a large modern wind turbine, the results proves that mainly the blade tips are more exposed. The findings formed part of IEC 61400-24, referred to as verification of lightning protection systems. Detail is shown in the next subheading.

Despite these computer developments, there are no standards as well as detailed experimental and numerical research covering receptor location, receptor size, pollution and general receptor performance considering upward initiated lightning.

## 2.10 Verification of Lightning Protection Systems

The ability of the lightning protection systems (air-termination system and down-conductor system) to intercept lightning flashes and conduct lightning currents is usually verified. The blade manufacturers usually produce documentation that describes the methods used and the results of the verification for their product. The methods of verification are given in IEC 61400-24 and are as follows:

1. High voltage and high current testing.

2. Demonstration of similarity with a previously verified design.

3. Using analysis tools (numerical simulations) previously verified against field data or laboratory results.

Various software has been very useful in lightning protection of wind turbines as shown above. COMSOL MULTIPHYSICS has introduced a new module called multibody dynamics in which it is possible to analyze multi bodies such as blade tip, trailing edge, leading edge, blade surface, nacelle, tower and the ground of a wind turbine in rotation mode simultaneously, this has made it a preferred choice in this work. Again, COMSOL MULTIPHYSICS is an analysis tools (numerical simulations) previously verified against field data and laboratory results in literature.

To ensure efficient lightning protection of wind turbines, high-voltage strike attachment tests in IEC 61400-24 are used to determine points of lightning attachments. These tests are usually conducted with a small blade sample as representative of full-scale blade length. However, incidences of lightning damage to wind turbines are still highly recorded indicating that small blade sample might not be an adequate representation of full-scale blade. Again, obtained results would be different if full blade length is used for the test.

Since there are no standards covering this subject, it is therefore very important to know the difference in results obtained with both small blade and full blade samples.

### 2.11 Lightning Protection Zones (LPZ)

Some further progress has been made on lightning protection of wind turbines, according to results obtained from the FEA wind turbine model conducted by [37], it was reiterated that the blades are at higher risk of lightning attachment, also, S.F. Madsen et.al [18, 120], presented a paper in which blades where divided into different zones and argue for a pattern of differentiating the lightning protection system and concluded that the tip is more exposed than other part of the blade, but [31], suggests that in lightning attaching to wind turbine blade, there is a possible sequence of events and according to them, due to the stepped leader interception, the first strike attaches to the tip of the blade, then, due to interception of dart leaders, the successive strike attaches to receptors inboard blade. This kind of lightning attachment process according to them, is due to the diverse properties of stepped and dart leaders, blade rotation as well as the blade angle as at when the stepped leader was intercepted. This support the argument that there is a blade length limit before lightning attachment to the middle part is not affected by the presence of the blade tip [18]. Multiple discharge in the turbine associated with nearby cloud to ground lightning has also been reported [30].

The zone where the lightning electromagnetic environment is defined is referred to as the lightning protection zone. S.F. Madsen et.al [18], conducted modeling and field surveys on three different sites. They extended their work in [120], and presented the revised Zoning Concept by evaluating the zones of protection afforded by a protection device eventhough such has not been extended to upward initiated lightning and suggest that it could help the

lightning engineers focus attention on the portion of the blades with highest lightning exposure. The zoning concept in [18], divides the blade into four different lightning protection zones. Figure 2-10,

*Zone 0A$_1$ is the outermost 1m tip section exposed to the full threat i.e., direct lightning attachment with a maximum peak current - 200kA, 10/350us*

*Zone 0A$_2$ is the section of the blade from 1m to 5 m inboard the tip, exposed to direct lightning attachment with current levels of only 100kA, 10/350us*

*Zone 0A$_3$ is the section of the blade from 5 m to 20 m inboard the tip, exposed to direct lightning attachment with current levels of only 50kA, 10/350us*

*Zone 0A$_4$ is the section of the blade from 20 m inboard the tip up to the root end of the blade, exposed to direct lightning attachment with current levels of only 10kA, 10/350us*

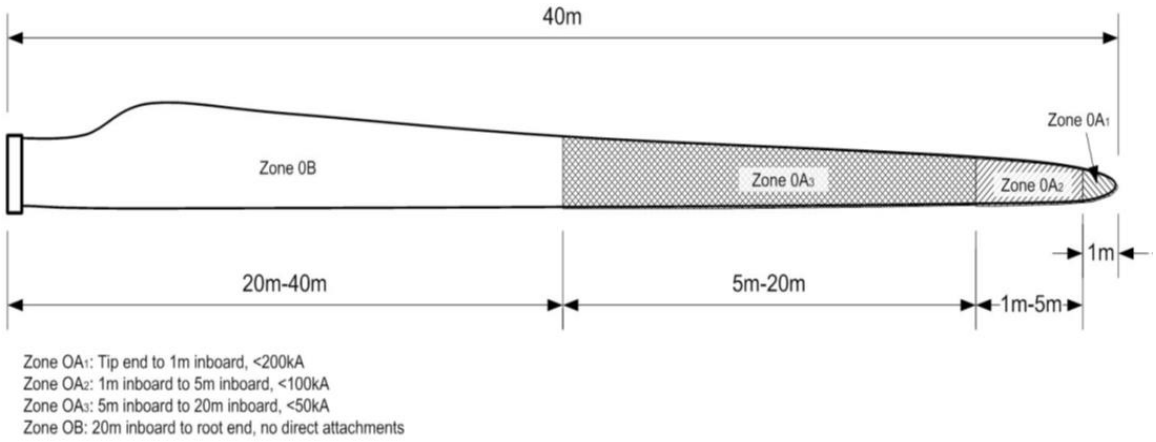


Figure 2-10: Zoning concept for wind turbine blade [120]

Accordingly, they suggested an equation relating distance from the blade tip with the probability of attachment for blade length of 40-80 m

$$\mathbf{P_{blade} = 0.4 \cdot exp\,(-0.4 \cdot d)} \qquad \mathbf{(2.2)}$$

Where $P_{blade}$ is the lightning attachment probability [%], and d is the distance [m] from the blade tip.

However, the zoning concept cannot show where to place air termination system or receptors, it only helps to assess the likely strike amplitudes to different areas on the blade.

## 2.12 Air-Termination Interception Efficiency

The interception efficiency of air-terminal systems used in wind turbine blade lightning protection is very important. The air-terminal must be more attractive to lightning than the blade surface otherwise, lightning can attach on the blade surface instead of the air-terminal resulting in damage to the blade and the wind turbine itself. The probability of lightning puncturing a non-conducting blade surface must be reduced to an acceptable level. Air-terminal placement should be such that the flashover voltage on the blade (non-conducting) surface is lesser than the blade skin breakdown voltage. However, in practice, these voltages will be difficult to establish due to expected variations caused by the following factors; different composite materials, change in blade surface conductivity due to pollution, humidity, cracks, ageing, changing blade length as well as its rotation.

Tip receptor has been very useful in protecting wind turbine, however, as the blade gets longer, the interception efficiency needs to be re-evaluated. Research has shown that the interception efficiency of receptors can be influenced by so many factors e.g., the presence of conducting materials inside the turbine blade [121].

High-voltage strike attachment tests are presently used on test specimens representing the design, though useful for revealing insufficient receptor protection, however, real lightning situations are not well represented in the laboratory. Also, certain other conditions such as pollution, aged blades, longer blades, blade rotation, lightning source orientations, receptor

materials, blade material etc. can play a critical role in the interception efficiency of air-terminal.

The reduced size wind turbine model has also helped in evaluating the interception efficiency of lightning protection systems of wind turbine but has also had its deficiencies.

As was discussed earlier, numerical simulation methods used to determine likely attachment points on blades and nacelles and to estimate the number of attachments of direct lightning flash to certain structures per annul are a focus of resent research. Thy have also been helpful in evaluating the interception efficiency.

### 2.13 Experimental Test

High voltage testing is given in section 8.1 of IEC 61400-24 to verify the functionality of a protection system. To ensure efficient lightning protection of wind turbines, experimental analysis is usually done in accordance with the test methods and as generated power capacity is increasing, offshore wind turbines are getting taller with longer blades, resulting in increased probability of lightning strike majorly due to upward lightning. Research has shown that the physics and properties of natural lightning are different from those in the laboratory. Also, the electric field present between a small test sample and the opposite electrode as it is currently the practice in the laboratory, is different than when the entire blade is present. Full scale blades tests are still complex [4], since modern wind turbine blades are as long as 80 m. Laboratory experiments are presently conducted with a small blade samples such as 3 m, 2 m cut from a full blade and also the reduced size (scaled model). Various test procedures and results can be found in literature such as in [109, 110, 122]. Also, various test methods are available in international standards for developing new

blade designs or verifying existing blade designs performances with respect to their capability. Some progress has been made with wind turbine lightning protection [6, 22, 33-35], as well as improved testing methods. Glushakow [123], discussed the formulation of the 10/350 test waveform and [124], presented a perspective on protection of direct lightning strike. Also, Zhou et al [125], gave a review of wind turbine blade's full-scale structural testing. Yang et al [126], give insight to nondestructive testing for wind turbine composite blade. For some reasons, it is impossible to duplicate lightning itself in testing: about 6 MV are the highest voltages that can be generated inside laboratories and for outdoor equipment, 10 MV. Laboratory size is another limitation as it is difficult to accommodate full blade with length as long as 80 m, and also preventing discharges much longer than 10 m or so. Again, there is no available equipment that can produce the high voltages and high currents of natural lightning, simultaneously with the same machine.

In order to assess the normal distribution of the points of discharge attachment on the blade surface, a large sized wind turbine hit by natural lightning strike is experimentally required while it is rotating, this can only be done in the natural lightning laboratory such as in Florida [14]. To ensure efficient lightning protection of wind turbines, high-voltage strike attachment tests in IEC 61400-24 are used to determine points of lightning attachments on wind turbines. These tests are usually conducted with a small blade sample as representative of full-scale blade length.

### 2.14 Laboratory Test in IEC 61400-24

Various test methods are available in IEC 61400-24 standards for developing new blade designs or verifying existing blade designs performances with respect to their capability of

handling the effect of a lightning discharge. These tests may also be applied to other objects such as spinner, hub, nacelle, etc.

Laboratory testing with high voltage equipment helps to compare the performance of unprotected wind turbine blades and those fitted with different designs of blade lightning protection systems. It simulates the electrical conditions on the blade during the formation of a lightning strike.

### 2.14.1 *High-Voltage Strike Attachment Tests*

High-voltage strike attachment tests are used to determine points of lightning attachment and breakdown paths through or across non-conducting materials. The High-voltage strike attachment tests in IEC 61400-24 that is considered in this work is the Initial leader attachment test.

### 2.14.2 *Initial Leader Attachment Test:*

#### *2.14.2.1 Test Purpose:*

Initial leader attachment test is used for wind turbine blades, but also applied to nacelles made of glass fibre or other non-conducting materials.

This test is used to assess;

1. Possible leader's attachment points locations and puncture or flashover paths on non-conducting structures such as blades.
2. Optimization of the location of protection devices and air-termination systems such as receptors.
3. Puncture or flashover paths along or through dielectric surfaces.

4. Performance of protection devices.

#### *2.14.2.2 Test Specimen:*

The specimen usually tested is a full-scale or blade section. Any section of the blade to be tested depends on the structural details and the lightning protection design of the blade. The principles are to expose all parts of the blade and its protection system design to the electric fields that usually precede lightning leader attachment.

#### *2.14.2.3 Test Setup:*

The general test arrangement of the Initial leader attachment test setup in IEC 61400-24 is illustrated in Figure 2-11. The blade specimen is usually tested in several positions representing different directions of the approaching leader.

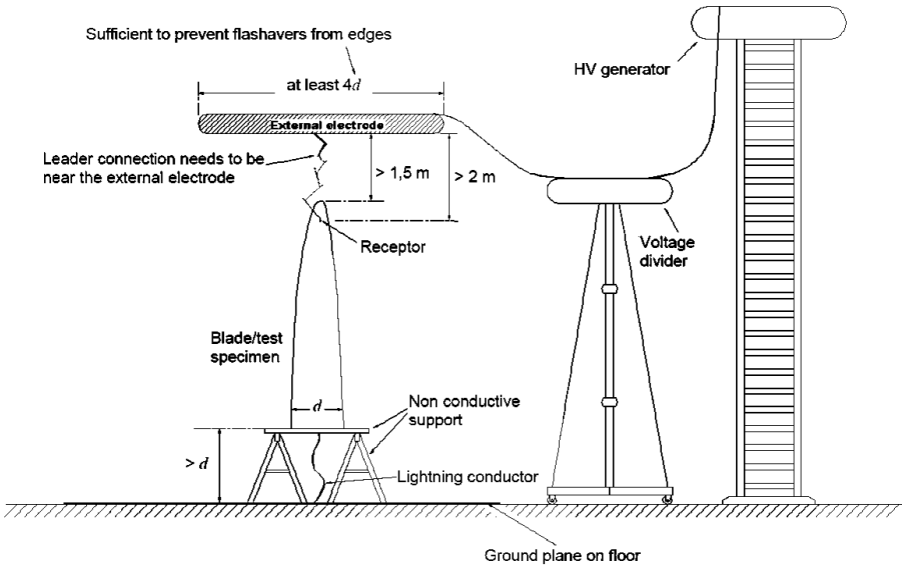


Figure 2-111: Initial leader attachment test setup in IEC 61400-24

### 2.14.3 *Initial Leader Attachment Test Voltage Waveform*

The voltage waveform that is the most representative of the electric field in the surrounding area of a structure in an initial leader attachment is the double exponential switching type impulse voltage. It has a time to peak 250 μs ± 20 % and decay time to half value of 2500 μs ± 60 %. In this case, the voltage is usually applied as a rise to flashover occurring before the crest of the voltage waveform. This type of voltage waveform in which the time between its initiation and the flashover to the structure must be at least 50 μs may be accomplished by using the switching type impulse voltage in IEC 60060-1 shown in Figure 2-12.

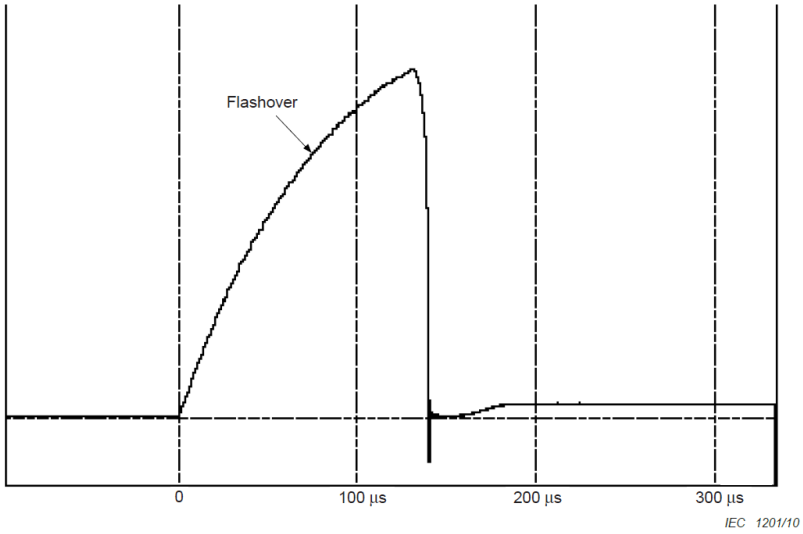


Figure 2-112: Switching impulse voltage (IEC 61400-24)

## 2.15 Protecting Wind Turbine from Upward Lightning Flashes

Upward lightning flashes have been observed to incept or initiate from tall towers [127], in America [6, 22], in Japan [128, 129], in Europe [130-132], and has been observed to be dominant at the Gaisberg Tower [130]. Upward lightning flashes has also been reported to

be triggered [133] by wind turbines [91, 93, 128]. An assessment of currents of upward lightning that were measured in tropical regions was presented in [54].

The lightning strike incidence to wind turbine is generally evaluated based on probability of downward lightning attachment and does not account for upward flashes. However, in the presence of a thundercloud, tall wind turbines are increasingly subjected to upward lightning attachment self-triggered by the wind turbine, this can significantly increase the number of lightning strike to a wind turbine per annual [134], and is considered to be the main mechanism of lightning damages [91]. Alex Byrne and Matthew Malkin [9], discussed wind turbine lightning protection system's field performance assessment and suggested that increased risk for investments and insurance premiums in wind industry is due to poorly understood interaction of lightning and wind turbines and also that the IEC 61400-24 approach to lightning damage risk assessment focuses more on downward lightning, and less on upward lightning. The design limits provided in IEC 61400-24 are for downward initiated lightning only, whereas, upward lightning has been found to have different characteristics than downward lightning [135, 136]. Also, upward leader's physical properties in nature have been found to be unlike those of leaders in the laboratory [107, 108]. Fundamentally, lightning attachment process of downward lightning are different to those of upward lightning, and as result, likely point of upward lightning attachments are uncertain. This is a major problem for modern wind turbine because lightning protection systems, the Electro Geometric Model (EGM) methods currently in use were designed considering downward lightning. These protection systems might not be effective for upward lightning. According to a paper by Vidyadhar Peesapati and Ian Cotton [37];

*Existing turbine lightning protection systems have been shown reasonably effective for downward initiated lightning but there is an underlying risk in assuming the same systems will work for upward initiated lightning [37]*.

Therefore, the interception efficiency of air-terminal assessment based on upward propagating lightning is very necessary, particularly due to varying blade conditions.

## 2.16 Estimating the Incidence of Upward Lightning to Wind Turbine

For a comprehensive lightning protection, it is necessary to estimate the incidence of upward lightning to wind turbine. lightning location systems (LLS) [137-142], has recently been used to study the occurrence of upward lightning flashes to wind turbine [143]. They have also been used to investigate lightning strokes characteristics forming a hot spot [144]. Sarajcev et al. [145], estimated lightning current amplitudes occurrence to wind turbines in exposed locations. [138], observed that some wind turbines have higher frequency in triggering upward flashes than others, however, this effect has not been fully studied. In [137], it is suggested that the incidence of upward lightning is a function of wind turbine height, the altitude and latitude of the location of the site. Also, [139, 140], approached it by divided the area surrounding wind turbines into different regions. However, in all, LLS is not able to detect a large percentage of upward lightning. Thus, the incident of upward flashes estimated using this method is undervalued.

Upward lightning flashes are initiated from the electric field enhancement produced by either thundercloud charge or from nearby lightning discharges [128, 130]. The level of electric field enhancement existing around the blade can affect the production of upward

initiated lightning [146]. However, the critical electric field essential for the initiation of upward lightning flashes has not been quantitatively analysed [128].

## 2.17 Electric Fields

Electric field strength around the blade and its distribution by the air-terminal is quite important for the prediction of lightning attachment points and will give information about the protection. Lightning is usually preceded by a high electric field in excess of 10 MV and could result in upward or downward initiated lightning. Cooray detailed the electric fields generated by thunderclouds, stepped leaders, dart leaders and from first and subsequent strokes [147], and various models have been used to replicate the thundercloud electric fields, but the electric field is very strong and not sufficiently represented in the laboratory and as mentioned above, its interaction with large and rotating wind turbines has not been well evaluated by the invalidated EGM.

### 2.17.1 *Electric Fields Generated by Thunderclouds*

Electric fields can appear around grounded structure either from a stepped leader descending from the cloud leading to downward initiated lightning strike or from thundercloud high static field conditions during a thunderstorm leading to upward initiated lightning strike which originates from the structure. In order to study the effect of blade conditions (dependent variable) on upward leader inception from wind turbines, only the thundercloud (independent variable) electric field is considered in this thesis.

During lightning strikes to structures like wind turbines, the maximum electric field strength on the surface of the structure and the air surrounding it can greatly influence the

lightning protection and are an important issue for designing effective lightning protection. Air terminations locations, their numbers and sizes can modify the maximum electric field strength.

Electric fields produced by thunderclouds are very important in the studies of lightning protection.

Placing an object in a constant electric field will cause corona emission from certain locations if the electric field is high enough. The emission of corona precedes leader formation. Leader is therefore expected to form at the points of corona formation. Marley Becerra [148], presented glow corona generation and streamer initiation at grounded objects tip during thunderstorms.

(a) Thundercloud generated electric fields at ground level causes the inception of upward flashes from high structures or structures situated on mountains

(b) Sharp, grounded tips and pointy leaves of plants due to electric fields generated by thunderclouds, can go into corona, which produces space charge

(c) Warnings on the threat of lightning strikes issuing can be based on the electric fields generated by thunderclouds.

Madsen et al. [149], presented floating electrodes for measuring static electric fields and [150], described horizontal electric field related with lightning return stroke. Barbosa et al. [151], published a paper on horizontal electric field at layered earth surface due to Lightning. Zhanqing et al. [152], calculated the surface electric field on transmission lines (UHV) under lightning stroke. Transient potential rise on wind turbines under lightning stroke was calculated in [153]. Wang et al. [154], presented electric field distribution in a wind turbine tower hit by lightning. Mohammad et al. [155], Investigated lightning

electromagnetic fields in wind farm's underground cables. Malinga et al. [156], modeled the behavior of lightning strike in the near field of elevated systems. Eriksson [157], in Pretoria, South Africa measured the electric fields distribution at ground level during thunderstorms and the maximum electric fields that were recorded are below 20 kV $m^{-1}$. Also, the measurements conducted by Soula and Chauzy [158], demonstrated that at altitudes of 603 m, thundercloud-generated electric fields can be as high as 60 kV $m^{-1}$, but, similarly, the electric field at ground level is below 10 kV $m^{-1}$. The ambient electric fields below thunderclouds was measured by Willett and colleagues [159] using rockets equipped with field-measuring devices.

As the thundercloud charges are produced at a rate of around 1 C $s^{-1}$, i.e. about 1 A charging current, the electric field between the ground and the cloud negative charge center increases. As the electric field at ground level reaches to about a few kV $m^{-1}$, sharp points, small protrusions, pointed leaves, and etc., go into corona. A space charge layer is produced by these corona discharges.

As the height of the cloud is lowered, the ambient field above ground intensely increases [37]. Electric field enhancement existing around the blade and their position initially affects the production of upward initiated lightning [38].

### 2.17.2 *Electric Fields Generated by Stepped Leaders*

Schonland experimentally showed that the stepped leader charge is uniformly distributed. Golde [160] assumed that with increasing height above ground, the line-charge density $\rho_S$ on the channel of the stepped leader decreases exponentially:

$$\boldsymbol{\rho s = \rho s o e^{-z/\lambda}} \qquad \textbf{(2.3)}$$

Where z is the height, λ is the charge decay height constant, and $\rho_{S0}$ the density of the charge at ground level.

Golde [160], used λ=1000 m for evaluation but Eriksson [161], assumed that charge is linearly distributed. As stepped leader descends, its charge distribution can be determined by the background electric field produced by cloud charges and field enhancement due to the ground. Cooray and colleagues [162], conducted a study and measured the charge transference by the first 100 μs of the first return strokes and generated the charge distribution along the leader channel. It was shown from their result that the following equation can be used to evaluate the variation of the stepped leader charge per unit length with height:

$$\mathbf{P\ (\zeta) = a_0\ (1- \frac{\zeta}{H-Z0})\ G\ (Z_0)I_p\ +\ \frac{Ip(a+b\zeta)}{1+c\zeta+d\zeta 2}\ Jz_0} \quad \textbf{(2.4)}$$

$$\mathbf{G\ (z_0)= 1\ -Z_0/H} \quad \textbf{(2.5)}$$

$$\mathbf{J\ (Z0)\ =\ 0.3\ \propto +0.7\beta} \quad \textbf{(2.6)}$$

$$\mathbf{\propto =\ e^{-(Z0-10)}/75} \quad \textbf{(2.7)}$$

$$\mathbf{\beta\ =\ (1\ -Z_0/H)} \quad \textbf{(2.8)}$$

Where $Z_0$ is the leader tip height (m) above ground, H the stepped leader channel total length (m), ρ(ζ) the per unit length charge (C $m^{-1}$), ζ the stepped leader channel length (m) (with ζ=0 at the leader tip), $I_p$ the return-stroke peak current (kA), $a_0$ = 1.476x$10^{-5}$, a =4.857x$10^{-5}$, b = 3.9097x $10^{-6}$, c= 0.522 and d=3.73x$10^{-3}$.

The equation can be used to calculate the variation of the electric field at ground level directly beneath the path of a stepped leader as a function of time.

## 2.18 Leader Inception Modelling

Various models have been put forth to predict the voltages and electric fields required for the inception of leader for an applied voltage wave shape and a certain electrode configuration from high-voltage electrode. These models were later used to investigate the initiation of upward leaders in natural conditions. Different models predict different conditions for upward leader inception. In order to study leader inception from grounded structures, numerous other models were similarly developed on the basics of either the laboratory long sparks observations or the physics of the streamer-to-leader transition. Recently, Candela et al. [163], presented computer modeling of wind turbine blade's lightning streamer formation and propagation, it was shown that computer modeling correlated experimental data.

### 2.18.1 *Models Assumptions Used in Lightning Inception Studies*

#### *2.18.1.1 The Critical Radius Concept*

positive polarity high-voltage electrode has been used to conduct high-voltage experiments in laboratories with different types of gap configurations to get information on streamer-to-leader transition physics and the consequent long laboratory gap electrical breakdown. An important result pertinent to lightning inception was obtained from the investigation of breakdown in rod–plane gaps carried out by Carrara and Thione [164], 'the critical radius concept'. It was shown that over a volume bounded by the critical radius, the initiation of a stable leader needs the realization of an ionization field, i.e. $3x10^{6}$ $V/m^{-1}$.

Les Renardieres group later extended the study to other voltage wave shapes and found that for different time to crest of the applied voltage, the value of the critical radius changes. In the arrangement used by Carrara and Thione [164] mentioned earlier, the rod is placed directly above the ground plane and raised to a high voltage. To make the experiments more realistic, it is also conducted with inverted rod–plane gaps. From such experiments, for 3-m gaps, Gary and colleagues [165], obtained 0.1 m to be the critical radius whereas for the same gap length, Carrara and Thione found 0.17 m. similarly Bernardi and colleagues [166], obtained 0.28 m. D'Alessandro and colleagues [167], conducted similar experiment with 5-m gaps and got 0.27 m as the critical radius. The reason for the differences in leader inception in the rod–plane gaps is not well understood whether the rod is at high voltage or when the rod is grounded.

Eriksson [157], was the first to apply the idea of the critical radius in lightning studies and since then, it has been widely used to evaluate the leader initiation conditions in rods, masts, power lines [168-170] and buildings [171]. In these approaches, any sharp point on a structure are rounded off to the critical radius. It is expected that when the surface electric field is equal to 3 MV $m^{-1}$ at atmospheric pressure a stable leader is initiated.

#### *2.18.1.2 Rizk's Generalized Leader Inception Equation*

Rizk [172] initially studied the leader inception criterion in the laboratory for rod–plane gaps, the findings were later revised for leader initiation from grounded structures influenced by thunderstorm electric fields. For a conductor– plane gap configuration, Rizk derived the following equation;

$$U_{ic} = 2247/\left[1+\frac{5.15-5.49\ln(a)}{h\ln(\frac{2h}{a})}\right] \quad \text{(Kv,m)} \qquad (2.9)$$

where $U_{ic}$ is the induced potential, h is the conductor height and a is the conductor radius

#### *2.18.1.3 Critical Streamer Length Concept*

Petrov and Waters [173], suggest that due to the effect of the electric field produced by the stepped leader, the streamer initiated from any point on a structure must go beyond a critical length before an upward leader can initiate from that point. Also, the total electric field (the sum of the ambient electric field and the generated electric field by the structure as a result of the induced charges on it by the ambient electric field) over the streamer zone must exceed a critical electric field.

Petrov and D'Alessandro [174], extended this study to include the conditions required for the continuous propagation of the leader after it is incepted.

the critical background electric field $E_0$ necessary for the initiation of an upward leader from a structure of height h is given by the following equation:

$$E_0 \approx 697/h^{0.68} \text{ (kV m}^{-1}\text{)} \quad (2.10)$$

Akyuz and Cooray [175], conducted a study in which 3 m was assumed as the critical streamer length required for leader inception.

#### *2.18.1.4 Bazelyan and Raizer's Empirical Leader Model*

In 1996, a model was proposed by Bazelyan and Raizer [176], to determine the conditions necessary to initiate upward leaders from grounded conductors founded on semi-empirical expressions derived from laboratory long gaps experiments.

the external background electric field $E_0$ that is required to sustain leader propagation from a grounded electrode of height h can be evaluate as

$$E_0 \approx 3700/h^{0.6} \ \text{(kV m}^{-1}\text{)} \qquad (2.11)$$

#### *2.18.1.5 Lalande's Stabilization Field Equation*

While trying to evaluate the leader inception condition, Lalande [177], applied a physical model for leader propagation in long gaps that was proposed by Goelian and colleagues [178], and in combination with the thermo-hydrodynamic model of the leader channel by Gallimberti [179], obtained equation for the background electric field required to initiate leaders from grounded structures. (i.e. the stabilization electric field $E_0$):

$$E_0 \geq \frac{240}{1+\frac{h}{10}} + 12 \quad \text{(kV m}^{-1}\text{)} \qquad (2.12)$$

where h is the height of the structure

#### *2.18.1.6 The Self-Consistent Leader Inception Model of Becerra And Cooray*

Becerra and Cooray [180, 181], introduced a model consisting of two parts; (a) static leader inception model and (b) dynamic leader inception model. In the streamer-to-leader transition process, the background electric field is assumed to be constant in the static leader inception model, but, the impact of the variation of the background electric field on the process of transition of the streamer-to-leader is included in the dynamic leader inception model. Thus, the static model is appropriate for cases in which the background electric field stays constant or is changing slowly. An example is the inception of upward leader from tall grounded structures influenced by the electric fields produced by thunderclouds.

Existing lightning protection standards are based on different concepts and models that neglect a lot of the physics related with the attachment process of lightning flashes to a structure.

#### *2.18.1.7 The cloud model*

An increased electric field at ground level produced by the electrical charge within a thundercloud can result in the production of upward leaders from a structure before the formation of a stepped leader. The attachment point is determined by the formation points of these upward leaders.

The charge structure in a thundercloud is usually replicated by three vertical stacked point charges or spherically symmetrical charge volumes. It consists of a vertical tri-pole made from a negative charge and two positive charges. In [50, 176], is contained various models that have been produced. The vertical tri-pole cloud charge distribution model is extended in this work and used to create ambient field representing uniform electric field at 200m above ground. The results of the electric field at ground from the system of three charges agrees with the report in [50] and lightning measurements.

## 2.19 Conclusion

Detailed literature review is presented in this chapter, previous research on lightning protection, air-termination systems, existing protection methods, numerical evaluations, upward lightning flashes, electric fields, leader inception models etc. are presented. The studied literature has shown that modern wind turbine due to height, blade rotation and varying blade conditions are at higher risk of lightning attachment due to upward initiated lightning. This can best be addressed with an extended cloud model instead of the stepped leader approach.

# Chapter 3

# Modeling Maximum Electric Field Strength Required for The Inception of Upward Leader from Wind Turbine

## 3.1 Introduction

Lightning can either be downward initiated or upward initiated. In the presence of a thundercloud, tall wind turbines are increasingly subjected to upward lightning attachment triggered by the wind turbine itself [91, 93, 128]. Report shows that upward lightning flashes are initiated from the enhancement of the electric field produced by thundercloud charge or close lightning discharges [128, 130]. The critical ambient electric field also known as the stabilization electric field for the initiation of upward leaders from wind turbines produced during thunderstorms consists of two main components; (a) the static or the slow increasing component $E_{\text{cloud}}$ due to the charging process of thunderclouds and (b) The fast-electric field change component $\boldsymbol{\Delta} E_{\text{cloud}}$. Upward leaders in self-initiated upward lightning [182] are majorly influenced by the static or the slowly increasing electric field component $E_{\text{cloud}}$, with a rise rate lower than 1 kV/m/s [183] i.e., during the inception of upward leaders, $E_{\text{cloud}}$ is considered to be constant because this process has a duration of around few hundred microseconds. However, the maximum electric field strength required for the initiation of upward leaders from wind turbines is highly dependent on the blade condition and upward leader models are still being investigated. For upward propagating lightning from wind turbine, as mentioned above, the electric field in the air is near uniform being produced by the cloud and not by a stepped leader. Therefore, for upward leader

formation, the strong influence of the stepped leader position is eliminated, and the formation will be dominated by the wind turbine geometry and the electric field distribution. In this chapter, ambient field representing uniform electric field due to cloud charge distribution at 200 m above ground is modeled from the cloud, whereas in the following chapters, the maximum electric field strength required for the initiation of upward leaders from wind turbines due to varying blade conditions will be applied to the wind turbine model and analyzed.

## 3.2 Simulation Method

This study utilizes the vertical tri-pole model made from two positive charges and a negative charge representing the idealized gross charge structure of a thundercloud. Even though the vertical tri-pole is usually used to replicate the electric fields found under a thundercloud, this model is further extended to investigate the maximum electric field strength required for the initiation of upward leaders from wind turbines due to varying blade conditions.

Initially, it is used to create an ambient field representing uniform electric field due to cloud charge distribution at 200 m above ground. By applying the extended model to two case studies of 3D electrostatics model of full-scale wind turbines; Vestas V100 with 2 MW rated power, 100 m rotor diameter and 49 m long blade, and a model of a 19.1 m blade length of 600 kW wind turbine, the maximum electric field strength is obtained. The peak current $I_{peak}$ is chosen as 30 kA because it represents the general situation of lightning strikes [184].

### 3.2.1 *Thundercloud*

A thundercloud is a cumulus cloud with a towering or spreading top, usually charged with electricity and capable of producing lightning and thunder. It may also be defined as a lightning-producing cumulonimbus. This definition is due to the fact that the cloud type termed cumulonimbus is the primary source of lightning and it is commonly referred to as the thundercloud. Though, not every cumulonimbus will produce a lightning [185]. Thunderclouds are complex, large and short-lived. A system of thunderclouds is referred to as thunderstorm. Rodrigues et al. [186], analyzed thunderstorm activity in Portugal.

### 3.2.2 *Gross Charge Distribution in a Thundercloud*

Basically, as generally accepted, the features of the cloud charge structure consist of, (a) A net positive charge near the top, (b) A net negative charge bellow it, and (c) An additional positive charge at the cloud bottom. It should be noted that positive and negative charge coexist in any region of the cloud, irrespective of the polarity of the net charge in the region [187].

### 3.2.3 *The Thunder Cloud Model*

The charge structure in a thundercloud is usually replicated by three vertical stacked point charges or spherically symmetrical charge volumes. It consists of a vertical tri-pole made from a negative charge and two positive charges. A summary of various cloud models have been listed in [50, 176]. The cloud model that has been implemented and simulated in this work is taken from [50]. The model is illustrated in Figure 3-1, it has positive charge at the top, negative in the middle, and a smaller positive at the bottom, and the ground modeled

as a perfect conductor. The top two charges are also called the main charges and are usually specified to be equal in magnitude. Sometimes, the lower positive charge is not present. The top two charges form a dipole, said to be positive because the positive charge is above the negative charge, this gives an upward-directed dipole moment.

In the simulation, the three charges of +40C, -40C and 3C are placed at height of 12, 7 and 2 km from the ground respectively and modelled as spheres of radii 900m for the 40C charges and 150 m for the charge of 3C [37, 50]. The size of the spheres is such that during meshing, the accuracy of the electric field in the area of interest within the model is ensured.

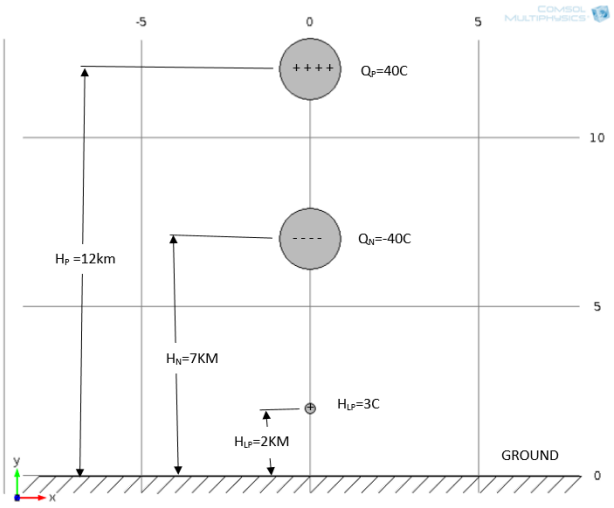


Figure 3-1: A vertical tri-pole made from two positive charges and a negative charge representing the idealized gross charge structure of a thundercloud.

Where $Q_p$ is the main positive charge, $Q_N$ is the main negative charge, $H_{LP}$ is the lower positive charge and $H_P$, $H_N$ and $H_{LP}$ are their various distances (in kilometer) from ground.

### 3.2.4 *Electric Field Intensity*

The electric field intensity (**E**) due to the system of three charges (Qp, $Q_N$ and $H_{LP}$) shown in Figure 3-1 is found by replacing the ground (perfectly conducting ground) with three image charges and by using the principle of superposition, the total electric field being the

vectorial sum of six (three from the actual charges and three from their images) contributions.

### 3.2.5 *Computation of Electric Field on Ground Surface*

Figure 3-2 shows the computation of the electric field on the ground surface owing to the main negative charge ($Q_N$) and its image. The actual charge's magnitude and that of its image are equal, and the contribution of each is found as in [188].

$$|\mathbf{E}^{(-1)}| = |\mathbf{E}^{(+1)}| = \frac{|Q|}{4\pi\varepsilon_0(H^2+r^2)} \quad \textbf{(3.1)}$$

The figure shows the method of images used for finding the electric field due to a negative point charge ($Q_N$) above ground (a perfectly conducting ground) at a field point located on the ground surface.

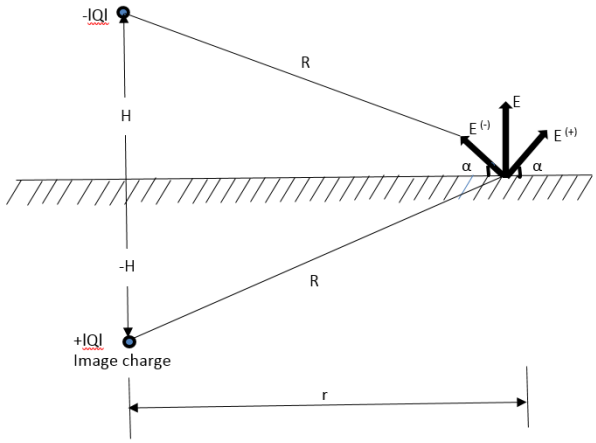


Figure 3-2: The method of images

From the method of image shown in Figure 3-2, it is apparent that, as expected from the boundary condition on the surface of a perfect conductor, the components of the electric field that is tangential to the ground plane due to the actual negative charge and its image cancel each other. The electric field components that is normal to the ground plane add,

and the total normal field magnitude is twice the contribution from either the actual negative charge or its image:

$$|\mathbf{E}| = 2|\mathbf{E}^{(-1)}|\cos(90^0 - \propto) = 2|\mathbf{E}^{(+1)}|\cos(90^0 - \propto)$$

$$= 2|\mathbf{E}^{(-1)}|\sin \propto = \frac{|Q|H}{2\pi\varepsilon_0(H^2+r^2)^{3/2}} \quad \textbf{(3.2)}$$

For the variation in |**E**| as a function of H and r with I**Q**I = constant. Rewriting Eq. 3.2:

$$|\mathbf{E}| = \mathbf{k}\frac{sin\propto}{R^2} \quad \textbf{(3.3)}$$

Where $\mathbf{k} = \frac{|Q|}{2\pi\varepsilon_0}$ **and R2** = $(H^2 + r^2)$**.**

Therefore, for two vertically stacked charges of equal magnitude, i.e., the main positive charge (Qp) and main negative ($Q_N$) charge (Figure 3-1), each of these two charge's relative contributions to **E** depends on r. The lower charge dominates the electric field at r = 0 because it is closer and sine α is the same for both charges. But the relative contribution from the upper charge increase just as r increases. The contribution from the upper charge becomes dominant at a certain distance and the total electric field i.e., the sum of the contributions due to the two charges, changes its polarity. This distance is referred to as the reversal distance. For two vertically stacked charges of opposite polarity but equal magnitude the reversal distance, $D_0$, is given by

$$\mathbf{D_0 = [(H_P H_N)^{2/3}(H_P^{2/3} + H_N^{2/3})]^{1/2}} \quad \textbf{(3.4)}$$

$H_p$ is the heights of the positive charge and $H_N$ is the heights of the negative charge. Therefore, for a positive dipole, it is expected that at far ranges the total electric field is positive, while at near ranges it is negative.

The materials used for the ground design is shown in table 1 below.

Table 1 Material used for a perfectly conducting ground (an ideal ground) design

| Property | Name | Value | Unit | Property Group |
|---|---|---|---|---|
| Relative permittivity | epsilonr | 1 | 1 | Basic |
| Relative permeability | mur | 1 | 1 | Basic |
| Electrical conductivity | sigma | $5.998x10^{-7}$[s/m] | s/m | Basic |
| Coefficient of thermal expansion | alpha | $17e^{-6}$ (1/k) | (1/k) | Basic |
| Heat capacity at constant pressure | $C_p$ | 385[J/(kg*k)] | J/(kg*k) | Basic |
| Density | rho | 8700[kg/m^3] | kg/m^3 | Basic |
| Thermal conductivity | k | 400[w/(m*k)] | w/(m*k) | Basic |
| Young's modulus | E | $110e^{-9}$[pa] | pa | Young's modulus and Poisson's ratio |
| Poisson's ratio | nu | 0.35 | 1 | Young's modulus and Poisson's ratio |
| Reference resistivity | Rho0 | $1.72e^{-8}$[ohm*m] | Ω*m | Linearized resistivity |
| Resistivity temperature coefficient | alpha | 0.0039[1/k] | 1/k | Linearized resistivity |
| Reference temperature | Tref | 298[k] | k | Linearized resistivity |

Let $E_2$ be the final electric field value after the charge removal due to lightning, and $E_1$ be the initial electric field value from original cloud charge distribution. Therefore, an electric field change is found as the difference between $E_2$ and $E_1$. The corresponding electrostatics field change for any charge removed from the cloud, is the negative of that charge contribution to the initial electric field. Assuming negative cloud charge's complete neutralization due to cloud-to-ground discharge, the resultant net electric field change at any distance will be negative, this is because the upward-directed positive electric field due to the negative charge (Figure 3-2) becomes zero. Polarity reversal will be exhibited by the resultant net field change as a function of distance if both main negative and main positive charges are neutralized via an intra cloud discharge. It should be noted that the positive field values are significantly smaller than the negative field values. The occurrence of the polarity reversal is because the net field change to the total electric field from these two charges, is the negative of the sum of the contributions, from these two charges. At close

ranges, this sum is positive and negative at far ranges. Electric field changes related to upward initiated lightning was observed in Gaisberg tower [189].

## 3.3 Ambient Field Representing Uniform Electric Field Due to Cloud Charge Distribution at 200 m Above Ground

An increased electric field at ground level produced by the electrical charge within a thundercloud can result in the production of upward leaders from a structure before the formation of a stepped leader. The attachment point is determined by these formation points of these upward leaders.

The results of the electric field at ground from the system of three charges shown in Figure 3-1 agrees with the report in [50], with maximum ambient field of just over 5kV/m. These values are used in this work and an upward-directed electric field is defined as positive [50].

In order to analyze the maximum electric field strength required for the initiation of upward leaders from wind turbines, the information from the cloud model is combined with the wind turbine model in the simulation. As mentioned above, the vertical tri-pole model is used to create an ambient field representing a uniform electric field due to cloud charge distribution at 200 m above ground. A uniform electric field produced by a plane electrode located 200 m above the ground is then applied on the wind turbine model. The magnitude of the applied electric field is 1MV/m (200 X 5KV/m = 1000000V/m). This is based on the results found from Malan's charged cloud model [50]. Figure 3-3 shows the simulation model while Figure 3-4 is the meshing. The electrode's polarity is negative; the

environment is modeled as air and the wind turbine is sited on the ground. The dimension of the electrode is large enough to prevent flashover from the edges.

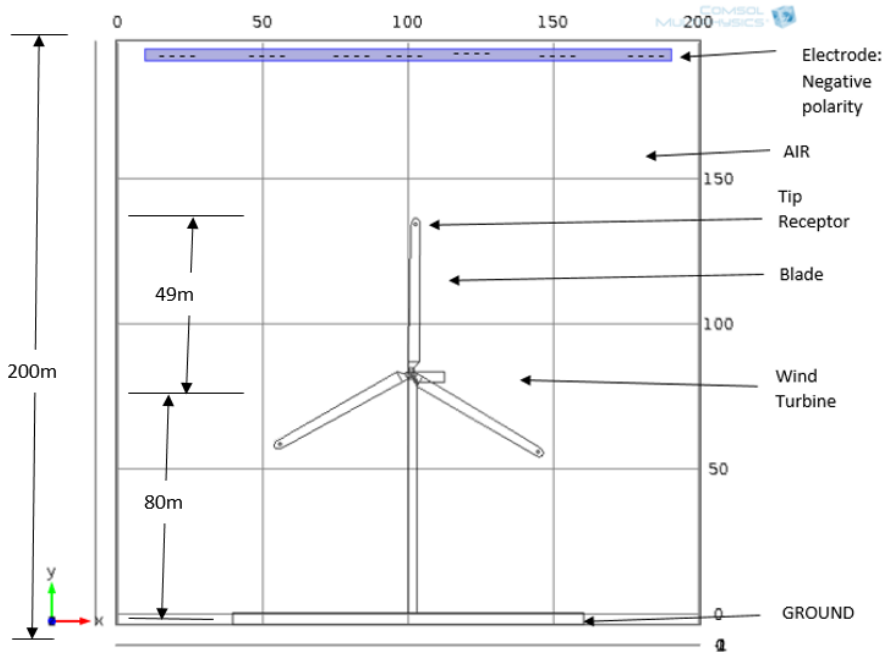


Figure 3-3: simulation model

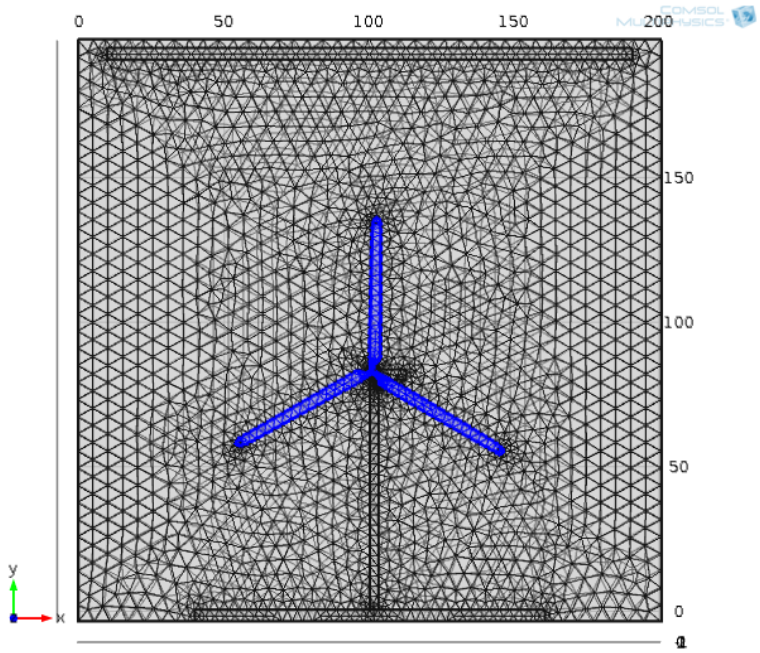


Figure 3-4: Model meshing

### 3.4 Wind Turbine Model

Two types of wind turbines are used as case studies in this work, chosen to ensure that various sizes of blades lengths (both small and long blades) are adequately considered. They are; Vestas V100 with 2 MW rated power, 100 m rotor diameter, swept area 7.854m$^2$ and 49 m long blade, and a 600-kW wind turbine with 19.1 m blade length.

V100 is a horizontal axis wind turbine with three blades. The blade is made of fibred glass with a relative permittivity: of 4.2, conductivity:$1.0 \times 10^{-14}$ S/m, blade thickness: 10 cm, chamber length: 0.9 m, maximum chord 3.9 m (varied at blade root and tip). The wind turbine nacelle and tower are conductive and are set to ground potential. Hub height (height from the lowest part of the tower to the Centre of the hub) is 80 m. The tower is tubular steel type. The nacelle is 10.4 m long and 3.5 m wide. V100 is shown below in Figure 3-5.

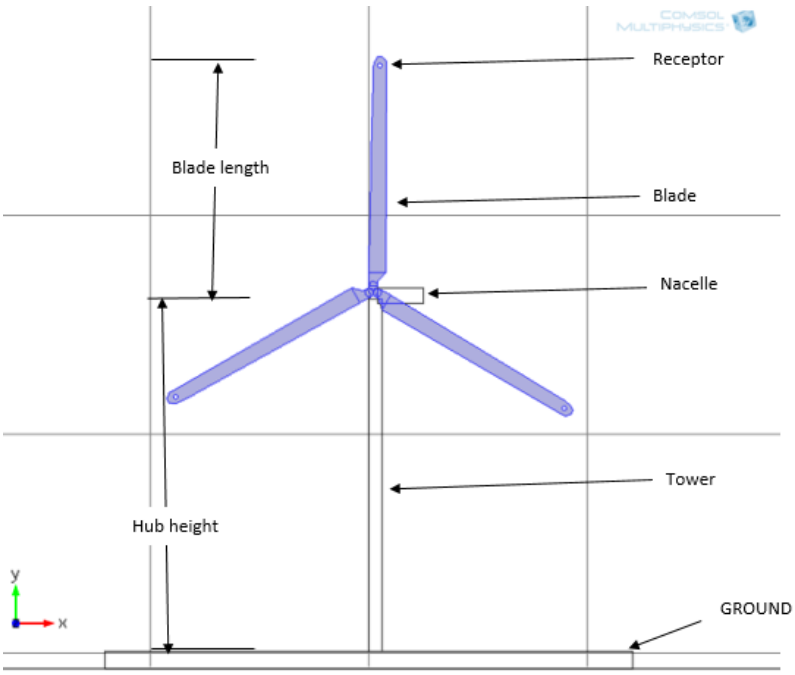


Figure 3-5: Wind turbine model

### 3.5 Full Scale Blade and 3 m blade tip section model

A sample of a full-scale blade is shown in Figure 3-6.


Figure 3-6: V164-80m long wind turbine blade [5]

Figure 3-7 is a full-scale blade model design

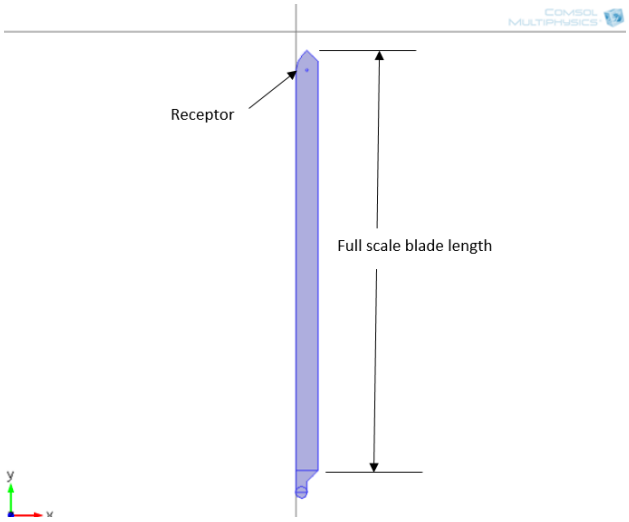


Figure 3-7 Full scale blade model

### 3.6 3 m blade tip section model

Figure 3-8 is a 3 m blade tip section model normally used for experimental analysis according to IEC 61400-24.

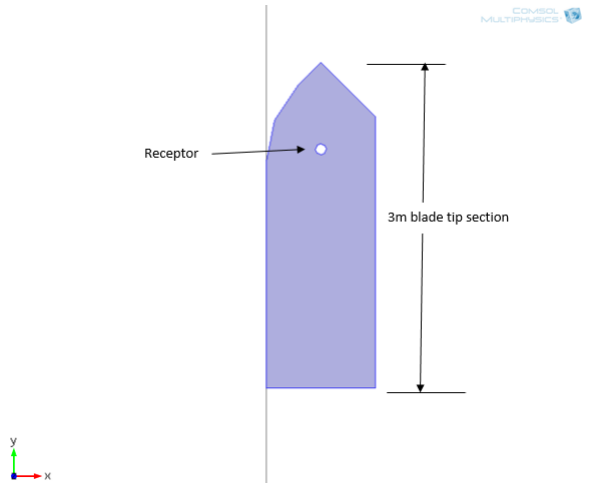


Figure 3-8: 3 m blade tip section model

## 3.7 Lightning Protection Air-Terminal

The lightning protection system is integrated into the model design. Wind turbine lightning protection systems usually consist of an internal down conductor with air-termination systems. The type of air-terminal used in this work includes tip receptor method and the metallic cap method. For receptor type, three receptors are designed and placed evenly across the blade length and the tip receptor is set at 2 m from the tip of the blade as default. The three receptors are grounded or earthed so as to take the lightning current to ground. The receptor's design is such that either of them, or two at a time or all of them can be activated or deactivated when the need arises during analysis. They are 10 mm in diameter and made of copper (conductivity: $6.0 \times 10^{-7}$S/m). The tip receptor (purple color) design is shown in Figure 3-8.

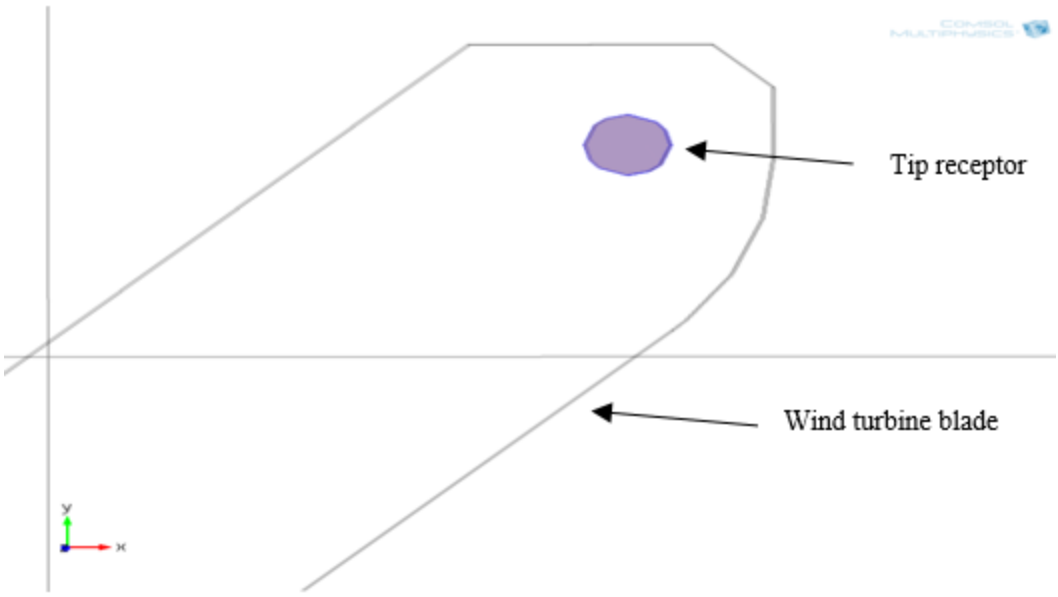


Figure 3-8: Tip receptor design

## 3.8 Material Content for The Design

The materials used for the turbine blade, air, thundercloud and the lightning protection systems model's designs are shown in tables 2, 3 and 4 respectively.

Table 2 Material used for Turbine blade design

| Property | Name | Value | Unit | Property Group |
|---|---|---|---|---|
| Relative permittivity | Epsilon | 4 | 1 | Basic |
| Relative permeability | mur | 1 | 1 | Basic |
| Density | Rho | 2200[kg/m^3] | kg/m^3 | Basic |
| Electrical conductivity | sigma | $1.0x10^{-14}$[s/m] | s/m | Basic |
| Thermal conductivity | K | 1.1[w/(m*k)] | w/(m*k) | Basic |
| Heat capacity at constant pressure | $C_p$ | 480[J/(kg*k)] | J/(kg*k) | Basic |
| Refractive index | N | 1.5 | 1 | Refractive index |
| Refractive index, imaginary part | Ki | 0 | 1 | Refractive index |
| Young's modulus | E | $74X10^9$[pa] | Pa | Young's modulus and Poisson's ratio |
| Poisson's ratio | Nu | 0.3 | 1 | Young's modulus and Poisson's ratio |

Table 3 Materials used for thunder cloud and lightning protection systems designs

| Property | Name | Value | Unit | Property Group |
|---|---|---|---|---|
| Electrical conductivity | sigma | $5.998x10^7$[s/m] | s/m | Basic |
| Coefficient of thermal expansion | alpha | $17x10^6$[1/k] | 1/k | Basic |
| Heat capacity at constant pressure | $C_p$ | 385[J/(kg*k)] | J/(kg*k) | Basic |
| Density | rho | 8700[kg/m^3] | kg/m^3 | Basic |
| Thermal conductivity | k | 400[w/(m*k)] | w/(m*k) | Basic |
| Young's modulus | E | $110X10^9$[pa] | pa | Young's modulus and Poisson's ratio |
| Poisson's ratio | nu | 0.35 | 1 | Young's modulus and Poisson's ratio |
| Reference resistivity | Rho0 | 1.72x108[ohm*m] | Ω*m | Linearized resistivity |
| Resistivity temperature coefficient | alpha | 0.0039[1/k] | 1/k | Linearized resistivity |
| Reference temperature | Tref | 298[k] | K | Linearized resistivity |

Table 4 Materials used for Air as the environment.

| Property | Name | Value | Unit | Property Group |
|---|---|---|---|---|
| Relative permittivity | epsilonr | 1 | 1 | Basic |
| Relative permeability | mur | 1 | 1 | Basic |
| Ratio of specific heat | gamma | 1.4 | 1 | Basic |
| Electrical conductivity | sigma | 0[s/m] | s/m | Basic |
| Dynamic viscosity | mu | Eta(T[1/K])[pa*s] | Pa*s | Basic |
| Density | rho | Rho(Pa[1/pa],T[1/k])[kg/m^3] | kg/m^3 | Basic |

## 3.9 Theory for Electric Field Interface

COMSOL Multiphysics contains physics interfaces for the modeling of static electric fields and currents. It is a computer simulation program that accommodate the physics of lightning interactions with grounded objects and can be used to evaluate protection procedures.

### 3.9.1 *Charge Relaxation Theory.*

The different physics interfaces can be interpreted in terms of the charge relaxation process. The fundamental equations involved are Ohm's law ($J = \sigma E$) the *equation of continuity*

$$\frac{\partial \rho}{\partial t} + \nabla . \mathbf{J} = 0 \tag{3.5}$$

and Gauss' law

$$\nabla . (\varepsilon \mathbf{E}) = \rho \tag{3.6}$$

By combining these, the following differential equation can be deduced for the space charge density in a homogeneous medium

$$\frac{\partial \rho}{\partial t} + \frac{\sigma}{\varepsilon \rho} = 0 \tag{3.7}$$

The solution to 3.7 is given as

$$\mathbf{P}\,(\mathbf{t}) = \rho_0 \mathbf{e}\text{^}(-\mathbf{t}/\boldsymbol{\tau}) \tag{3.8}$$

Where $\boldsymbol{\tau} = \epsilon/\sigma$, and $\boldsymbol{\tau}$ is called the charge relaxation time. For a good conductor, such as copper, $\tau$ is of the order of $10^{-19}$s but for a good insulator such as silica glass, it is of the order of $10^{3}$s. It becomes infinite for a pure insulator.

### 3.9.2 *Electrostatics Interface*

The electric potential V for static conditions, is defined by the relationship;

$$\boldsymbol{E} = -\boldsymbol{\nabla} V \tag{3.9}$$

With equation (3.5) combined with the constitutive relationship $\boldsymbol{D} = \varepsilon_0 \mathbf{E} + \mathbf{P}$ between the electric displacement **D** and the electric field **E**, it is possible to represent Gauss' law

as the following equation:

$$-\nabla.(\varepsilon_0 \nabla V - \mathbf{P}) = \rho \quad (3.10)$$

In the above equation, the physical constant, $\varepsilon_0$ (SI unit: F/m) is the permittivity of vacuum, ρ (SI unit: C/m$^3$) is space charge density and P (SI unit: C/m2) is the electric polarization vector. The electrostatic field in dielectric materials is described by this equation.

For in-plane 2D modeling, the electrostatics interface adopts a symmetry where the electric potential varies in the x and y directions only and is constant in the z direction. This suggests that the electric field, **E**, is tangential to the xy-plane. Due to this symmetry, the same equation is also solved in the 3D case. The interface evaluates the following equation where d is the thickness in the z direction:

$$-\nabla.\mathbf{d}(\varepsilon_0 \nabla \mathbf{P} - \mathbf{P}) = \rho \quad (3.11)$$

The axisymmetric type of the interface considers the situation in which the fields and geometry are axially symmetric. For this case the electric potential, V is constant in the φ direction, which infers that the electric field is tangential to the rz-plane.

### 3.10 Procedure for Evaluation

The electric field due to thunder cloud charge can be calculated using these electrostatics equations. The governing equations are solved with FEA software and the computational domain is shown in Figure 3-3.

Different configurations are applied on the wind turbine to investigate the effect of blade conditions on initiation of upward leader. In each case, the evaluation is done as the blade is rotated through -60$^0$ and 60$^0$ from the vertical position. The blade in the vertical position

in Figure 3-3 is referred to in this thesis as blade A and only the results for blade A are provided. Also, values are obtained from the blade tip, leading edge, trailing edge, the receptor tip and sometimes the blade surface.

The focus is on evaluating the efficiency of the lightning protection systems by obtaining the maximum electric field strength required for the initiation of upward leader due to thunder cloud charge. The positions with higher electric field strength are considered to have higher possibility of inception of upward leader. Results are plotted and compared for values obtained from the blade tip, leading edge, trailing edge and the receptor tip. The most efficient situation in this analysis is the one with highest electric field on the receptor and minimum at the tip, leading edge, trailing edge and the entire blade surface.

In order to investigate the effect of blade conditions on the electric field strength, the simulation is first conducted on the wind turbine without the receptor and then the receptors are used as the blades are rotated.

### 3.10.1 *Unprotected Wind Turbine*

Figure 3-9 shows an unprotected wind turbine model under the influence of thunder cloud electric field. The receptors are disabled; leaders can incept from any part of an unprotected wind turbine with a consequence of lightning damage.

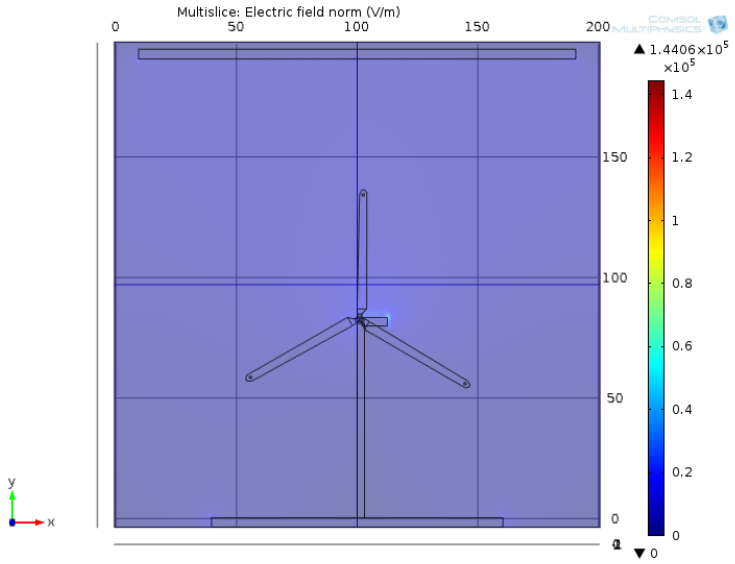


Figure 3-9: Unprotected wind turbine

### 3.10.2 *Protected Wind Turbine.*

A protected wind turbine model is shown Figure 3-10 below; the receptors are enabled. When the wind turbine is put in the electric field, field enhancement is observed at certain positions as shown. The level of electric field intensification is predominantly high around the lightning protection system of the wind turbine model and at the blade tip receptor. This intensification will allow the formation of upward streamers. From the diagram, field enhancement is seen, it is apparent that upward leader will first incept from the blade in the vertical position. Lightning strike might initially attach to the lighting protection device depending on its ability to emit leader relative to the ability of the surrounding surface.

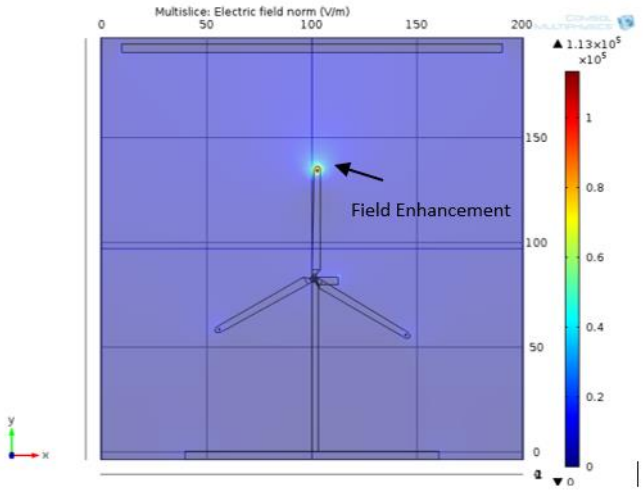


Figure 3-10: Protected wind turbine

As mentioned above, the simulation result shows a high probability of inception of upward streamer from the blades. The highest been the blade (blade tip and receptor) at the vertical position, then the nacelle, and also the receptor of the other two blades. Upward initiated lightning production, at first, depends on a given level of electric field enhancement existing around a component and also their position [38]. The results correlate with experimental and actual lightning data on points of leader attachment and upward leader initiation points. However, the electric field is affected by the blade conditions as is shown in the successive chapters.

### 3.10.3 *Rotated Wind Turbine.*

Blade A is moved counterclockwise for analyzing rotation. The evaluation is done as the blade is rotated through $-60^0$, $-55^0$, $-50^0$, $-45^0$, $-40^0$, $-35^0$, $-30^0$, $-25^0$, $-20^0$, $-15^0$, $-10^0$, $-5^0$, $0^0$, $5^0$, $10^0$, $15^0$, $20^0$, $25^0$, $30^0$, $35^0$, $40^0$, $45^0$, $50^0$, $55^0$ and $60^0$ from the vertical position. The model used for rotation mode is shown in Figure 3-11.

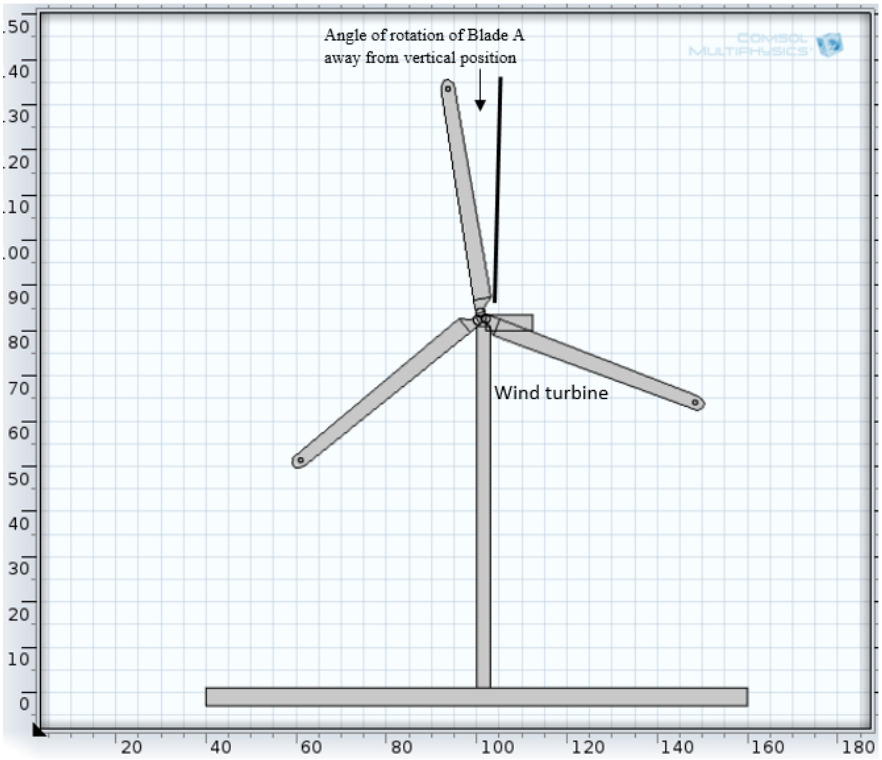


Figure 3-11: Rotation model

Figure 3-12 shows the simulation for the rotated blade. The maximum electric field strength required for the initiation of upward leader from the wind turbine is found to change as the blade is rotated.

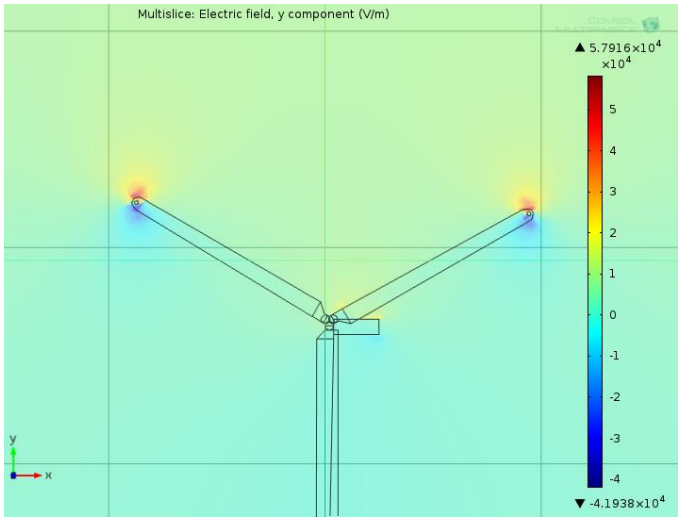


Figure 3-12: Rotated state

As mentioned earlier, when the wind turbine is protected, by activating the receptors, field enhancement is seen. Figure 3-13 shows the detailed activities around the receptor, these include; the upward positive polarity for streamer activities, the negative polarity going to ground through ground wire, positive polarity on the blade surface. Also shown is the produced corona charge (qc) which lowers the electric field on the tip inhibiting the occurrence of a streamer.

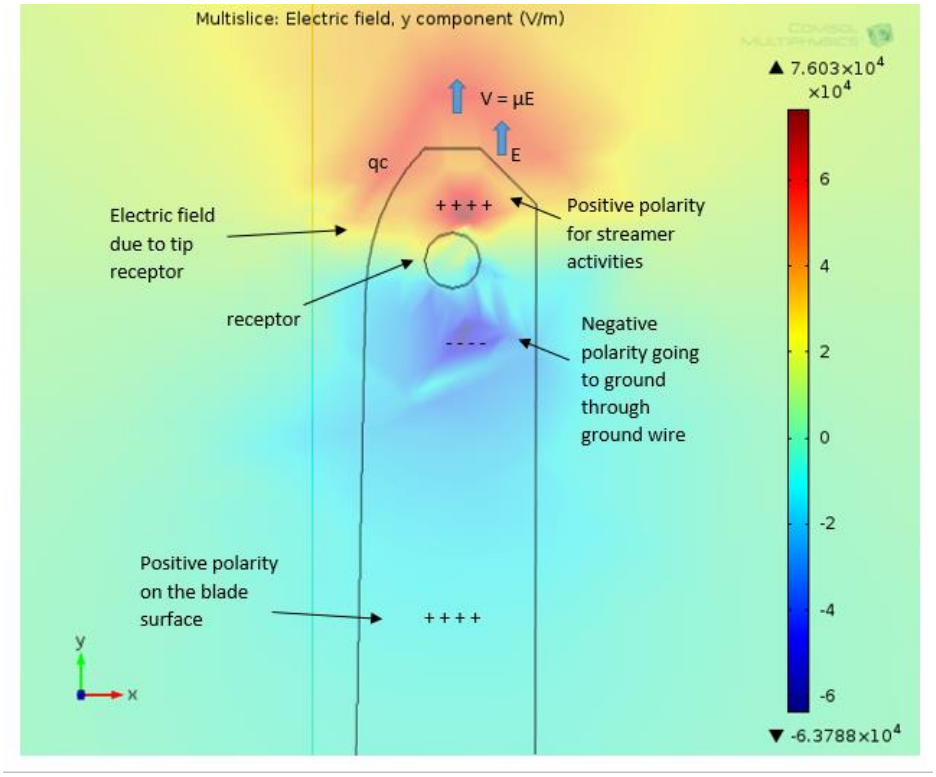


Figure 3-13: Activities around the receptor preceding leader initiation

Figure 3-14 shows the maximum electric field distribution as blade A is rotated from $-60^0$ to $+60^0$ from the vertical position: (a) $30^0$; (b) vertical position; (c) $-30^0$; (d) $60^0$; and (e) $-60^0$. It is generally observed that the electric field strength at the tip region appears to be higher than that at the inboard region. This is corroborative of laboratory experiments and field observations indicating that the tip is more exposed than other part [1], and that upward leader is more likely to initiate from the tip receptor. When lightning attaches to

the receptor, it will be conducted to ground through ground wire without causing damage to the turbine. This is the intent of the lightning protection design. If lightning is attached to the blade surface instead of the receptor, the blade and even the entire wind turbine can be destroyed. The positions with higher electric field strength are considered to have higher possibility of inception of upward leader. The negative polarity going to ground through ground wire as shown in Figure 3-14 is usually confined to the ground wire and not on the surface of the blade, therefore, only the positive parts of the electric field strength are relevant.

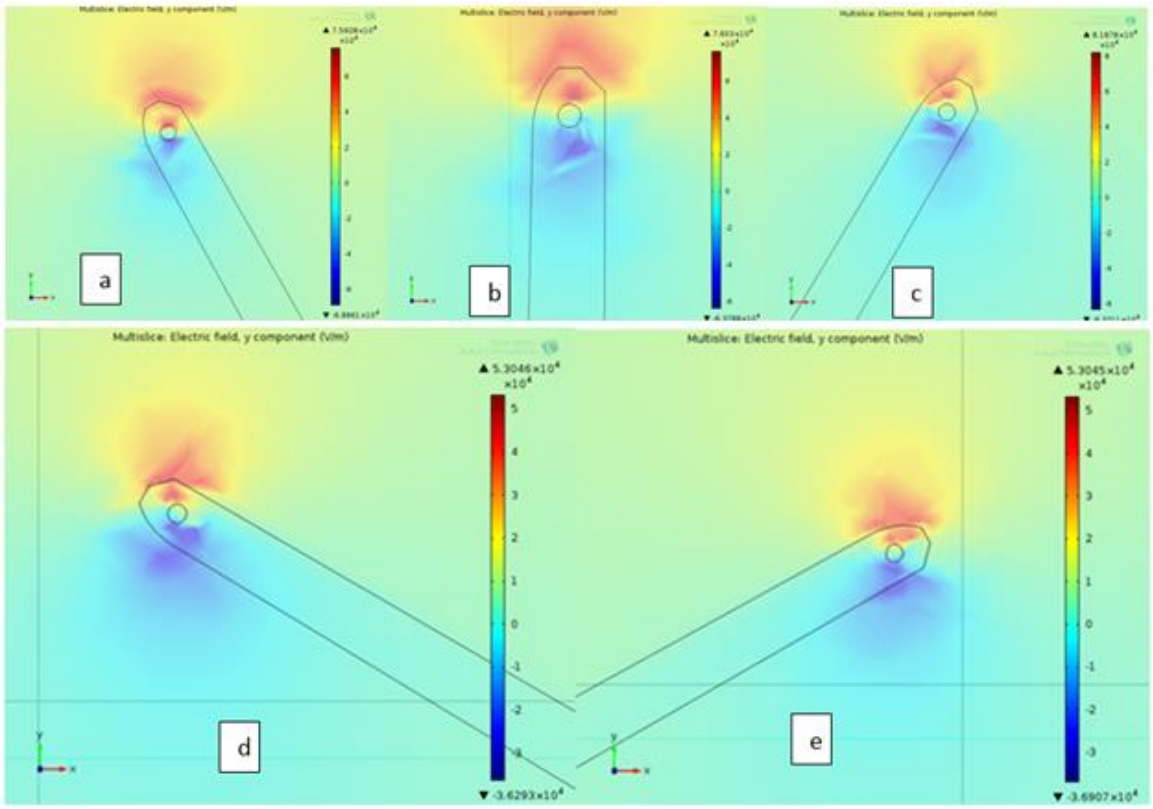


Figure 3-14: Maximum electric field distribution as blade A is rotated from -60 to +60 degrees from the vertical position: (a) 30; (b) vertical position; (c) -30; (d) 60; and (e) -60.

### 3.11 Conclusion

In this chapter, ambient field representing uniform electric field due to cloud charge distribution at 200 m above ground was modeled.

The study utilizes the vertical tri-pole model made from two positive charges and a negative charge representing the idealized gross charge structure of a thundercloud. Although the vertical tri-pole is usually used to replicate the electric fields found under a thundercloud, this model is extended to investigate the maximum electric field strength required for the initiation of upward leaders from wind turbines due to varying blade conditions.

The extended model is then applied to a 3D electrostatics model of a full-scale wind turbine and the maximum electric field strength is obtained.

The simulation result shows a high probability of inception of upward streamer from the blades which correlates with experimental and actual lightning data on points of leader attachment and upward leader initiation points.

# Chapter 4

# Effect of Receptor Size and Receptor Position on Wind Turbine Lightning Protection Systems

## 4.1 Introduction

The size of receptor and its position on the blade can influence the maximum electric field strength required for the initiation of upward leader from wind turbine. In chapter 3, ambient field representing uniform electric field due to cloud charge distribution at 200 m above ground was created from the cloud, the extended model was then applied to a 3D electrostatics model of a full-scale wind turbine and the maximum electric field strength was obtained. In the next chapter, the effect of pollution on offshore wind turbine is evaluated. Initially, in this chapter, receptor sizes are investigated to know the best size. Secondly, discrete receptor position from the blade tip are evaluated to find the best position for efficient lightning protection.

## 4.2 Receptor Sizes

The receptor though effective [19], also failed in many instances [28, 29]. The efficiency of the receptor is dependent on its interception proficiency which is its ability to intercept a lightning stroke. This strongly dependents on the size of the receptors [39]. The effect of receptor size has not been well considered in literature and standards. An attempt was made by Wang et al. [40], to evaluate the effect of receptor, however, only the shape (tip shape receptor, also referred to as metallic cap and disk shape receptor) were considered and not on various sizes.

Since there are no standard governing receptor sizes, choices are made randomly by researchers. For instance; Abd-Elhady et al. [44], used 20mm diameter, Wang et al. [40], used 0.2 m and 0.3 m radius, Naka et al. [45], used 25 mm diameter, in IEC61400-24, 15 mm diameter was applied, Peesapati and Cotton [37], used 10 mm diameter, Minowa et al. [11], used 20 mm diameter, Shindo et al. [19], used 35 mm in diameter, Yokoyama et al. [17], used 25 mm diameter and Danoon et al. [16], used 30 mm diameter. This is not healthy for an efficient lightning protection because the results are affected as the size of the receptor has been found to significantly affect its efficiency. It is therefore necessary to harmonize on the most efficient receptor size for an efficient lightning protection of wind turbines.

In this section, the receptor size is evaluated and optimized by comparing the electric field strength as the receptor size is changed and the blade is rotated. Six receptor sizes (10 mm, 15 mm, 20 mm, 25 mm, 30 mm and 35 mm receptor diameters), encompassing adopted sizes in literature are investigated. The point of upward leader inception is predicted by the magnitude of the electric field strength.

Figure 4-1 shows six receptor sizes applied on the wind turbine model to investigate the effect of receptor size on initiation of upward leader. In each case, the blade is rotated through $-60^0$, $-30^0$, $0^0$, $30^0$ and $60^0$ from the vertical position. The rotation is useful in evaluating the influence of blade position on every part of the blade such as tip, leading edge, trailing edge and the entire blade surface. The receptor is placed 1.5 m from the blade tip as recommended [190]. The blade in the vertical position in Figure 3-3 in previous chapter, is referred to as blade A. Values obtained from the blade tip, leading edge, trailing edge and the receptor tip for blade A only are provided.

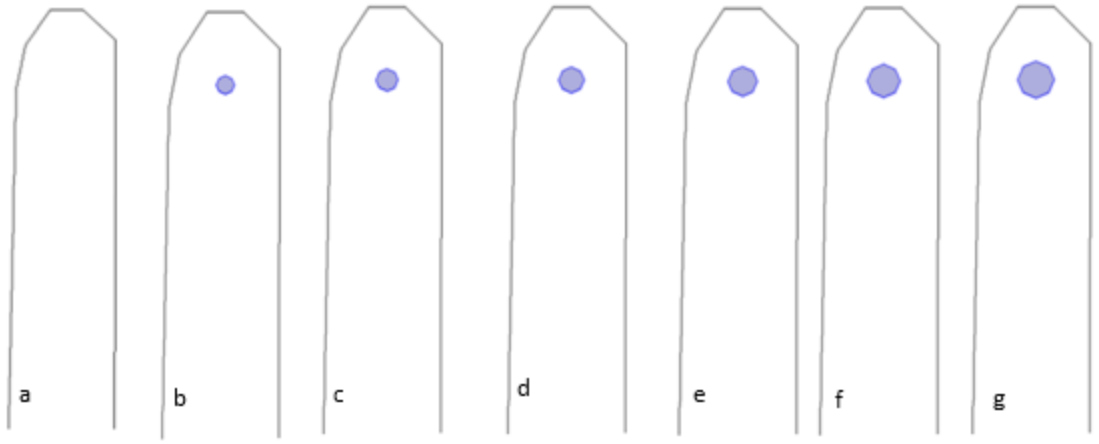


Figure 4-1. Different receptor sizes: (a) No receptor (b) 10 mm; (c) 15 mm; (d) 20 mm; (e) 25 mm; (f) 30 mm and (g) 35 mm diameters

Figure 4-2 shows the simulation for different receptor sizes used in the comparison of the maximum electric field strength distribution: (a) 10 mm; (b) 15 mm; (c) 20 mm; (d) 25 mm; (e) 30 mm and (f) 35 mm diameters respectively.

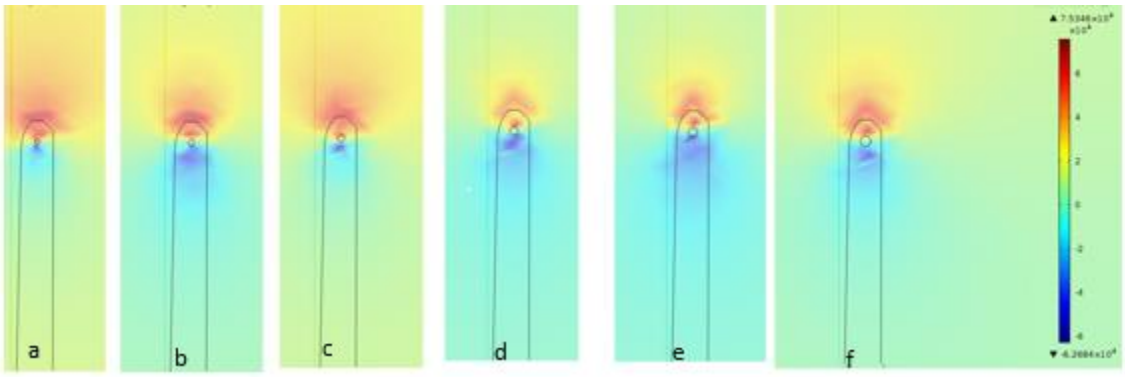


Figure 4-2. Receptor sizes and their various maximum electric field strength distribution: (a) 10mm; (b) 15 mm; (c) 20 mm; (d) 25 mm; (e) 30 mm and (f) 35 mm diameters respectively

The results for different receptor sizes are shown in table 5 and are plotted (Figure 4-3 to Figure 4-8).

Table 5 . Maximum electric field strength distribution (kV/m)

| Angle from vertical | Blade tip | Leading Edge | Trailing edge | Receptor |
|---|---|---|---|---|
| Receptor 10mm diameter | | | | |
| $-60^0$ | 20.12 | 36.25 | 0.43 | 60.78 |
| $-30^0$ | 43.96 | 42.64 | 21.93 | 121.0 |
| $0^0$ | 58.29 | 26.93 | 45.70 | 193.0 |
| $30^0$ | 45.03 | 2.04 | 51.43 | 135.0 |
| $60^0$ | 21.27 | -14.83 | 37.41 | 61.35 |
| Receptor 15mm diameter | | | | |
| $-60^0$ | 20.45 | 36.58 | -0.69 | 43.79 |
| $-30^0$ | 47.09 | 42.87 | 25.37 | 79.96 |
| $0^0$ | 57.54 | 28.03 | 52.57 | 89.22 |
| $30^0$ | 44.10 | 4.02 | 57.29 | 59.87 |
| $60^0$ | 20.51 | -13.09 | 41.06 | 14.76 |
| Receptor 20mm diameter | | | | |
| $-60^0$ | 20.95 | 36.66 | -0.15 | 40.49 |
| $-30^0$ | 44.87 | 40.81 | 25.36 | 74.01 |
| $0^0$ | 57.49 | 27.58 | 52.17 | 82.63 |
| $30^0$ | 44.93 | 2.16 | 57.83 | 56.58 |
| $60^0$ | 19.88 | -14.05 | 39.65 | 13.60 |
| Receptor 25mm diameter | | | | |
| $-60^0$ | 18.22 | 38.36 | 0.18 | 32.83 |
| -30 | 41.18 | 42.18 | 20.91 | 82.58 |
| $0^0$ | 55.01 | 28.06 | 44.47 | 98.13 |
| $30^0$ | 46.35 | 1.04 | 53.38 | 79.29 |
| $60^0$ | 20.37 | -15.01 | 36.93 | 33.74 |
| Receptor 30mm diameter | | | | |
| $-60^0$ | 18.33 | 38.81 | -0.06 | 31.23 |
| $-30^0$ | 43.33 | 45.64 | 20.90 | 70.08 |
| $0^0$ | 55.96 | 28.83 | 43.62 | 93.47 |
| $30^0$ | 46.87 | 2.10 | 53.07 | 83.28 |
| $60^0$ | 20.72 | -14.55 | 37.73 | 31.62 |
| Receptor 35mm diameter | | | | |
| $-60^0$ | 19.77 | 39.74 | -0.66 | 29.24 |
| $-30^0$ | 41.75 | 43.88 | 21.82 | 68.24 |
| $0^0$ | 56.05 | 29.31 | 46.48 | 88.84 |
| $30^0$ | 48.88 | 1.27 | 56.42 | 68.55 |
| $60^0$ | 21.12 | -14.36 | 38.30 | 30.84 |

### 4.2.1 *Receptor 10mm diameter*

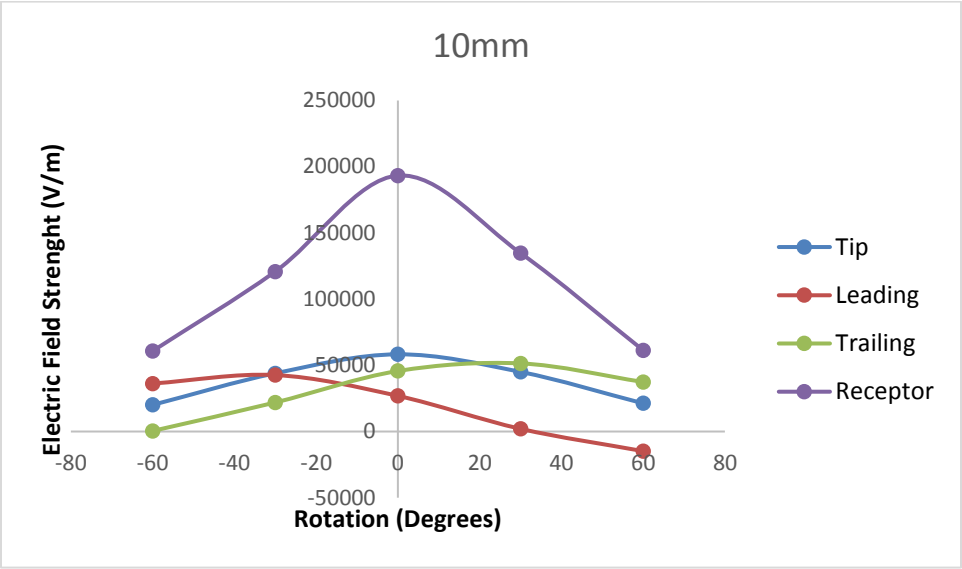


Figure 4-3. Maximum electric field strength distributions due to 10mm diameter receptor as blade A is rotated.

A receptor 10 mm in diameter is used on the model, the simulation result is shown in Figure 4-3. The electric field distribution on the blade is shown. The maximum electric field plot shows that the value at the receptor tip is highest at the vertical position, followed by the blade tip also at the vertical position, the leading edge at $-60^0$ and then, trailing edge at $30^0$. The electric field distribution is highest at the receptor and as such, leader will incept from it first followed by other part of the blade in the sequence as depicted by the plot.

### 4.2.2 *Receptor 15mm diameter*

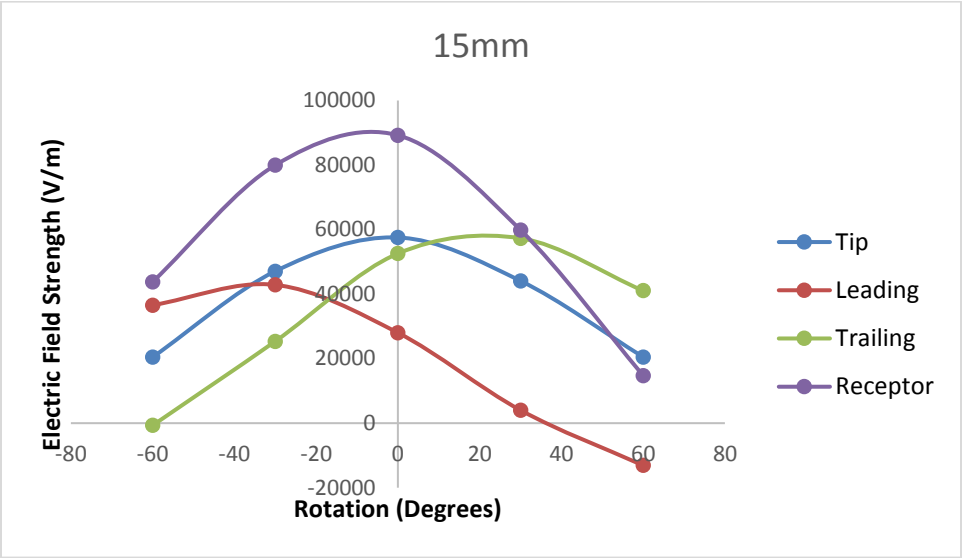


Figure 4-4. Maximum electric field strength distributions due to 15mm diameter receptor as blade A is rotated.

The receptor size is changed to 15 mm and the process is repeated, obtained result is plotted in Figure 4-4. It is observed that the change in receptor size has significantly affected the result as shown by the plot, the maximum electric field plot shows that the value at the receptor tip is highest at $-20^0$ from the vertical position, followed by the blade tip also at $-20^0$, trailing edge at $30^0$, and then, the leading edge at $-40^0$. The electric field strength on the receptor is higher.

### 4.2.3 *Receptor 20mm diameter*

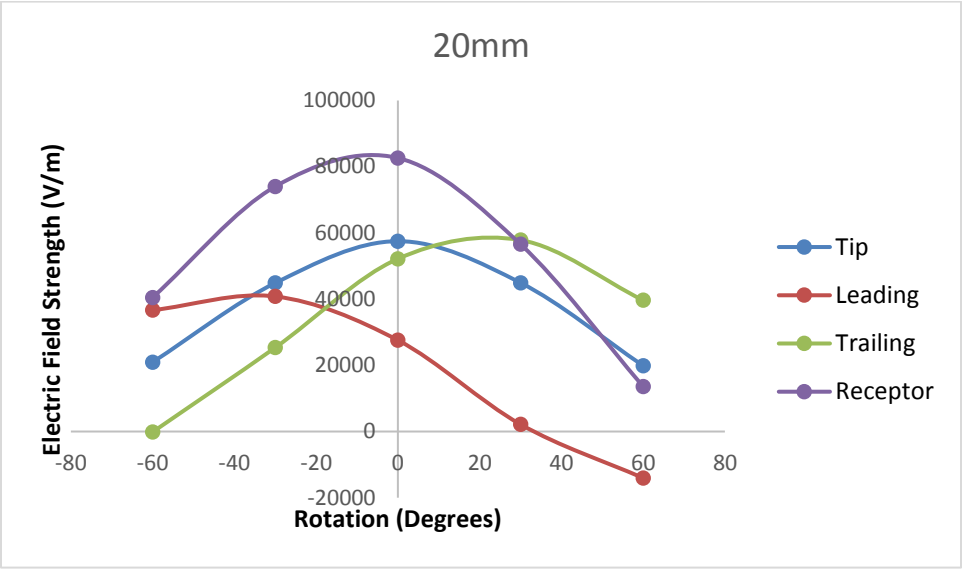


Figure 4-5. Maximum electric field strength distributions due to 20mm diameter receptor as blade A is rotated.

As shown in Figure 4-5 above, the effect of receptor size is seen. In this instance, the size is increased to 20 mm. It is observed again that the change in receptor size has significantly affected the result as shown by the plot, the maximum electric field plot shows that the value at the receptor tip is highest at $-10^0$ from the vertical position, followed by the trailing edge at $20^0$, blade tip at $-10^0$, and then, the leading edge at $-60^0$. The electric field strength on the receptor is higher. Here, there is a possibility of leader incepting from the trailing edge before the receptor at between $40^0$ and $60^0$.

### 4.2.4 *Receptor 25 mm diameter*

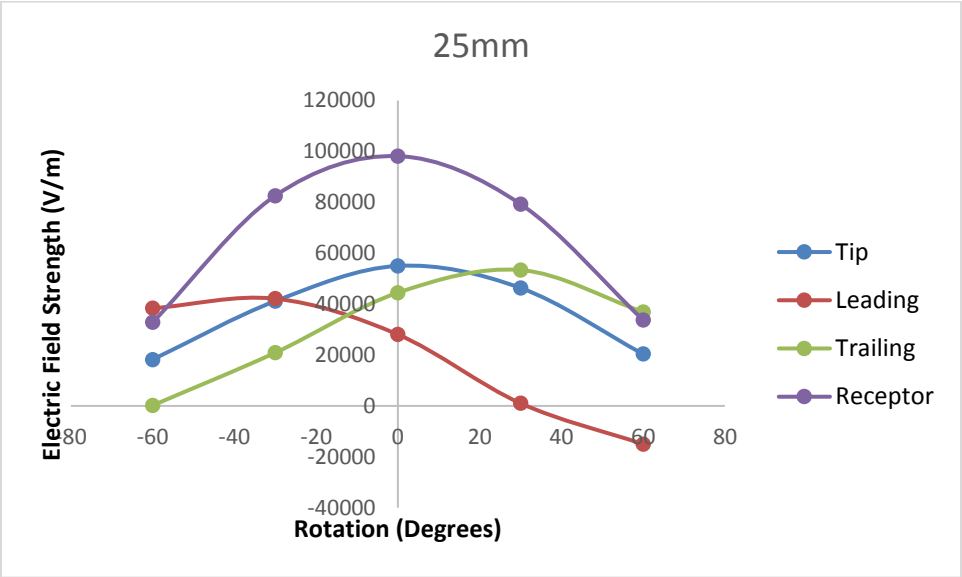


Figure 4-6. Maximum electric field strength distributions due to 25mm diameter receptor as blade A is rotated.

The receptor size is increased to 25 mm and the effect is shown in Figure 4-6 above, the maximum electric field plot shows that the value at the receptor tip is highest at the vertical position, followed by the trailing edge at $30^0$, leading edge at $-60^0$, and then, the blade tip at the vertical position. The electric field strength on the receptor is higher but leader can incept simultaneously at the receptor and the leading edge at $-60^0$, also at the receptor and the trailing edge at $60^0$.

### 4.2.5 *Receptor 30 mm diameter*

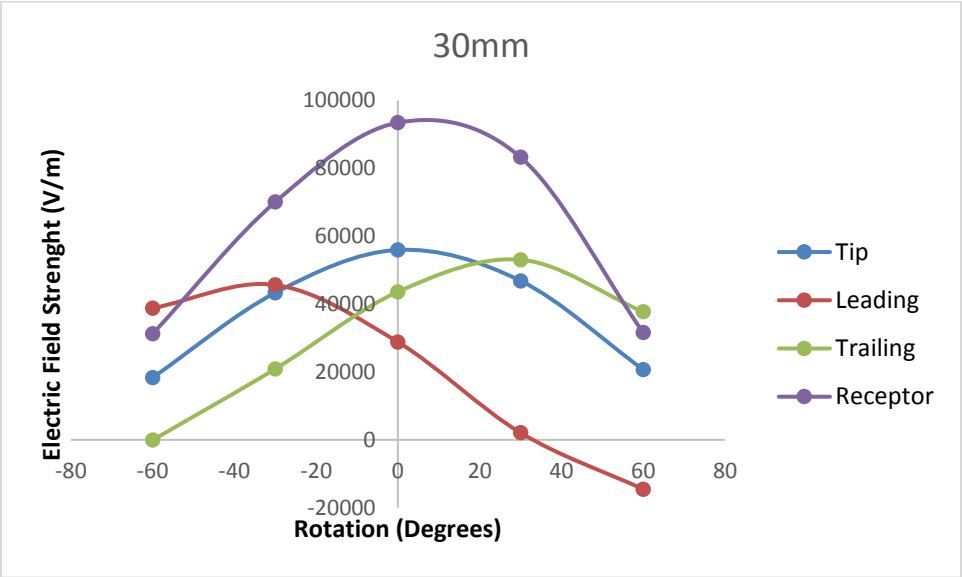


Figure 4-7. Maximum electric field strength distributions due to 30mm diameter receptor as blade A is rotated.

Again, the receptor size is increased to 30 mm diameter and the effect is shown in Figure 4-7 above. The maximum electric field plot shows that the value at the receptor tip is highest at $10^0$ from the vertical position, followed by blade tip at the vertical position, trailing edge at $25^0$, and then, leading edge at $-40^0$. The electric field strength on the receptor is higher but leader can incept first from the leading and trailing edges at $-60^0$, and $60^0$ respectively before the receptor.

### 4.2.6 *Receptor 35 mm diameter*

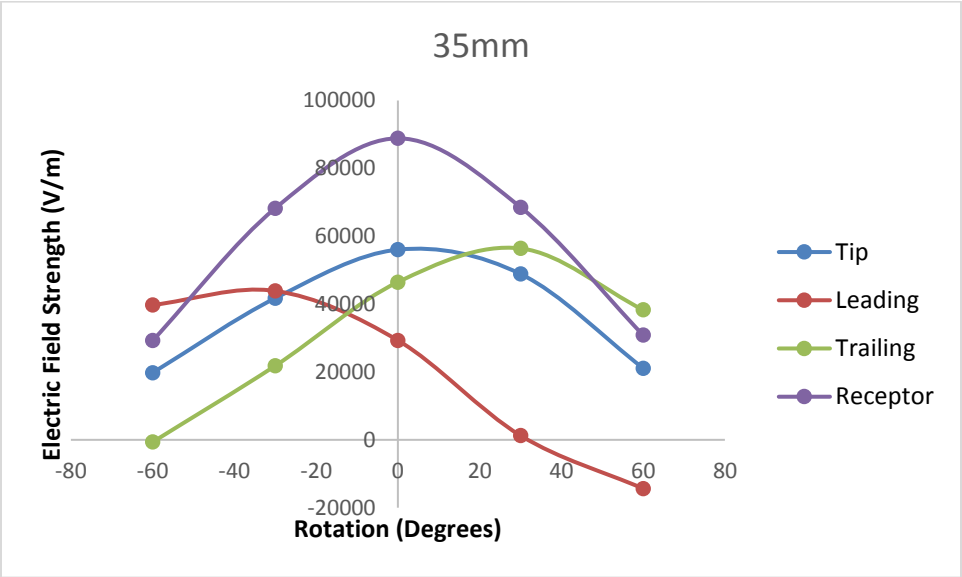


Figure 4-8. Maximum electric field strength distributions due to 35 mm diameter receptor as blade A is rotated.

Finally, the receptor size is increased to 35 mm in diameter. The result is shown above in Figure 4-8. In this case, it is also observed that it is possible for leader to incept from other part of the blade before the receptor. The maximum electric field plot shows that the value at the receptor tip is highest at the vertical position, followed by trailing edge at $25^0$, blade tip at the vertical position, and then, leading edge at from $-40^0$ to $-60^0$. As in the previous scenario, the electric field strength on the receptor is higher but leader can incept first from the leading and trailing edges at $-60^0$, and $60^0$ respectively before the receptor.

### 4.2.7 *Comparison*

The comparison for various receptor sizes is shown in; (Figure 4-9) for blade tip, (Figure 4-10) for leading edge, and (Figure 4-11) for trailing edge.

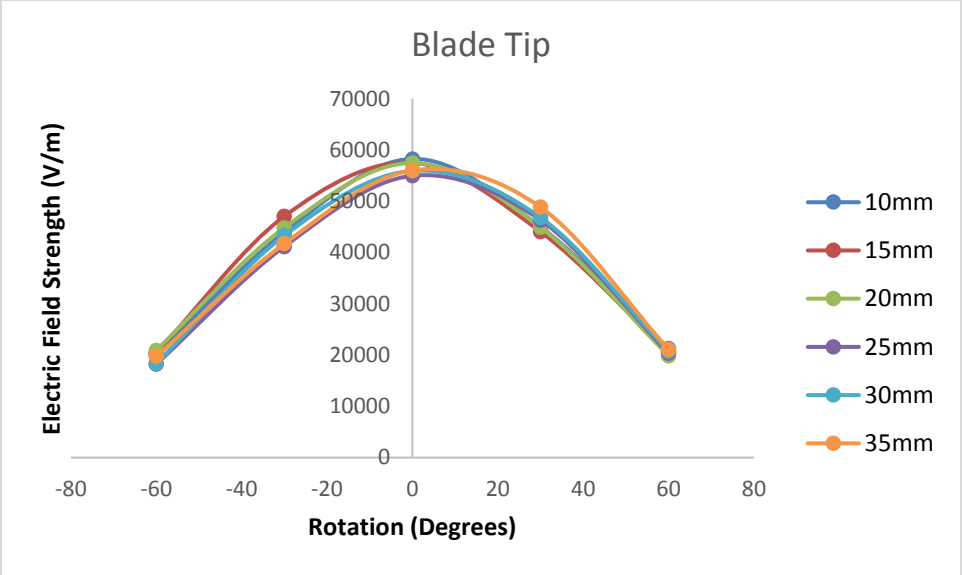


Figure 4-9. Comparison for various receptor sizes at the blade tip

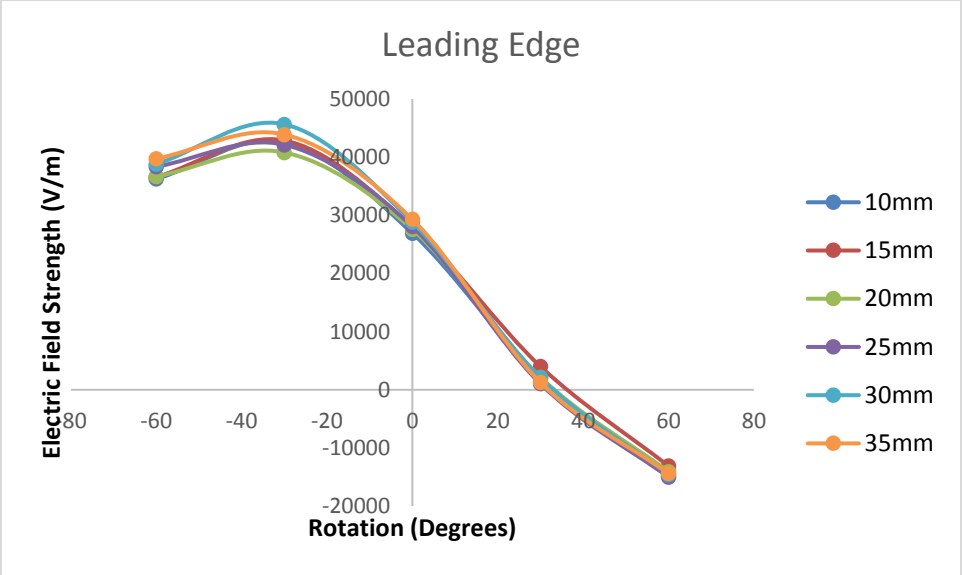


Figure 4-10. Comparison for various receptor sizes at the leading edge

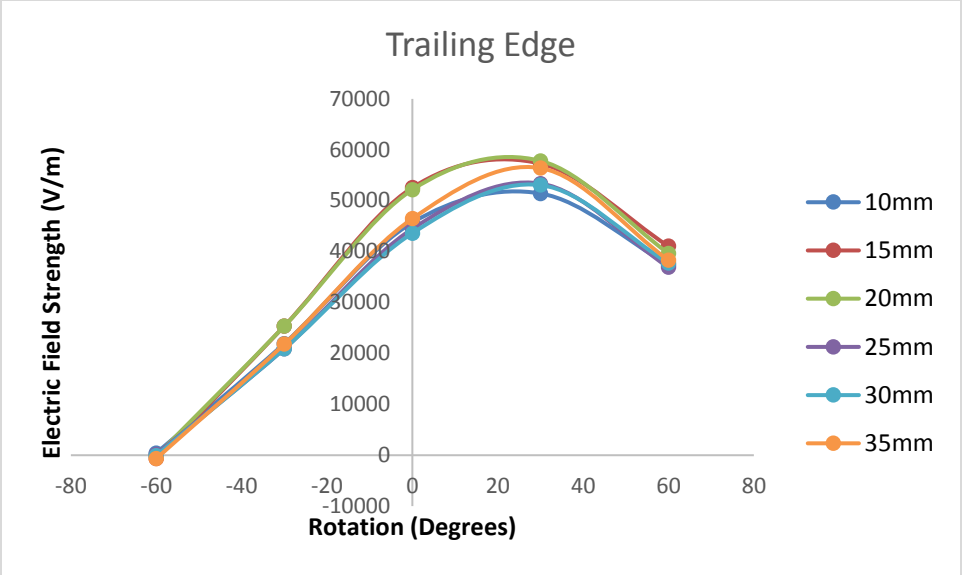


Figure 4-11. Comparison for various receptor sizes at the trailing edge

Making comparison at the blade tip as shown above in Figure 4-9, the electric field plot shows that 35 mm diameter has the highest value at the vertical position, followed by 15 mm, 30 mm, 25 mm, 20 mm and finally 10 mm.

Also, at the leading edge as shown in Figure 4-10 above, the values of the electric field strength are in the sequence 15 mm, 25 mm, 35mm, 20 mm, 10 mm and 30 mm.

Finally, for the trailing edge as shown in Figure 4-11 above, the sequence is 20 mm, 35 mm, 30 mm,15 mm, 15 mm, 25 mm and 10 mm.

Figure 4-12 shows the comparison of maximum electric field strength on the receptor for various receptor sizes.

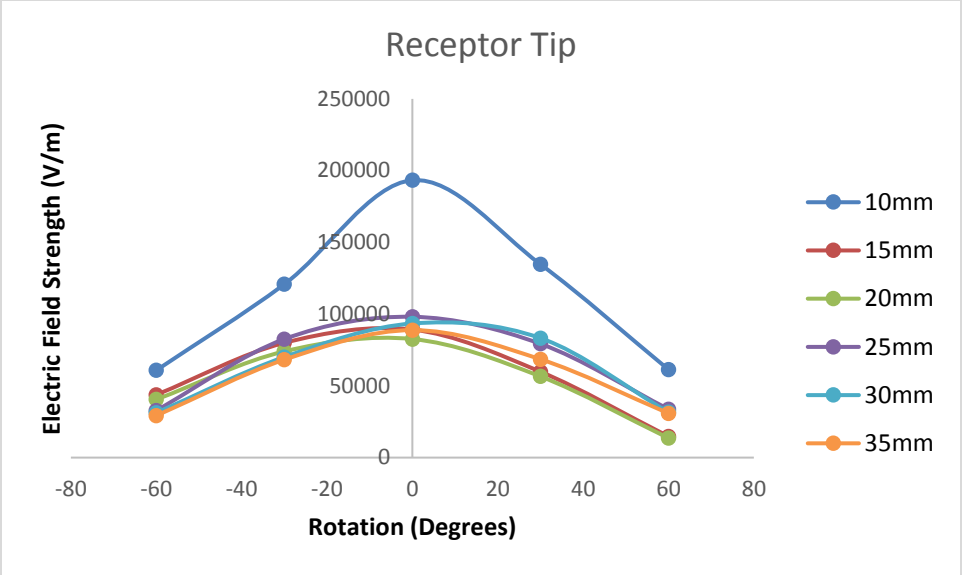


Figure 4-12. Comparison for various receptor sizes at the receptor tip

Comparing values for the receptor tip as shown above in Figure 4-12, the electric field plot shows that 10 mm diameter has the highest value at the vertical position, followed by 25 mm, 30 mm, 35 mm, 15 mm and finally 20 mm.

It is found that 10 mm receptor diameter presents the highest electric field strength on the receptor than other receptor sizes. Also, relatively, the electric field distribution at the blade tip, leading edge, trailing edge for 10 mm receptor diameter is lower than that of other sizes. This indicates that 10 mm receptor diameter will allow leader to be initiated from the receptor before any other part of the blade or wind turbine and as a result prevent damage. This receptor size will therefore provide higher protection efficiency than other receptor sizes and is therefore recommended. 10 mm is the smallest amongst the sizes considered and would be thought least in withstanding high current, however, it has been shown in literature that this size is adequate for an average peak stroke current and if need be, this can be improved by increasing the diameter of the down conductors. With proper scaling, findings can be extended to other wind turbine sizes.

### 4.3 Optimum Receptor Position on The Blade

The effect of receptor type and size on lightning protection of wind turbine have recently been evaluated in [40, 41], however, the obtained results would be affected if the position of the same size of receptor is changed. It is therefore more important to know the optimum position of the receptor on a blade. Again, there are also no standards as well as detailed experimental and numerical research covering receptor location.

In this section, by comparing the electric field strength as the receptor position is changed and the blade is rotated, the receptor position is evaluated and optimized.

Figure 4-13 shows the discrete receptor position model. Four different configurations of receptor positions Figure 4-14 are applied on the wind turbine to investigate the effect of receptor position on initiation of upward leader. In the configurations, the receptor (10 mm in diameter) is fixed at discrete positions from the blade tip. These positions are 2 m, 1.5 m, 1 m and 0.6 m respectively. In each case, the evaluation is done as the blade is rotated through $-60^0$, $-30^0$, $0^0$, $30^0$ and $60^0$ from the vertical position. As in previous analysis, the blade in the vertical position in Figure 3-3 is referred to as blade A and only the results for blade A are provided. Also, values are obtained from the blade tip, leading edge, trailing edge and the receptor tip.

The focus is on evaluating the efficiency of the receptor by obtaining the maximum electric field strength required for the initiation of upward leader due to thunder cloud charge.

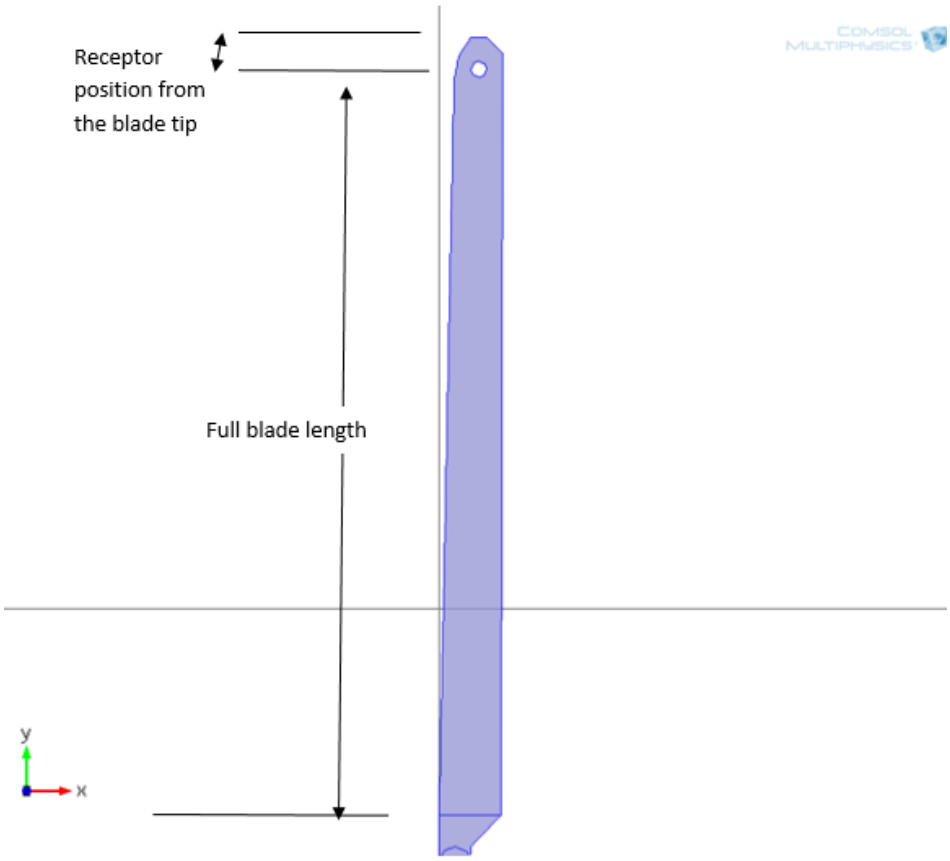


Figure 4-13: Discrete receptor position model

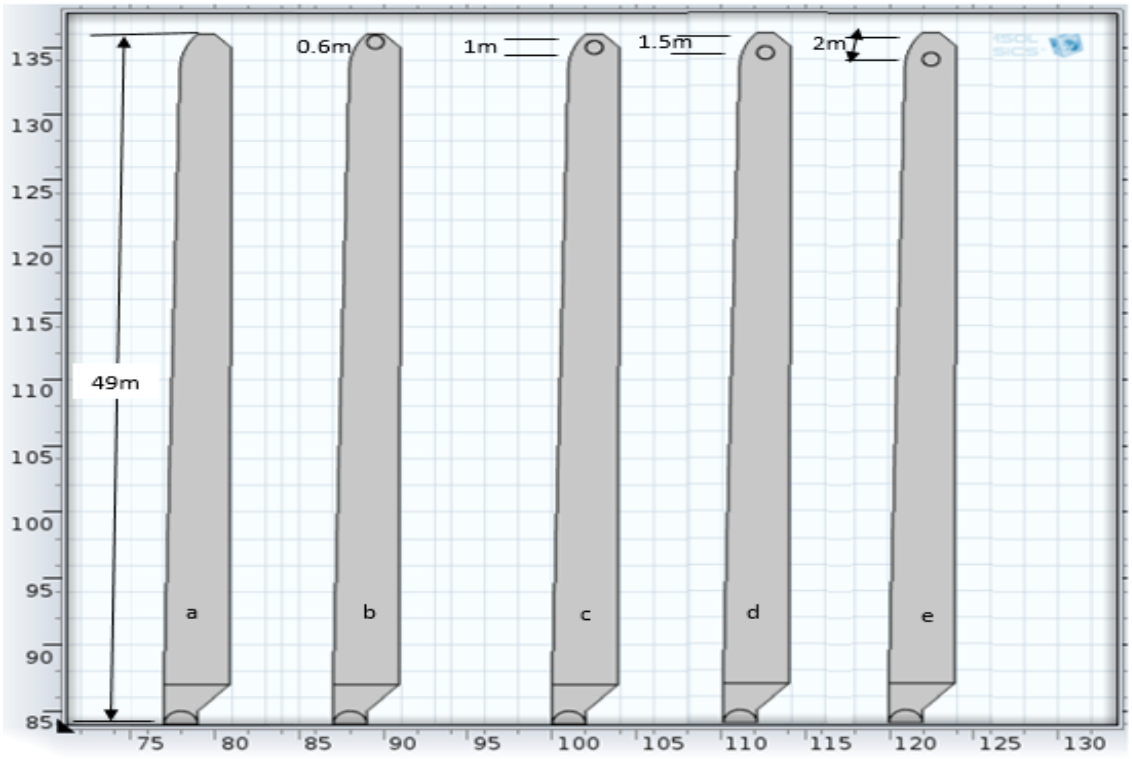


Figure 4-14: Different configurations of receptor positions from the blade tip used in the study: (a) No receptor; (b) 0.6 m; (c) 1 m; (d) 1.5 m; and (e) 2 m.

In order to investigate the effect of receptor position on the electric field strength, the simulation is first conducted on the wind turbine without the receptor and then the receptors are used on discrete positions as the blades are rotated.

The results of maximum electric field strength distributions for various configurations obtained from the blade tip, leading edge, trailing edge and the receptor tip, as blade A is rotated are shown in table 5 and plotted for blade tip; (b) leading edge; (c) trailing edge; (d) receptor; (e) without receptor; and (f) with receptor, respectively.

Table 6 Values of maximum electric field strength (kV/m) obtained from the blade tip, leading edge, trailing edge and the receptor tip, as blade A is rotated for various configurations.

| Angle from Vertical | Blade tip | Leading Edge | Trailing edge | Receptor |
|---|---|---|---|---|
| Receptor 2m from blade tip | | | | |
| $-60^0$ | 19.79 | 39.80 | -0.67 | 29.28 |
| $-30^0$ | 41.93 | 44.10 | 21.91 | 68.68 |
| $0^0$ | 56.43 | 29.46 | 46.81 | 89.72 |
| $30^0$ | 49.31 | 1.12 | 56.96 | 69.39 |
| $60^0$ | 21.33 | -14.70 | 38.75 | 31.30 |
| Receptor 1.5 m from blade tip | | | | |
| $-60^0$ | 23.37 | 39.52 | -7.79 | 42.06 |
| $-30^0$ | 50.34 | 38.82 | 16.78 | 95.81 |
| $0^0$ | 70.52 | 18.98 | 53.18 | 124.10 |
| $30^0$ | 55.30 | -9.01 | 64.94 | 91.38 |
| $60^0$ | 23.92 | -22.96 | 47.05 | 24.85 |
| Receptor 1 m from blade tip | | | | |
| $-60^0$ | 28.85 | 40.09 | -20.62 | 15.86 |
| $-30^0$ | 67.51 | 34.40 | 7.69 | 35.38 |
| $0^0$ | 86.67 | 4.73 | 36.72 | 50.39 |
| $30^0$ | 67.77 | -26.24 | 62.91 | 36.60 |
| $60^0$ | 32.50 | -33.26 | 47.63 | 19.80 |
| Receptor 0.6 m from blade tip | | | | |
| $-60^0$ | 35.83 | 40.27 | -36.59 | 6.49 |
| $-30^0$ | 72.39 | 28.69 | -19.55 | 14.10 |
| $0^0$ | 103.58 | -7.00 | 14.84 | 1.69 |
| $30^0$ | 79.59 | -35.66 | 56.92 | 9.36 |
| $60^0$ | 39.08 | -39.82 | 56.85 | 7.60 |

### 4.3.1 *Receptor 2 m Away from Blade Tip.*

The maximum electric field strength due to the configuration with the receptor 2 m away from the blade tip is shown below, wind turbine in Figure 4-15, blade in Figure 4-16 and Figure 4-17. The corresponding plot for the blade tip, leading edge, trailing edge, without receptor and with receptor are shown in Figure 4-18 to Figure 4-23. Note that with or

without receptor simply means that in the comparison, the values for the receptor is inclusive or not.

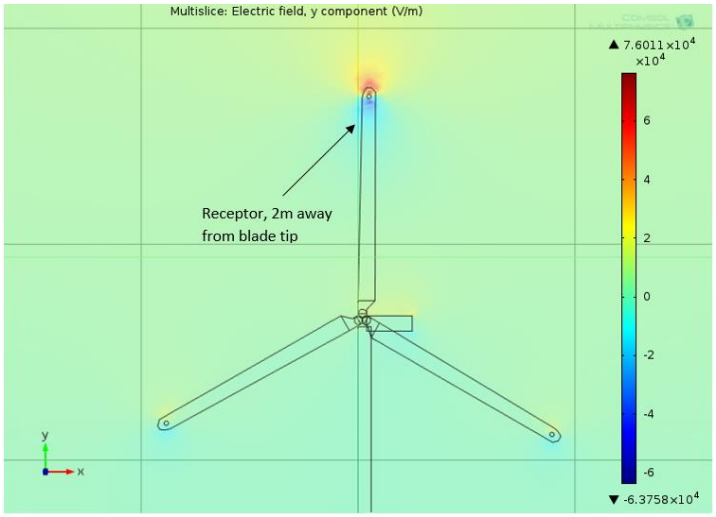


Figure 4-15: Wind Turbine

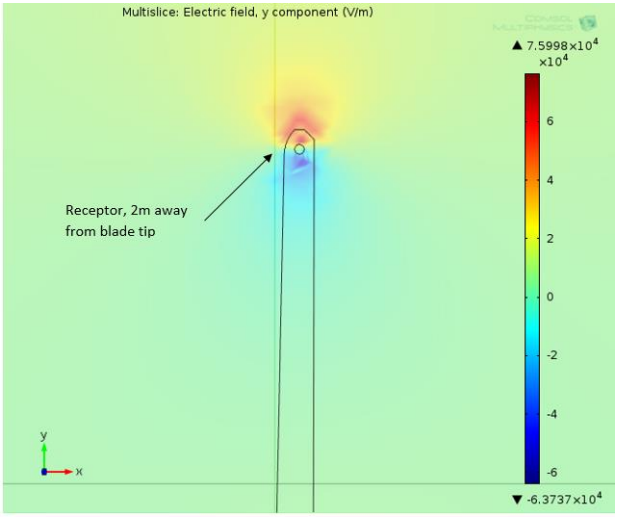


Figure 4-16: Blade

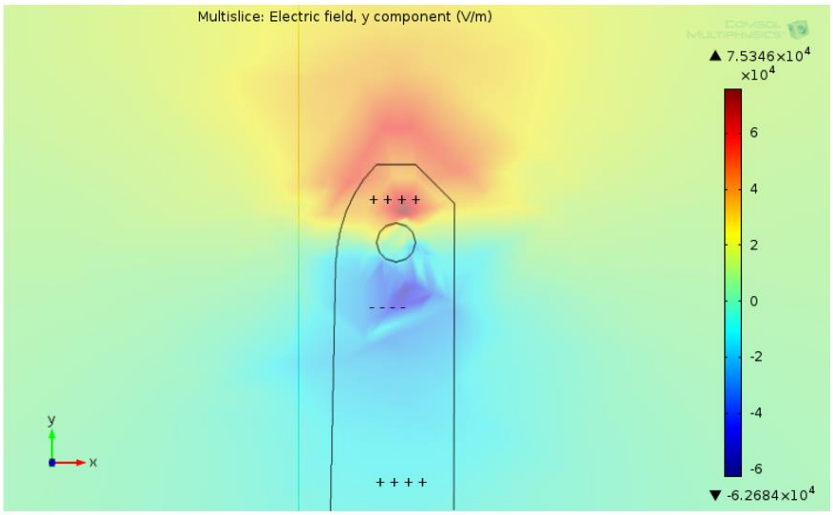


Figure 4-17: Blade

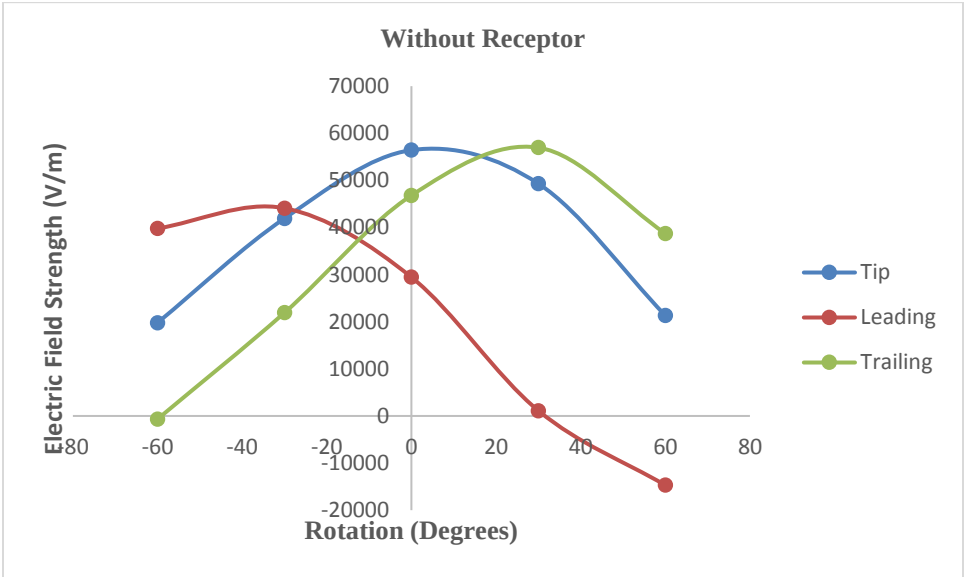


Figure 4-18: Comparing Blade Tip, Leading and Trailing Edge without considering Receptor.

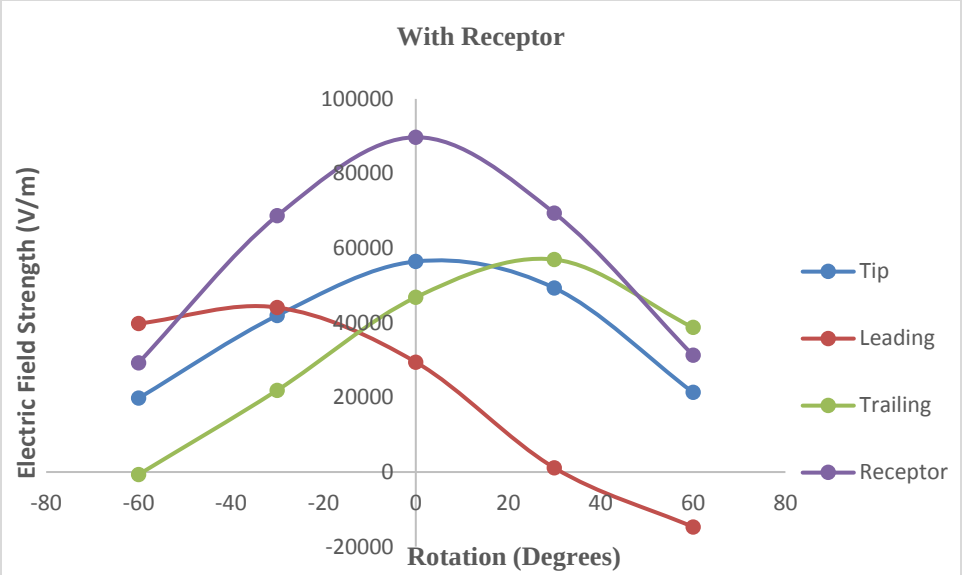


Figure 4-19: Comparison with the receptor inclusive

In this configuration, with the receptor 2 m away from blade tip, the maximum electric field plot shows that the value at the receptor tip is highest at vertical position (89.72 kV/m), followed by the blade tip at vertical position (56.43 kV/m), the trailing edge at $30^0$ from the vertical position (56.96 kV/m), and then, the leading edge at $-35^0$ from the vertical position (43.10 kV/m). The electric field strength on the receptor is higher but leader can incept first from the leading and trailing edges at $-60^0$, and $60^0$ respectively before the receptor.

### 4.3.2 *Receptor 1.5 m Away from Blade Tip.*

The maximum electric field strength due to the configuration with the receptor 1.5 m away from the blade tip is shown below, wind turbine in Figure 4-24 and blade in Figure 4-25. The corresponding plot for the blade tip, leading edge, trailing edge, without receptor and with receptor are shown in Figure 4-26 to Figure 4-31.

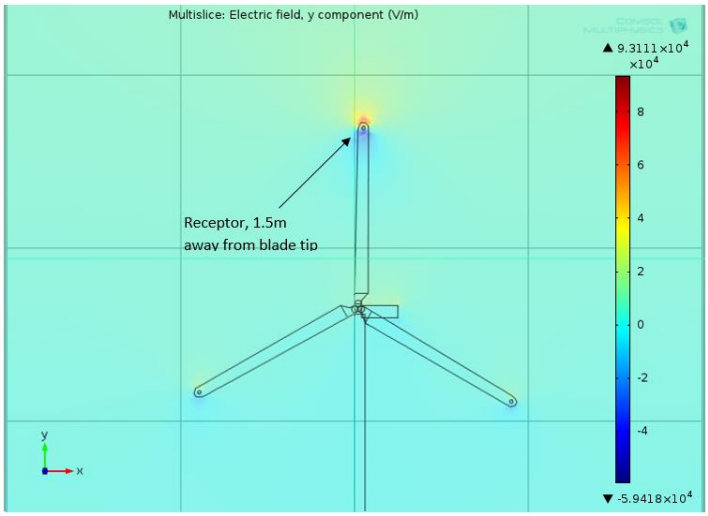


Figure 4-20: Wind Turbine

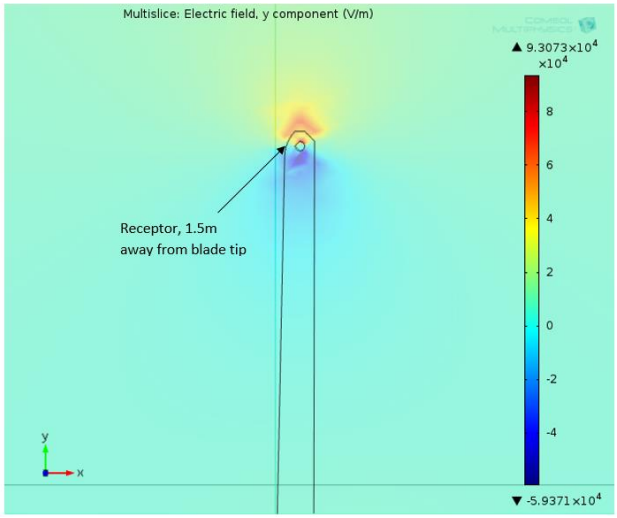


Figure 4-21: Blade

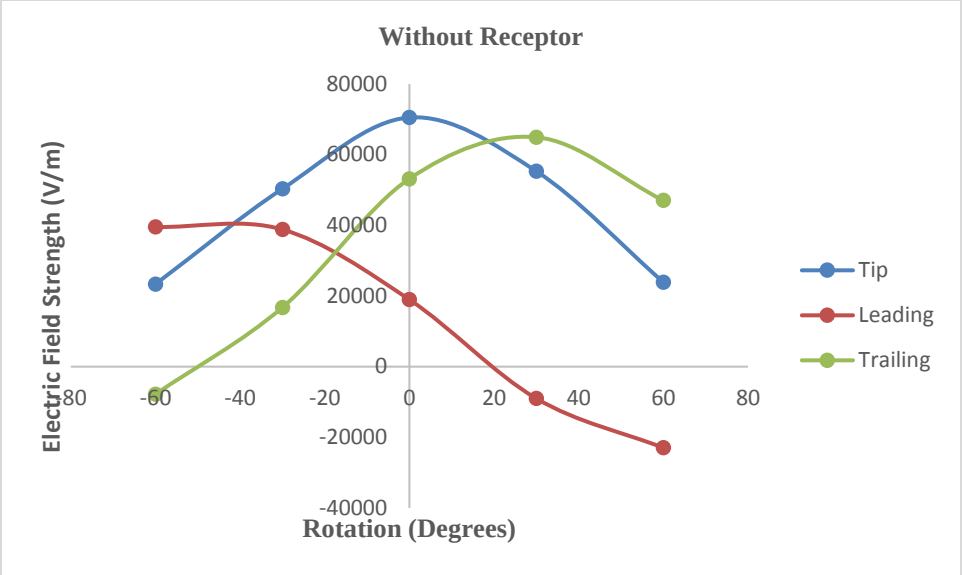


Figure 4-22: Comparing Blade Tip, Leading and Trailing Edge without considering Receptor.

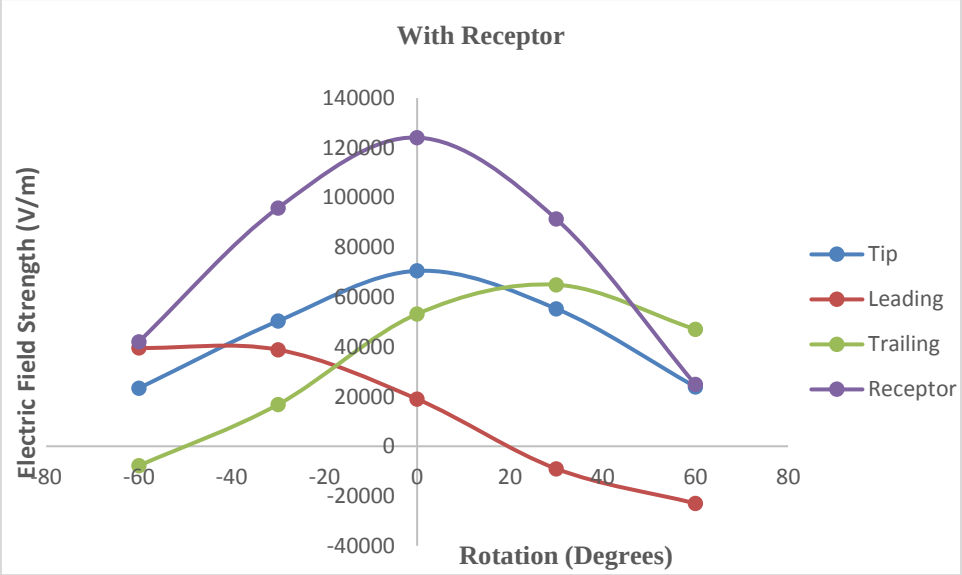


Figure 4-23: Comparison with the receptor inclusive

The configuration, with the receptor 1.5 m away from blade tip, the maximum electric field plot show that the receptor has the highest value at vertical position (124.10 kV/m), followed by the blade tip at vertical position (70.52 kV/m), the trailing edge at $30^0$ from the vertical position (64.94 kV/m), and then, the leading edge at $-60^0$ from the vertical position (39.52 kV/m). Also, as before, the electric field strength on the receptor is higher

but leader can incept first from the leading and trailing edges at $-60^0$, and $60^0$ respectively before the receptor.

### 4.3.3 *Receptor 1 m Away from Blade Tip.*

The maximum electric field strength due to the configuration with the receptor 1 m away from the blade tip is shown below, wind turbine in Figure 4-32 and Figure 4-33, then blade in Figure 4-34. The corresponding plot for the blade tip, leading edge, trailing edge, without receptor and with receptor are shown in Figure 4-35 to Figure 4-40.

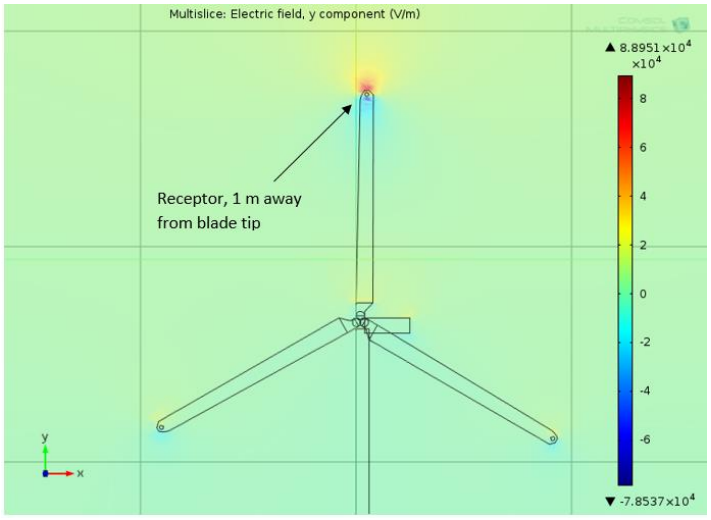


Figure 4-24: wind Turbine

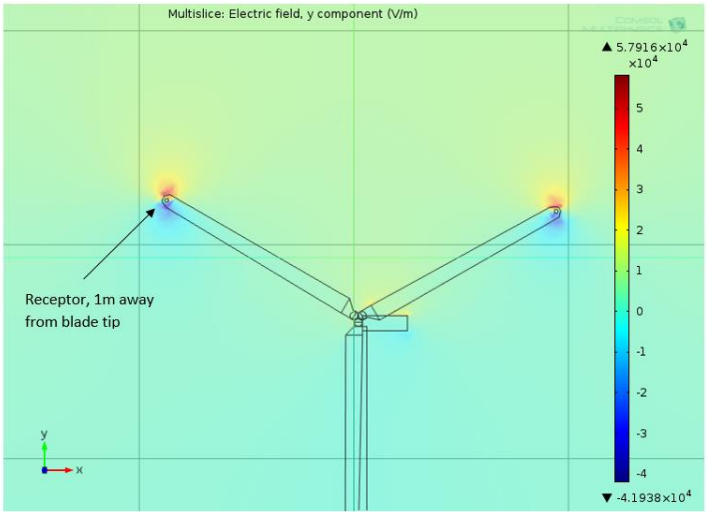


Figure 4-25: Rotated wind Turbine

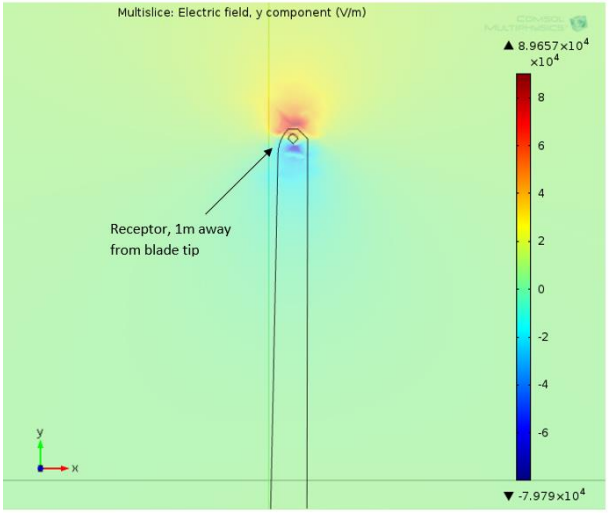


Figure 4-26: Blade

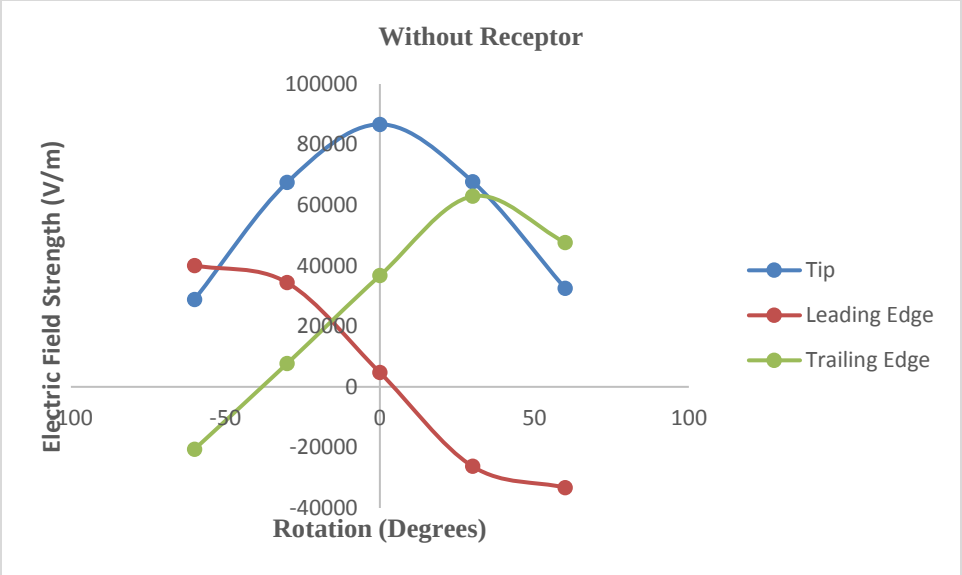


Figure 4-27: Comparing Blade Tip, Leading and Trailing Edge without considering Receptor.

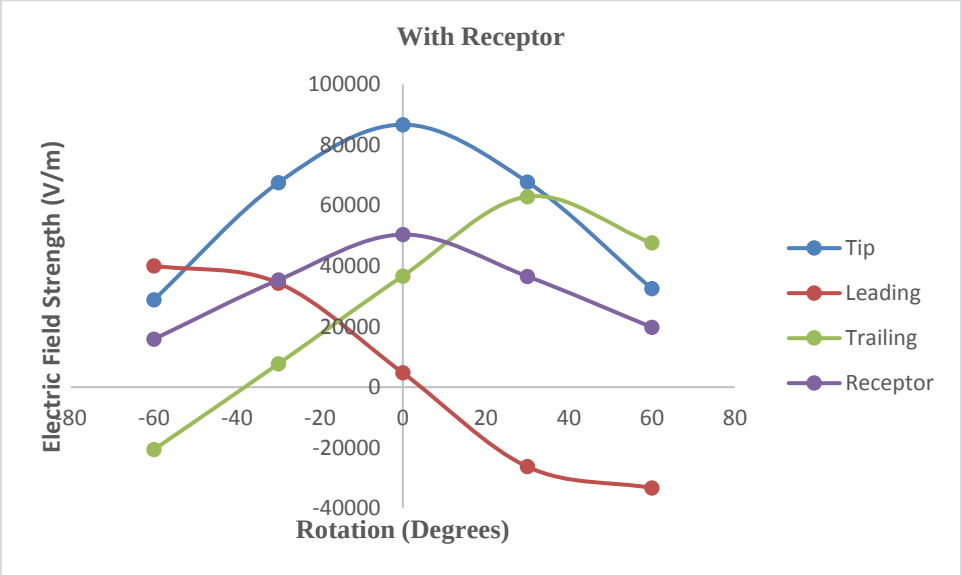


Figure 4-28: Comparison with the receptor inclusive

For the configuration, with the receptor 1 m away from blade tip, the maximum electric field plot shows that the blade tip has the highest value at vertical position (86.67 kV/m), followed by trailing edge at $60^0$ (47.63 kV/m), the receptor tip at vertical position (50.39 kV/m), and then, the leading edge with a value of (40.09 kV/m). It is observed here that in the case of 2 m and 1.5 m, the highest values were at the receptor tip which is different in

this case. Therefore, leader will incept from the blade tip, the trailing edge before the receptor. This is not a desired situation.

### 4.3.4 *Receptor 0.6 m Away from Blade Tip.*

The maximum electric field strength due to the configuration with the receptor 0.6 m away from the blade tip is shown below, wind turbine in Figure 4-41 and blade in Figure 4-42. The corresponding plot for the blade tip, leading edge, trailing edge, without receptor and with receptor are shown in Figure 4-43 to Figure 4-48.

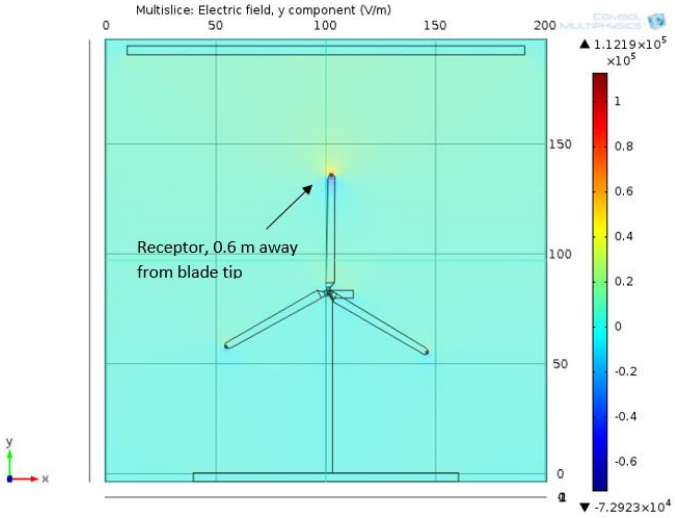


Figure 4-29: Wind Turbine

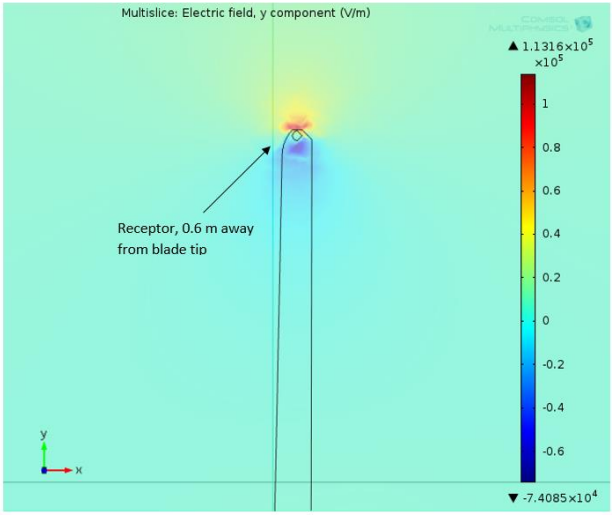


Figure 4-30: Blade

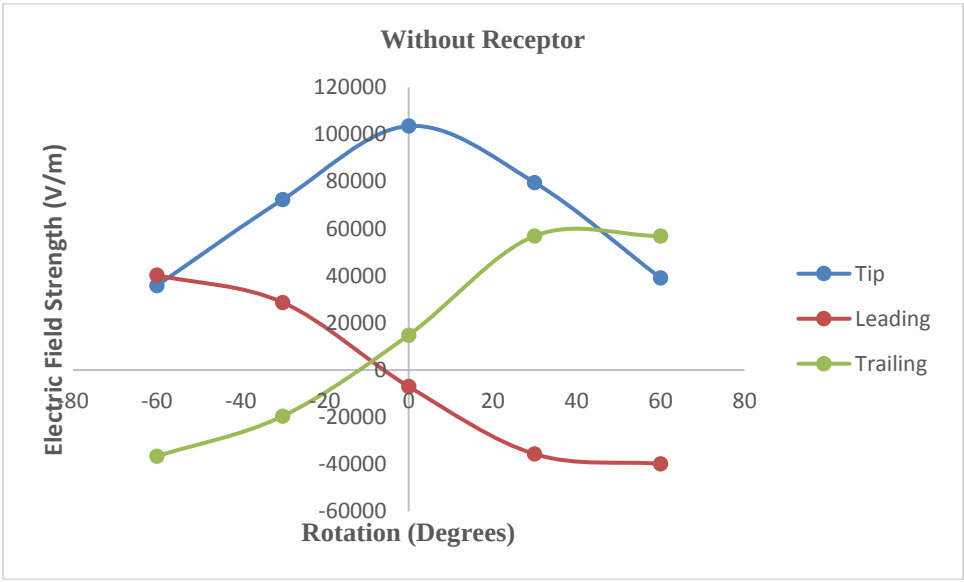


Figure 4-31: Comparing Blade Tip, Leading and Trailing Edge without considering Receptor.

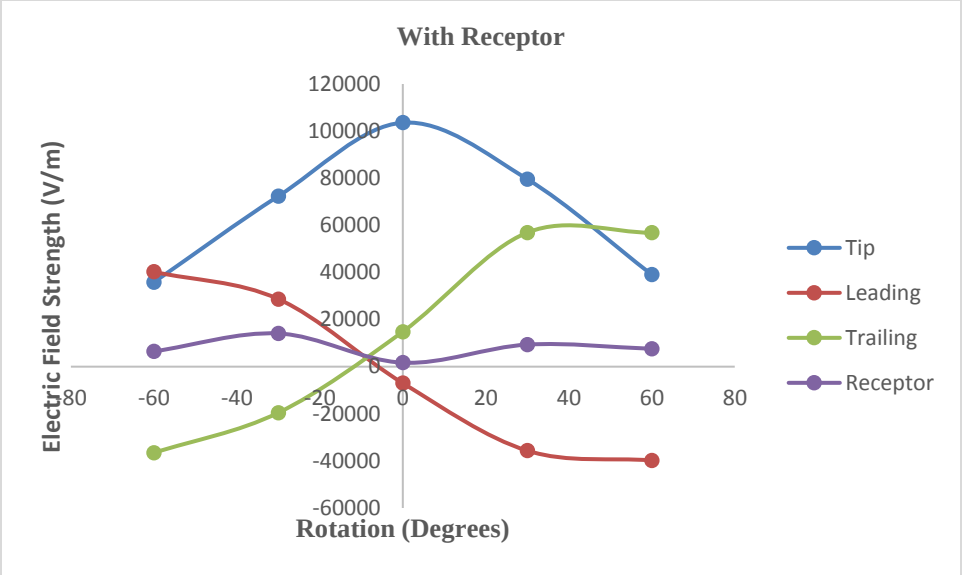


Figure 4-32: Comparison with the receptor inclusive

Finally, for the configuration, with the receptor 0.6 m away from blade tip, the maximum electric field plot shows that the blade tip has the highest value at vertical position (103.58 kV/m), followed by trailing edge at $60^0$ (56.85 kV/m), the leading edge at $-60^0$ (40.27 kV/m), and finally the receptor at $-30^0$ with the lowest value of (14.10 kV/m). This is the worst-case scenario as the receptor, even though close to the blade tip, has the least maximum field strength. This suggests that it is not good for the receptor to be too close to the blade tip except it is placed on the tip itself as in the case of metallic cap. The reason for this is not well understood and requires further investigation.

### 4.3.5 *Comparison*

The comparison for various configurations without the receptor is shown in Figure 4-49 blade tip, Figure 4-50 leading edge, Figure 4-51 trailing edge. Figure 4-52 Shows the comparison of receptor maximum electric field strength for various configurations.

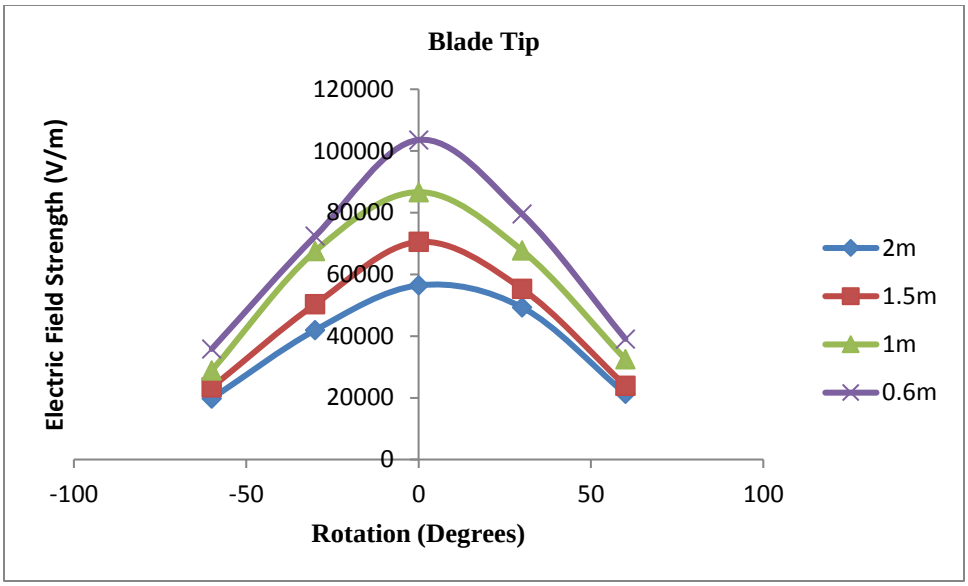


Figure 4-33: Blade Tip Comparison

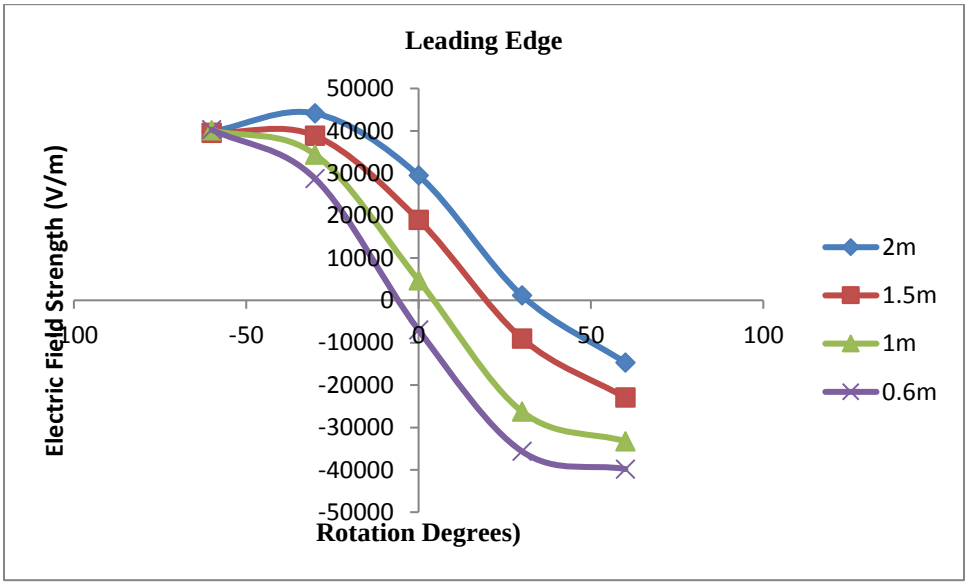


Figure 4-34: Leading Edge Comparison

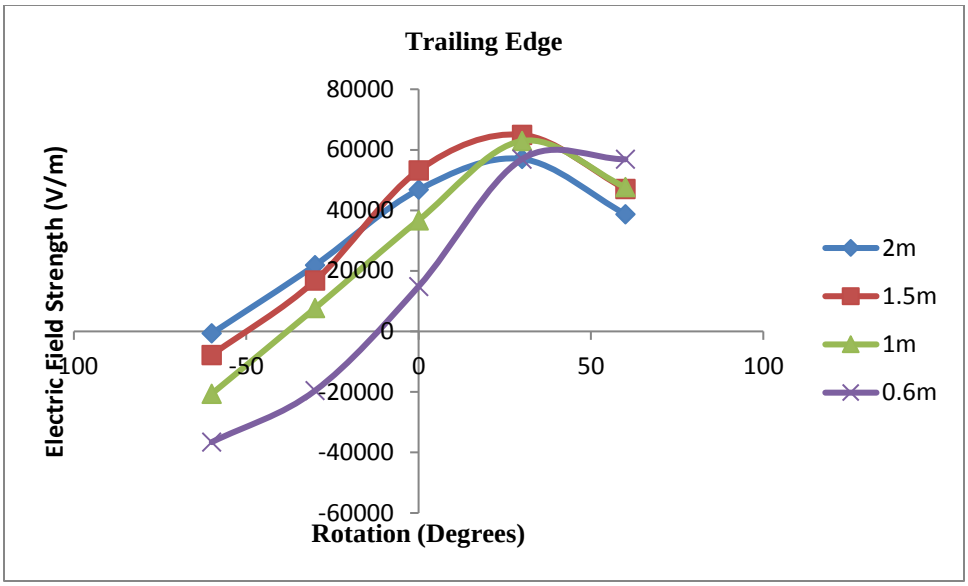


Figure 4-35: Trailing Edge Comparison

The electric field distribution is compared for the blade tip, trailing and leading edges as shown above. Initially comparison is done for the blade tip for all the configuration considered, the plot in Figure 4-49 shows that 0.6 m has the highest value at the vertical position, followed by 1 m, 1.5 m and 2 m.

Secondly, comparison is done for the leading edge. The electric field plot in Figure 4-50 shows that at the leading edge, 2 m has the highest value at the vertical position, followed by 1.5 m, 1m and 0.6 m the least.

Finally, comparison is done for the trailing edge. The electric field plot in Figure 4-51 shows that though the values are not distinct as in previous cases, 1.5 m has the highest value at the vertical position, followed by 2 m, 1 m and 0.6 m as the least. The comparison is further shown in the table below.

Table 7 Relative efficiencies on the blade surface due to the positions of the receptor from the blade tip

| Blade Tip | Leading Edge | Trailing Edge |
|---|---|---|
| 0.6 | 2 | 1.5 |
| 1 | 1.5 | 2 |
| 1.5 | 1 | 1 |
| 2 | 0.6 | 0.6 |

For an efficient lightning protection, it is desirable that the value of electric field at the blade surface be kept to a minimum as a result of the presence of the receptor, whereas, most importantly, it should be maximum on the receptor so that leader will incept from it first. The configuration with the highest maximum electric field on the receptor is 1.5 m from the blade as shown below in Figure 4-52.

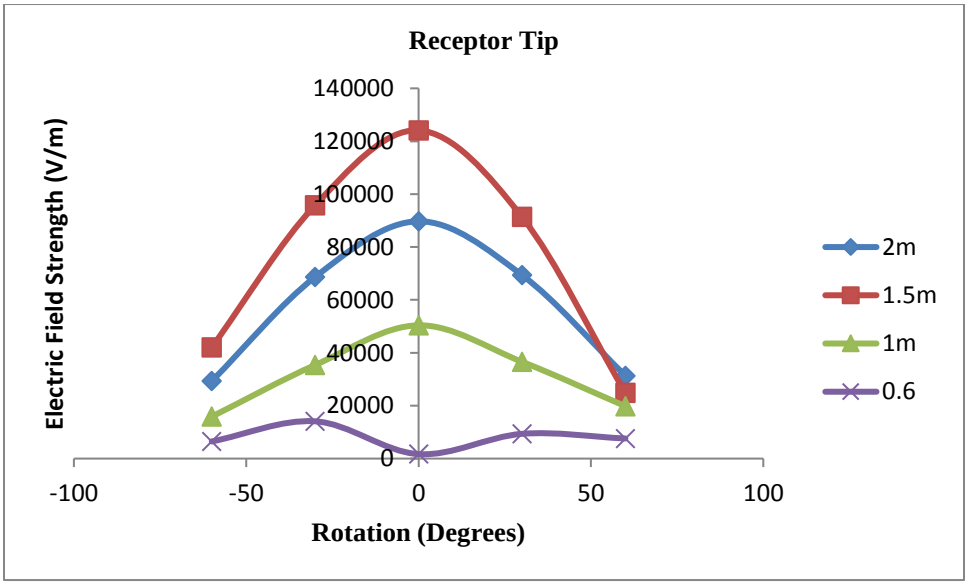


Figure 4-36: Receptor Tip Comparison

Similarly, comparison is done for the receptor tip considering the various configurations. The electric field plot shows that 1.5 m has the highest value at the vertical position,

followed by 2 m, 1 m and finally 0.6 m. The comparison is further shown in the table below.

Table 8 Relative efficiencies of the receptor Tip due to its positions from the blade tip

| Receptor Tip |
|---|
| 1.5 |
| 2 |
| 1 |
| 0.6 |

The maximum electric field strength and their corresponding locations on the blade tip, leading edge, trailing edge and the receptor are shown in table and plots above. It is found that the configuration with the receptor 1.5 m away from the blade tip presents the highest electric field strength on the receptor, whereas the maximum electric field strength on the configuration with the receptor 0.6 m away from the blade tip is the lowest among all the configurations. It should be noticed that 0.6 m is closer to the tip than other configuration and would be thought that it should perform better but result have shown otherwise. This indicates that locating the receptor 1.5 m away from the blade tip will allow the leader to be initiated from the receptor before any other part of the blade and as a result prevent damage. This configuration therefore provides higher protection efficiency than other configurations and is therefore recommended.

If the receptor locations are properly scaled as shown above, the results and findings in this thesis could be extended to different wind turbine sizes.

## 4.4 Conclusion

The extended vertical tri-pole cloud charge model has been used to evaluate the maximum electric field strength required for the initiation of upward leader from wind turbine. In this chapter, the size of receptor and its position and their influence on the maximum electric

field strength is investigated. Initially, the receptor was placed in discrete position; 2 m, 1.5 m, 1 m and 0.6 m from the tip of the blade to find the best position that will allow leader incepted from the receptor before other part of the blade. It is found that locating the receptor 1.5 m away from the blade tip provides higher protection efficiency than other configurations. Secondly, six receptor sizes (10 mm, 15 mm, 20 mm, 25 mm, 30 mm and 35 mm receptor diameters), encompassing adopted sizes in literature are investigated. It is found that 10 mm receptor diameter presents the highest electric field strength on the receptor than other receptor sizes. Also, relatively, the electric field distribution at the blade tip, leading edge, trailing edge for 10 mm receptor diameter is lower than that of other sizes. This indicates that 10 mm receptor diameter will allow leader to be initiated from the receptor before any other part of the blade or wind turbine and as a result prevent damage. This receptor size will therefore provide higher protection efficiency than other receptor sizes and is therefore recommended.

# Chapter 5

# Pollution and Offshore Wind Turbine Lightning Protection

## 5.1 Introduction

Pollution of the blade can influence the maximum electric field strength required for the initiation of upward leader from wind turbine. In chapter 4 above, the size of receptor, and its position on the blade, and their effect on lightning protection systems were investigated. Initially, in this chapter, the effect of pollution on the performance of the receptor is evaluated and estimated on a full-scale offshore wind turbine. Secondly, two lightning protection systems (metallic cap and receptor methods) commonly in use are applied on a full scale polluted offshore wind turbine and compared. A new protection system with higher lightning protection efficiency is developed. Vesta V100-2MW wind turbine model is used.

## 5.2 The Effect of Pollution on Offshore Wind Turbine Blade Lightning Protection System's Performance

As the number and size of modern wind turbines are increasing, lightning damages has also increased with the blades at the highest risk [1]. Offshore windfarm data shows that most lightning strikes to wind turbines happen during winter months [37], and that winter lightning occurs frequently [191]. Characteristics of winter lightning on wind turbines [192] in coastal Part of the sea of Japan was discussed in [193]. Compared to summer clouds, winter clouds which develop at lower altitudes are more capable of developing

higher electric fields at ground. The current duration of winter lightning is usually very long, and it tends to strike tall structures such as wind turbines intensively. Since its energy is remarkably large, winter lightning causes considerable damage. Sinha et al. [194], did a study of offshore wind farm maintenance optimization by using risk based failure analysis. Nearshore regional behavior of lightning was studied by [195] regarding its interaction with wind turbines. Soloot et al. [196], studied switching overvoltage observed in offshore wind farm. Temporal and spatial measurements was used for detecting salt deposit on a Glass Fibre Reinforced Plastic (GFRP) Material in [197]. Attachment of lightning to wind turbine surfaces due to internal blade conditions was shown in [198]. Winds are stable and strong at the ocean owing to the absence of structures blocking the wind. When wind turbine is located offshore and in contact with salt water, it gets polluted with salt deposit which causes its insulation strength to decrease and raising the conductivity which could result in the blade going into competition with the receptors for lightning attachment. The problem with this is that Streamers can propagate from the surface of the blade instead of the receptors and as an unintended lightning part, the blade is severely damaged when hit by lightning. As compared to unpolluted blade surface, the conductivity as well as the relative permittivity are increased as observed from the distributed electric potential on the surrounding air and the blade surface.

The relative electric permittivity of water decreases as the temperature rises, for example, at 0°C its relative permittivity is 88, at 20°C it is 80.1, at 100°C it is 55.3 and at 200°C it is 34.5. Hasted (1948) experimentally conducted study on the dielectric properties of salt-water solutions, a dielectric decrement with salt concentration was observed. This means that the addition of sodium chloride to water results in a reduction in electrical permittivity.

There is an electric field between sodium and chloride ions when they dissociate in solution. The polarized water molecules, under the effect of the electric field get oriented so that their oxygen atoms (a partial negative charge carrier) face toward the sodium ion then their hydrogens (partial positive charges carrier) face toward the chloride ion. The polar water molecules orientation causes its own electric field that cancels out most of the electric field that would be present if the ions were in a vacuum. The result is that the sodium and chloride ions are well 'shielded' by a 'hydration shell' of polarized water molecules which effectively reduces the applied external field and hence lowering the electric permittivity (dielectric constant) as the ionic concentration increases.

The risk of lightning striking offshore wind turbine is higher because they are subjected to moisture, contaminations such as dust, sand and salt. When these contaminations accumulate on the surface of the blade, for instance, if it gets polluted with salt deposit, it can cause its insulation strength to decrease and raise the conductivity which can greatly affect the interception efficiency of the receptor. The problem with this is that on lightning strike, streamers can initiate and propagate from the surface of the blade instead of the receptors and as an unintended lightning part, the blade is severely damaged, and puncture of the blade can occur. This is a major problem for the wind industry.

Lightning protection of wind turbine has attracted research. Wang et al. [40], investigated the effects of receptors on lightning protection of wind turbine blades. Kumar et al. [199], used a remote laser-induced breakdown spectroscopy (LIBS) technique for the detection and quantification of salt deposits on wind turbine blade surface.

It has been found that pollution affects the performance of the receptor. i.e., if receptor A is used on an unpolluted blade, and the same receptor is also used on a polluted blade, that

same receptor will perform better in an unpolluted blade condition. Therefore, understanding the extent pollution can affect the receptor, will enable the design engineer to improve on the properties of the receptor.

The effect of Pollution on wind turbines has been experimentally evaluated as in [44, 45] however, a small blade tip section was used and not full blade length, more also, the performance of the receptor considering pollution has not been considered in literature and are not suggested in the current lightning protection standards. Up to date, the level of pollution influence on receptor performance has not been estimated and simulation studies associated to this topic have rarely been reported. The effect of pollution on offshore wind turbine receptor performance is very important to enable improvement on the protection systems.

In this section, by comparing the electric field strength as the blade surface conductivity is changed and the blade is rotated, the effect of pollution on lightning protection systems is evaluated. The wind turbine model used in this investigation is Vesta V100-2MW and the receptor is 1.5 m away from the blade tip. The evaluation is done as the blade is rotated through $-60^0$, $-55^0$, $-50^0$, $-45^0$, $-40^0$, $-35^0$, $-30^0$, $-25^0$, $-20^0$, $-15^0$, $-10^0$, $-5^0$, $0^0$, $5^0$, $10^0$, $15^0$, $20^0$, $25^0$, $30^0$, $35^0$, $40^0$, $45^0$, $50^0$, $55^0$ and $60^0$ from the vertical position. As in previous analysis, the blade in the vertical position in Figure 3-3 is referred to as blade A and only the results for blade A are provided. Also, values are obtained from the receptor tip. The focus is on evaluating the maximum electric field strength required for the initiation of upward leader due to thunder cloud charge. The simulation for polluted blades condition is done with values of the conductivity of the blades at 0.9 S/m and relative permittivity

80, this corresponds to the value of salt-water [45], the relative permittivity for normal water is higher than this value.

### 5.2.1 *Unpolluted Wind Turbine Blades*

The model is first simulated without protection by deactivating the three receptors. The turbine is then protected by activating the receptors. When the receptors are activated, field enhancement is seen around them. It is also possible to have field enhancement on the blade surface instead of the receptor. Note that in this case, the turbine is protected but not polluted. Figure 5-1 and Figure 5-2 shows the simulation model for unpolluted wind turbine blade condition used in the comparison of the maximum electric field strength distribution.

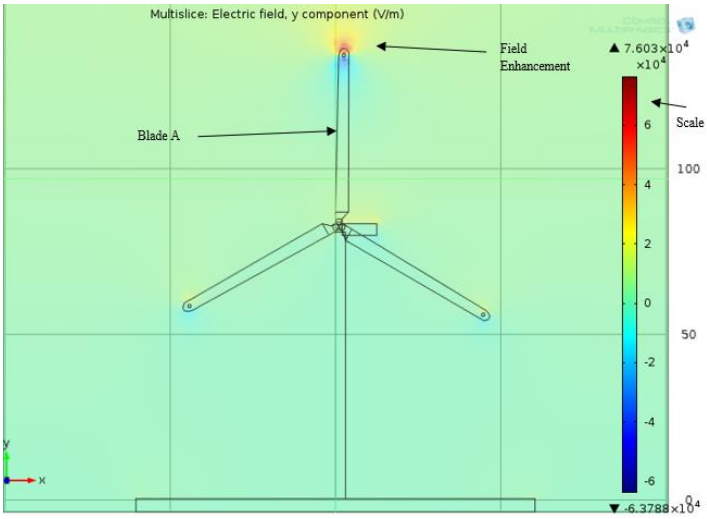


Figure 5-1. unpolluted wind turbine

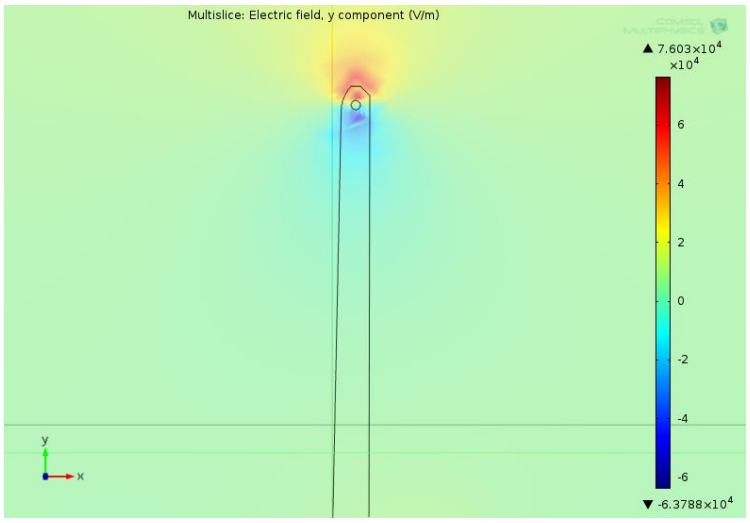

Figure 5-2. unpolluted wind turbine blade

The protected model was simulated with a single receptor at the tip of each blade. As compared to the unprotected condition, the blade is protected but unpolluted. The tip enhancement around various receptors is shown and the value for the maximum electric field strength for blade A is shown in table 9. This value is 89.71 kV/m when blade A is in the vertical position. Note that the relative permittivity for the blade is 4.2 and Conductivity:$1.0 \times 10^{-14}$ S/m.

When upward lightning does not incept from the receptor, then, any part of the blade with the highest stress corresponding to largest electric field strength will be the likely attachment point. There are reports of multiple discharge in the turbine associated with nearby cloud to ground lightning [30], and also strikes attaching inboard on the blade due to dart leader [31].

### 5.2.2 *Polluted Wind Turbine Blades*

The turbine model is protected and polluted. In this condition, the simulation for polluted turbine blades condition is done with values of the conductivity of the blades at 0.9 S/m

and relative permittivity 80, this corresponds to the value of salt-water. Figure 5-3 and Figure 5-4 shows the simulation model for polluted wind turbine blade condition used in the comparison of the maximum electric field strength distribution.

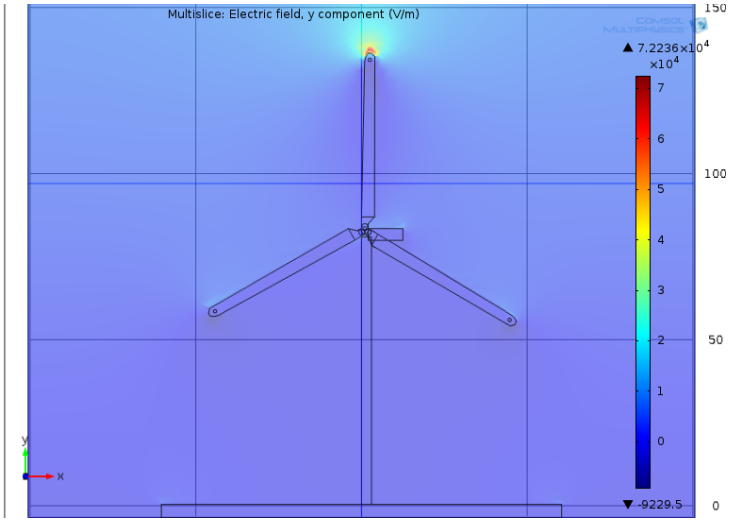


Figure 5-3. Polluted wind turbine

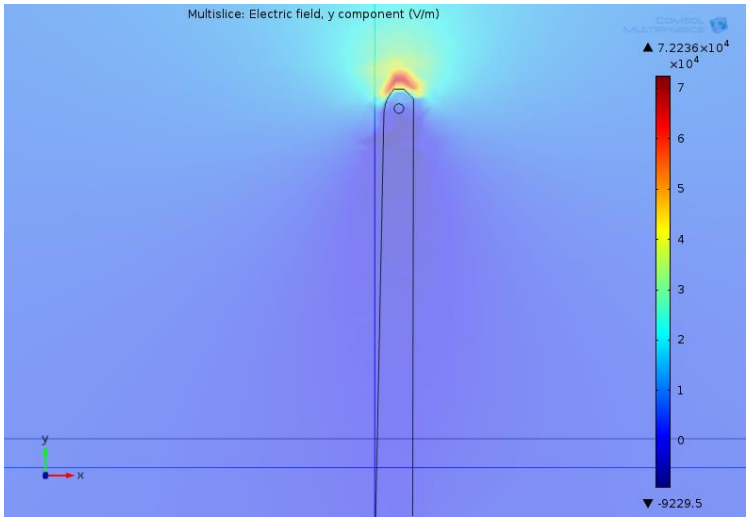


Figure 5-4. Polluted wind turbine blade

The polluted condition was simulated and the tip enhancement around various receptors is also shown and the value for the maximum electric field strength for blade A is shown in table 6. This value is 5.96 kV/m when blade A is in the vertical position. This is a significant reduction on the field enhancement by the receptors.

Table 9. Maximum electric field strength distribution (kV/m) at the receptor tip on blade A for various blade condition

| Maximum electric field strength Kv/m on the Receptor tip | | |
|---|---|---|
| Angle from Vertical | Unpolluted | Polluted |
| $-60^0$ | 29.28 | 1.93 |
| $-55^0$ | 36.34 | 2.41 |
| $-50^0$ | 42.89 | 2.87 |
| $-46^0$ | 29.16 | 1.95 |
| $-40^0$ | 56.13 | 3.73 |
| $-35^0$ | 65.96 | 4.47 |
| $-30^0$ | 68.67 | 4.60 |
| $-20^0$ | 80.44 | 5.45 |
| $-15^0$ | 82.15 | 5.52 |
| $-10^0$ | 90.46 | 5.99 |
| $0^0$ | 89.71 | 5.96 |
| $10^0$ | 85.26 | 5.71 |
| $15^0$ | 86.04 | 5.72 |
| $20^0$ | 63.41 | 4.30 |
| $26^0$ | 76.08 | 5.10 |
| $30^0$ | 69.39 | 4.57 |
| $35^0$ | 66.20 | 4.41 |
| $40^0$ | 56.87 | 3.76 |
| $45^0$ | 61.44 | 4.22 |
| $50^0$ | 43.12 | 2.83 |
| $55^0$ | 35.38 | 2.29 |
| $60^0$ | 31.29 | 2.04 |

The table above shows the effect of pollution on the receptor. The interception efficiency is dampened by pollution. As the blade is rotated from $-60^0$ to $+60^0$, it is observed that the values of the maximum electric field strength required for the initiation of upward leader is uniformly reduced for the polluted condition when compared with the unpolluted condition. Therefore, leader might incept from the blade surface earlier than the receptor in the polluted blade condition, which might cause severe damage to the wind turbine. The values for when blade A is in the vertical position which represents the critical position is plotted below in Figure 5-5. The percentage damping at this instance is evaluated.

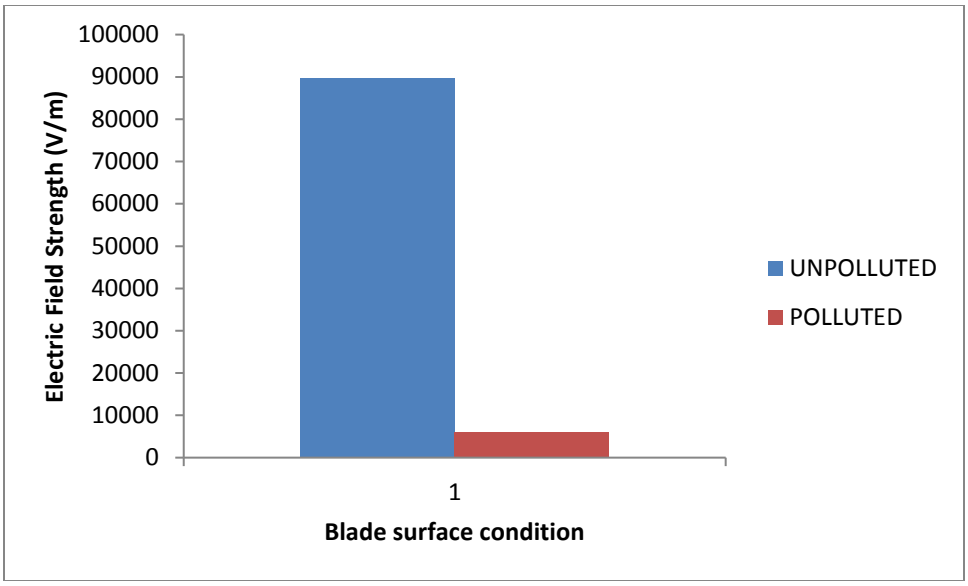


Figure 5-5. Pollution effect on the receptor

The effect of pollution on the receptor is depicted in the plot above. A damping of

89707.9712V/m - 5961.671163V/m = 83746.300037V/m is estimated.

Therefore, % damping,

$$X = \frac{83746 \times 100}{89708}$$

$$= 93\%$$

is estimated at blade A in the vertical position.

The maximum electric field strength at the receptor tip as the blade is rotated and at different positions of the blade are shown in table and plots above. It is found that pollution dampens the performance of the receptor by 93% and on average, the general performance of the receptor in a polluted blade condition is found to be less than 10%. If receptor A for instance, is used on an unpolluted blade, and the same receptor is also used on a polluted blade, that same receptor will perform better in an unpolluted blade condition, i.e. under the same condition, upward leader can initiate from a receptor used in an unpolluted blade condition earlier than the polluted blade condition. This indicates that offshore wind

turbines are at higher risk of failure of its lightning protection systems and are prone to higher probability of damage.

In this section, the effects of pollution on the efficiency of lightning protection system of wind turbine has been investigated. The vertical tri-pole model has been used to create an ambient field which is used to study the variations in maximum electric field strength required for the initiation of upward leader from wind turbine, this is done with COMSOL Multiphysics software. By comparing the electric field strength as the blade surface condition is changed from unpolluted to polluted and the blade is rotated, the damping effect of pollution on the proficiency of the receptor is estimated. Point of initiation of upward leader was compared with experimental data to validate the efficiency of applied numerical model. Results show that pollution dampens the performance of the receptor by 93% and on average, the general performance of the receptor in a polluted blade condition is found to be less than 10%. Indicating that offshore wind turbines are at higher risk of failure of its lightning protection systems and are prone to higher probability of damage.

## 5.3 Performance Enhancement for Offshore Wind Turbine Blade Lightning Protection Systems

In this section, two lightning protection systems commonly in use are applied on a full scale polluted offshore wind turbine and compared initially. The blades are polluted and rotated. Finally, an enhanced system, a new method comprising a metallic cap at the tip of the blade and a receptor at the middle of the blade is designed, investigated and compared with the two methods. This was found to influence the electric field distribution immensely.

The proposed method will increase the lightning protection efficiency of offshore wind turbines.

### 5.3.1 *Lightning Protection Systems on the Blade*

Two configuration of blade protection systems commonly used with offshore wind turbine are considered with various specification;

(1) Receptor: A disk type receptor made of copper (conductivity: $6.0 \times 10^{-7}$S/m), 10 mm in diameter, inserted at 1.5 m away from the blade tip [190], and connected to ground. This is shown in Figure 5-6.

(2) Metallic cap: In this system, 150 mm tip part of the blade is completely covered with copper foil and connected to ground, Figure 5-7.

The protection systems are connected to the down conductor inside the blade shell.

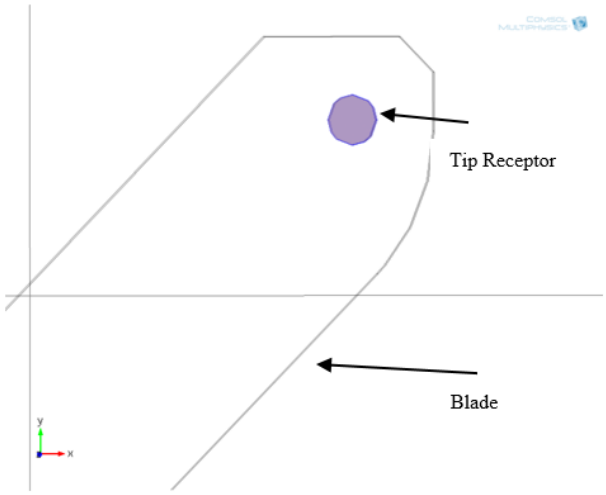


Figure 5-6. Tip receptor design

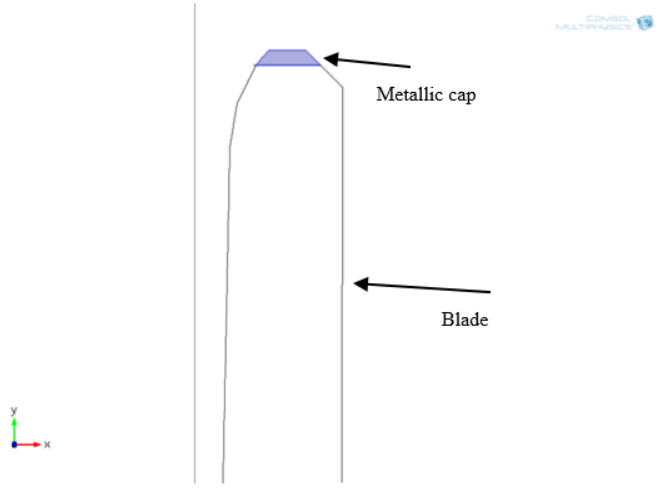


Figure 5-7. The metallic cap design

### 5.3.2 *Evaluation Conditions*

Figure 5-8 (a). Shows the model for rotation mode. As the blade rotates, it was tested in selected five positions to investigate the performance of offshore wind turbine lightning protection systems on initiation of upward leader. The positions of the blade are chosen to determine the complete successes and failures of each protection systems. These positions are shown in Figure 5-8. They are; (b) vertical, (c) $45^0$ (Trailing edge facing the cloud) (TEFC), (d) $45^0$ (Leading edge facing the cloud) (LEFC), (e) horizontal (Trailing edge facing the cloud) (TEFC), and (f) horizontal (Leading edge facing the cloud) (LEFC).

The blade in the vertical position in Figure 5-8 (a) is referred to as blade A and only the results for blade A are provided.

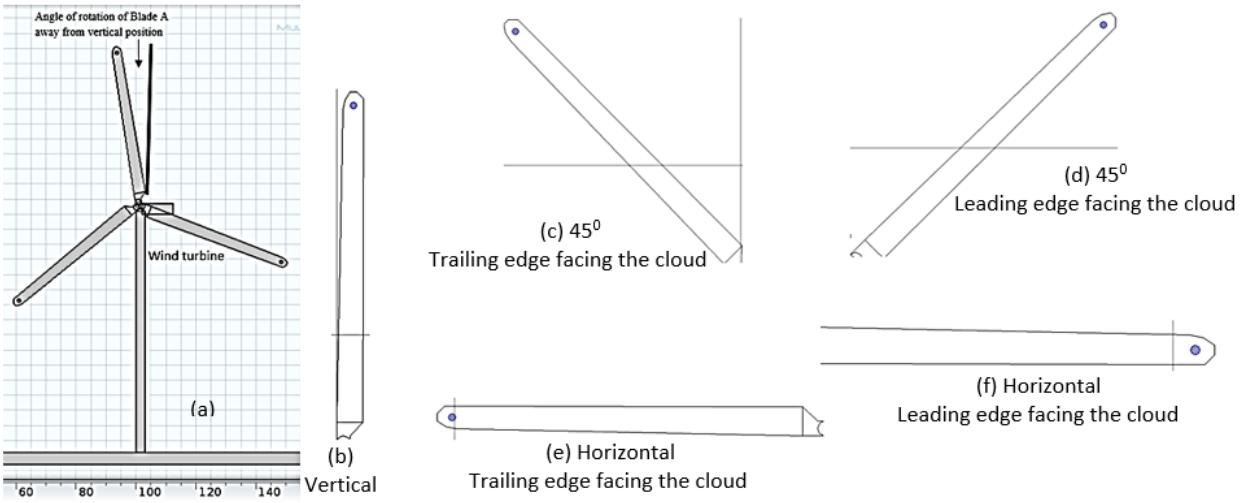


Figure 5-8. (a) Model for rotation mode, (b, c, d, e and f) Arrangement of blade sample

The results for each protection system are discussed in the following subsections. Results are plotted and compared for values obtained from the blade surface and the lightning protection system. The most efficient method is the one with highest electric field on the lightning protection system and minimum on the blade surface. For a better understanding of the reader, the initial comparison plot between the receptor method and the metallic cap method are not shown separately but are shown with the three methods combined.

### 5.3.3 *Receptor Method*

The simulation is conducted with the receptor method considering the arrangements shown in Figure 5-8. Initially, the model is simulated for unpolluted blade (shown in Figure 5-9), and then the blade is polluted. Details of results for the unpolluted blade were already shown in previous chapters as such not repeated here. The polluted blade condition is exclusively for offshore wind turbines. Due to pollution, offshore wind turbines condition is different than that of onshore wind turbines. This is particularly important for wind

turbines owners who can apply the results for unpolluted blade condition for onshore wind turbines only.

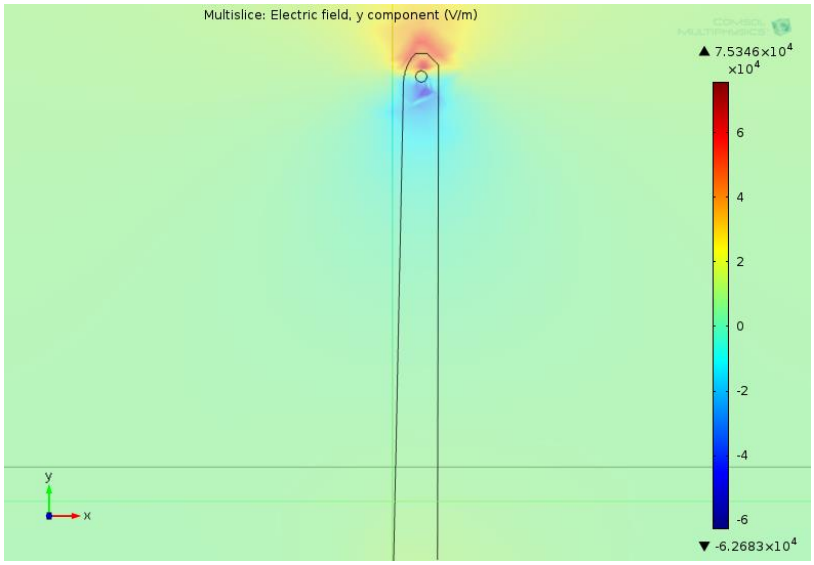


Figure 5-9. Unpolluted blade with receptor method

Details of the activities such as field enhancement around the protection methods for unprotected, unpolluted and polluted wind turbine blade were already given in [190].

The simulation for the polluted blade arrangement for the receptor method is shown below in Figure 5-10.

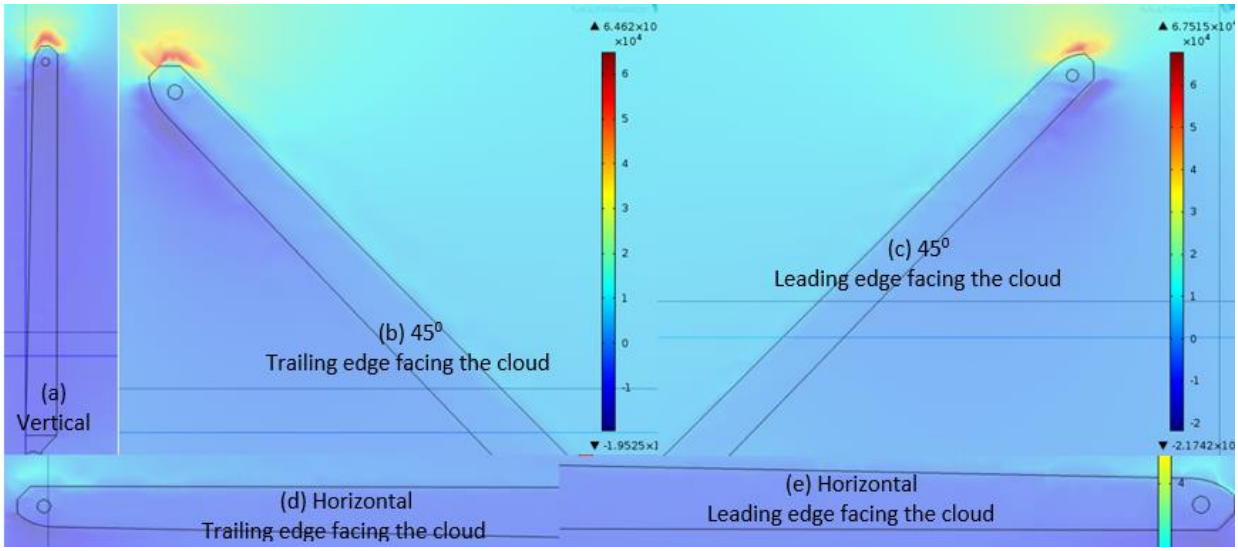


Figure 5-10. Polluted blade arrangement for the receptor method

It shows the maximum electric field distribution as blade A is rotated through; (a) vertical, (b) $45^0$ (Trailing edge facing the cloud), (c) $45^0$ (Leading edge facing the cloud), (d) horizontal (Trailing edge facing the cloud), and (e) horizontal (Leading edge facing the cloud).

Generally, the electric field strength around the tip region is higher than that at the inboard region. This is supportive of laboratory experiments and field survey demonstrating that the tip is more exposed than other parts [1], and that upward lightning leader is more likely to originate from the tip of the lightning protection system. The locations with higher electric field strength are considered to have higher possibility of inception of upward leader.

The results for the maximum electric field distribution on the receptor as well as on the blade surface for various arrangements are tabulated in Table below and the comparison with other methods are plotted.

### 5.3.4 *Metallic Cap Method*

The simulation is also conducted with the metallic cap method considering the arrangements shown in Figure 5-8. The simulation for unpolluted blade (shown in Figure 5-11), and then the blade is polluted.

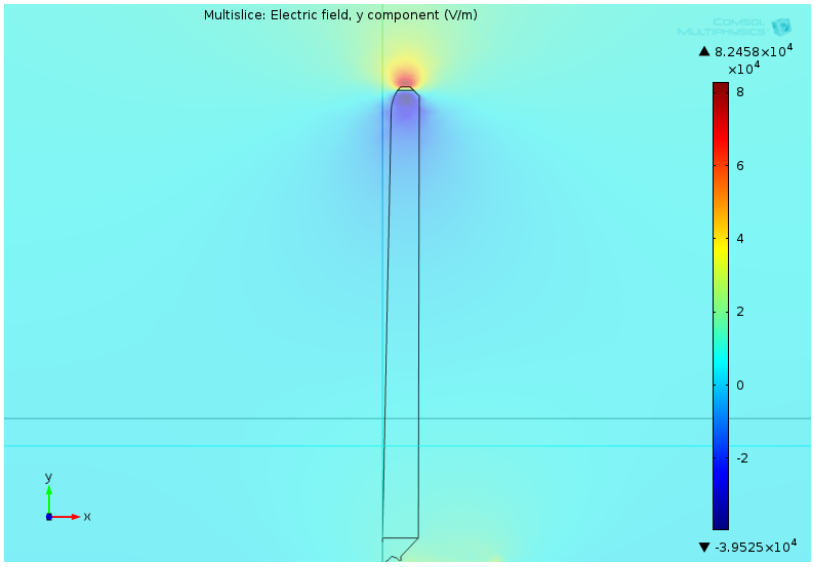


Figure 5-11. Unpolluted bade with metallic cap method

The simulation for the polluted blade arrangement for the metallic cap method is shown below in Figure 5-12.

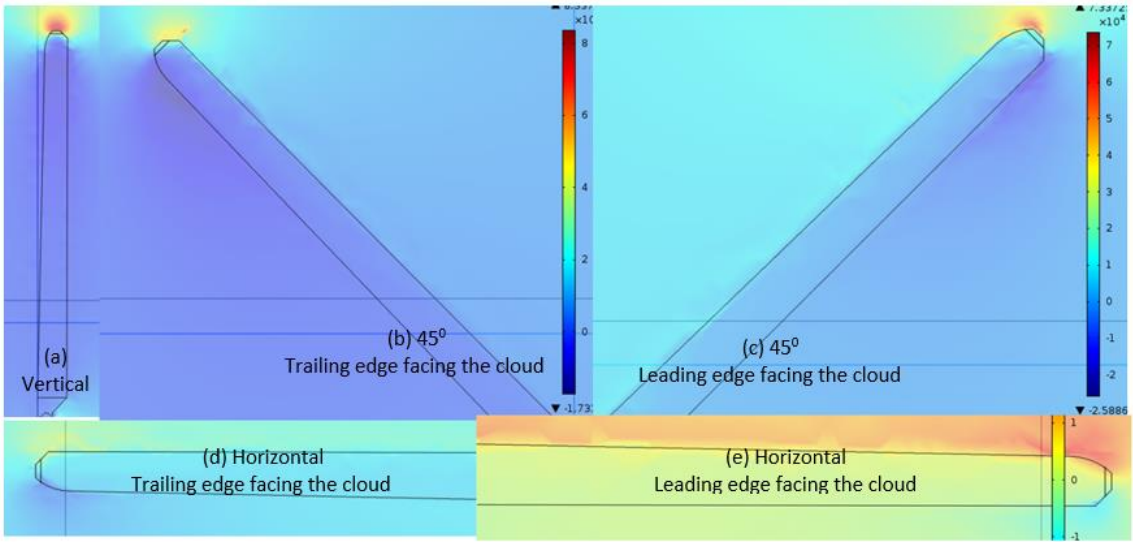


Figure 5-12. Polluted blade arrangement for the metallic cap method

The results for the maximum electric field distribution on the tip of the metallic cap as well as on the blade surface for various arrangements are tabulated in Table 8 and the comparison with other methods is also plotted.

### 5.3.5 *Performance Enhancement method*

Research has shown that pollution has been found to dampen the performance of the protection devices. Existing protection systems, even though they perform well in unpolluted wind turbines, the same protection system performs poorly when applied on a polluted wind turbine. The metallic cap method performs better than other method in some arrangements but failed in some others [44].

In the performance enhancement method, the performance of the metallic cap was improved by adding a receptor at the middle of the blade. The model is shown in Figure 5-13.

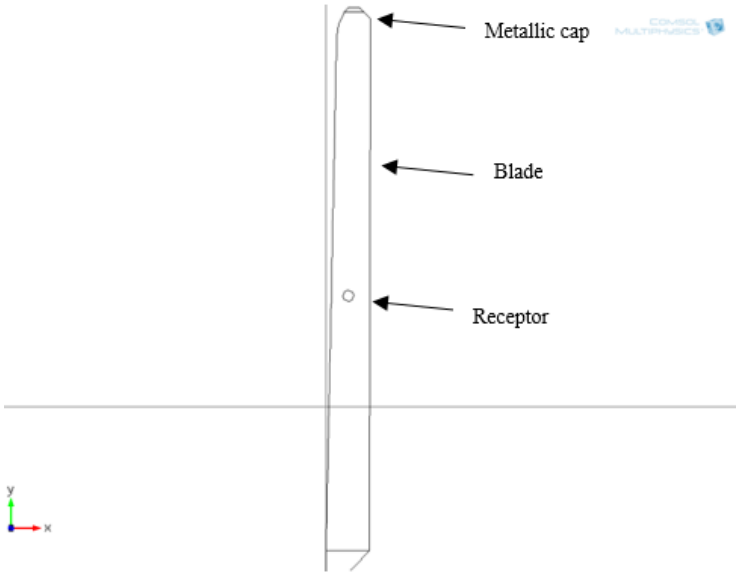


Figure 5-13. Enhanced method

The enhanced method is applied on the polluted wind turbine, evaluated and compared considering the arrangements shown in Figure 5-8. The simulation is shown in Figure 5-14.

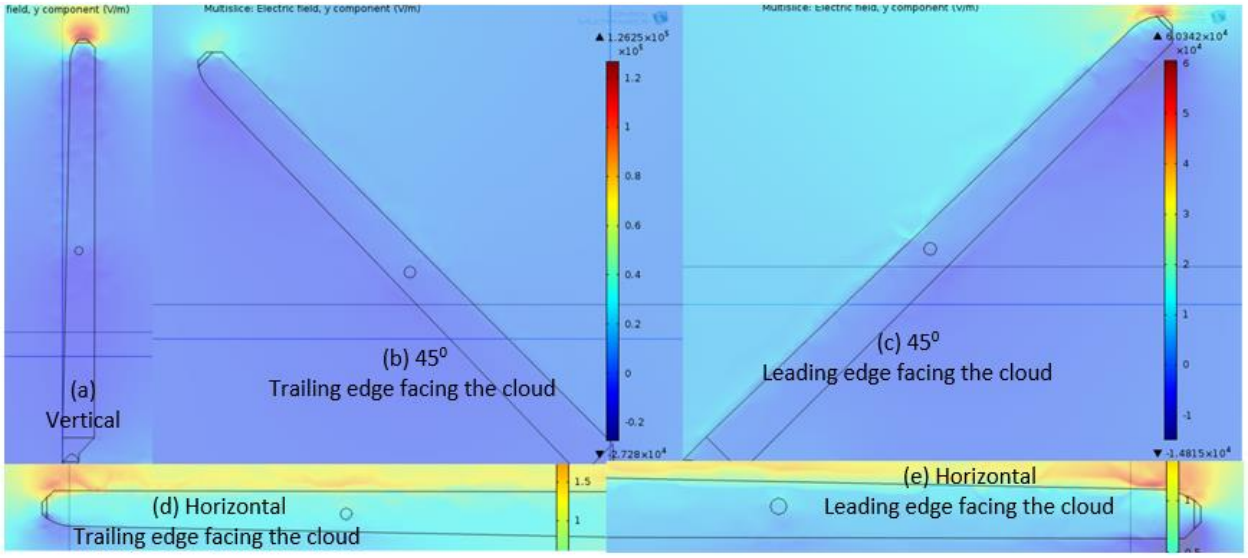


Figure 5-14. Polluted blade arrangement for enhanced method

The results for the maximum electric field distribution for the new method as well as on the blade surface for various arrangements are tabulated and the comparison with other methods are shown.

Table 10, 11 and 12 provides details of the maximum electric field strength on various protection systems and on the polluted blade surfaces for various arrangement.

Table 10 Maximum electric field strength Kv/m with the Receptor method

| Blade position | Maximum electric field strength | |
|---|---|---|
| | Receptor tip | Blade surface |
| Vertical | 7.12 | 0.43 |
| $45^0$ (TEFC) | 5.66 | 0.64 |
| Horizontal (TEFC) | 0.54 | 2.13 |
| $45^0$ (LEFC) | 3.97 | 0.46 |
| Horizontal (LEFC) | 1.66 | 1.16 |

Table 11 Maximum electric field strength Kv/m with the Metallic cap method

| Blade position | Maximum electric field strength | |
|---|---|---|
| | Metallic Cap tip | Blade surface |
| Vertical | 54.39 | 0.26 |
| $45^0$ (TEFC) | 30.87 | 0.34 |
| Horizontal (TEFC) | 0.37 | 1.74 |
| $45^0$ (LEFC) | 17.47 | 1.44 |
| Horizontal (LEFC) | 2.43 | 1.31 |

Table 12 Maximum electric field strength Kv/m with the Enhanced Method

| Blade position | Maximum electric field strength | |
|---|---|---|
| | Metallic Cap tip | Blade surface |
| Vertical | 53.68 | 0.25 |
| $45^0$ (TEFC) | 31.87 | 0.33 |
| Horizontal (TEFC) | 0.55 | 1.63 |
| $45^0$ (LEFC) | 26.10 | 0.45 |
| Horizontal (LEFC) | 2.43 | 0.75 |

The results for maximum electric field strength distributions for various configurations obtained from the protection systems and the blade surfaces as blade A is rotated are plotted in Figure 5-15 to Figure 5-24. As was said earlier, the most efficient method is the one with highest electric field on the lightning protection system and minimum on the blade surface.

*(a) Vertical (Protection System)*

The plot for the maximum electric field strength distribution on the three protection systems while the blade is in the vertical position is shown in Figure 5-15

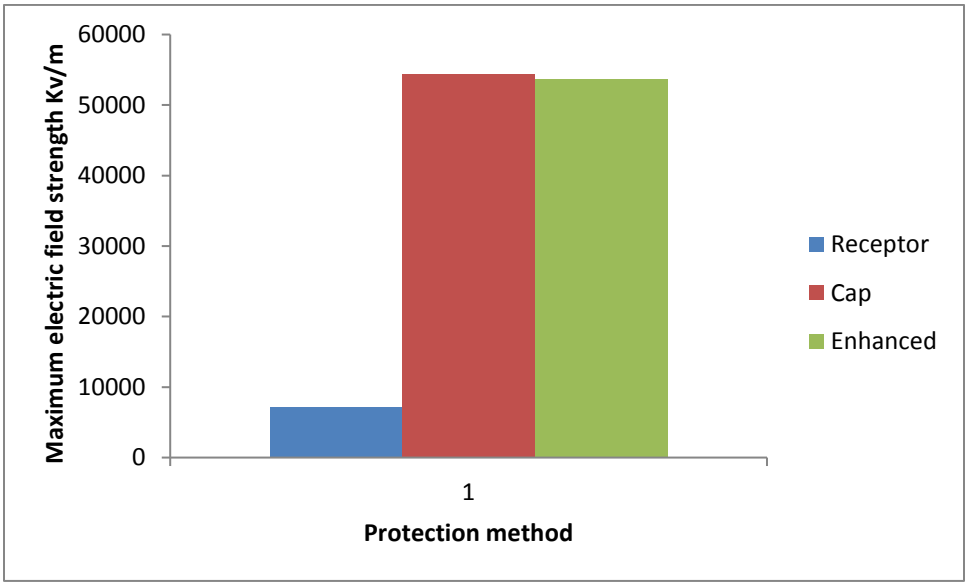


Figure 5-15. Maximum electric field strength distributions on the protection system for vertical position

It is observed that with blade A in the vertical position, the maximum electric field strength for the metallic cap method is higher followed by the enhanced method and lowest for the

receptor method. Since the metallic cap method has the highest value on the cap, it is more proficient at this position than other methods.

*(b) Vertical (Blade Surface)*

The plot for the maximum electric field strength distribution on the blade surface for the three protection systems while the blade is in the vertical position is shown in Figure 5-16

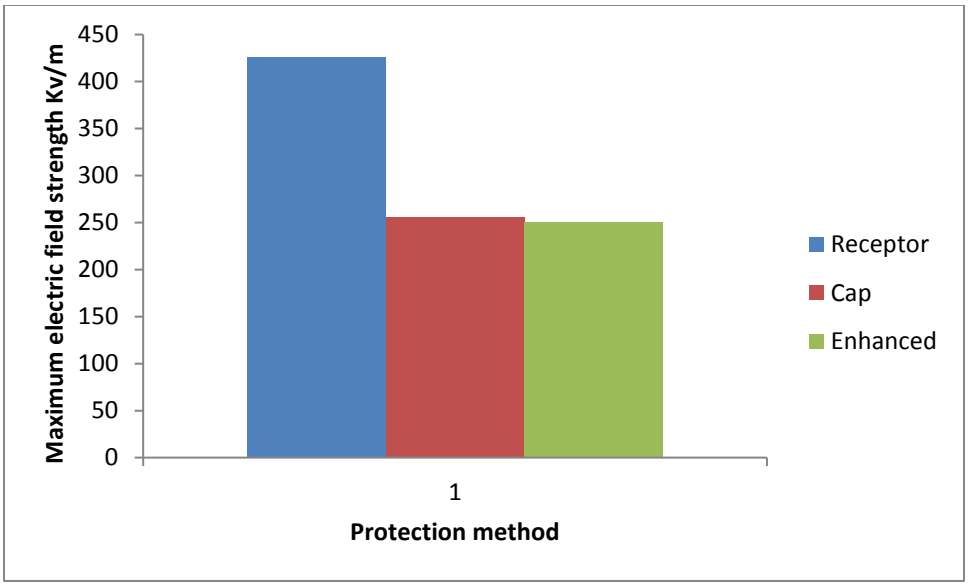


Figure 5-16. Maximum electric field strength distributions on the blade surface for vertical position

From Figure 5-16 above, with blade A in the vertical position, the maximum electric field strength for the receptor method is higher followed by the metallic cap method and lowest for the enhanced method. Since the enhanced method has the lowest value on the blade surface, it is more proficient at this position than other methods.

*(c)$45^0$ (TEFC) (Protection System)*

The plot for the maximum electric field strength distribution on the protection system on the three protection systems while the blade is in the $45^0$ (TEFC) from the vertical position is shown in Figure 5-17 below

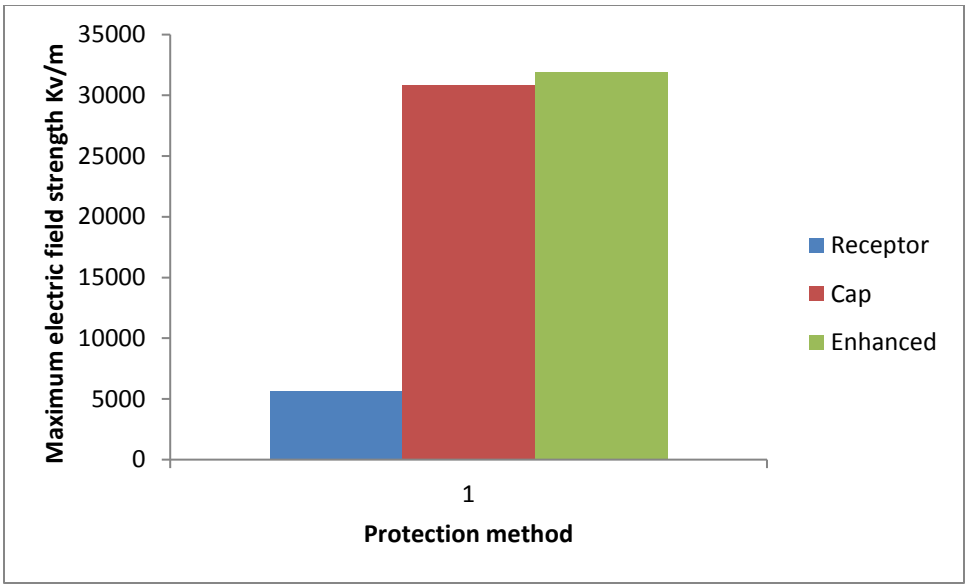


Figure 5-17. Maximum electric field strength distributions on the protection system for $45^0$ (TEFC) position

From the plot above, with blade A $45^0$ (TEFC) from the vertical position, the maximum electric field strength for the enhanced method is higher followed by the metallic cap method and lowest for the receptor method. Since the enhanced method has the highest value on the cap, it is more proficient at this position than other methods

*(d) $45^0$ (TEFC) Blade Surface*

The plot for the maximum electric field strength on the blade surface for the three protection systems while the blade is $45^0$ (TEFC) from the vertical position is shown in Figure 5-18 below

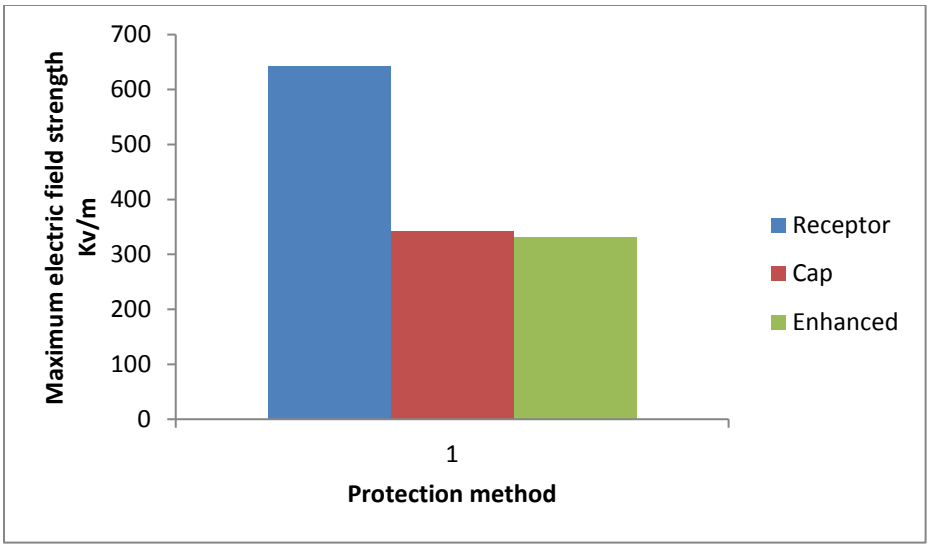


Figure 5-18. Maximum electric field strength distributions on the blade surface for $45^0$ (TEFC) position

From Figure 5-18 above, with blade A $45^0$ (TEFC) from the vertical position, the maximum electric field strength for the receptor method is higher followed by the metallic cap method and lowest for the enhanced method. Since the enhanced method has the lowest value on the blade surface, it is more proficient at this position than other methods.

*(e) Horizontal (TEFC) (Protection System)*

The plot for the maximum electric field strength at the tip of the protection system on the three protection systems while the blade is in the horizontal (TEFC) position is shown in Figure 5-19. below

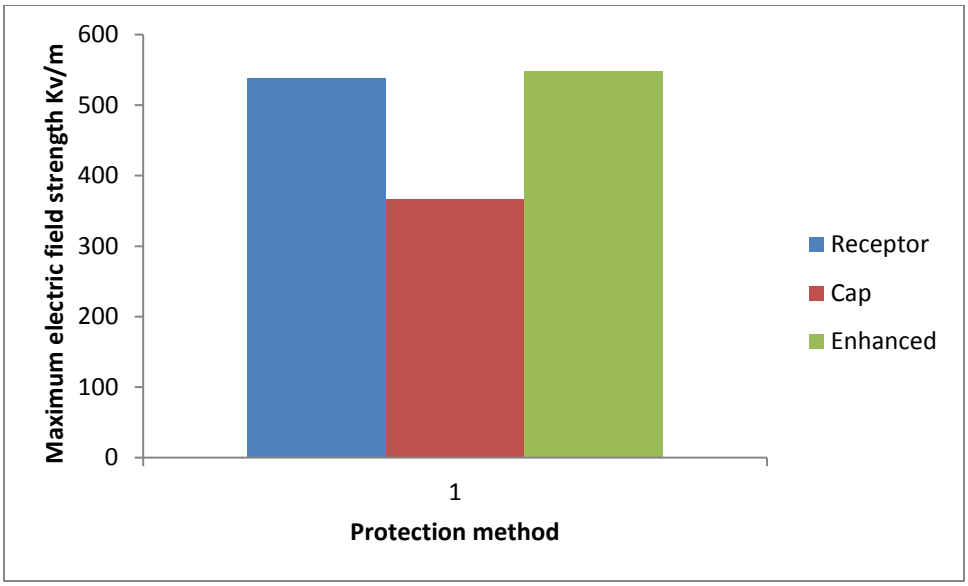


Figure 5-19. Maximum electric field strength distributions on the protection system for horizontal (TEFC) position

From the plot above, with blade A in the horizontal (TEFC) position, the maximum electric field strength for the enhanced method is higher followed by the receptor method and lowest for the metallic cap method. Since the enhanced method has the highest value on the cap, though with a small margin, it is more proficient at this position than other methods

*(f) Horizontal (TEFC) (Blade Surface)*

The plot for the maximum electric field strength distribution on the blade surface for the three protection systems while the blade is in the horizontal (TEFC) position is shown in Figure 5-20 below

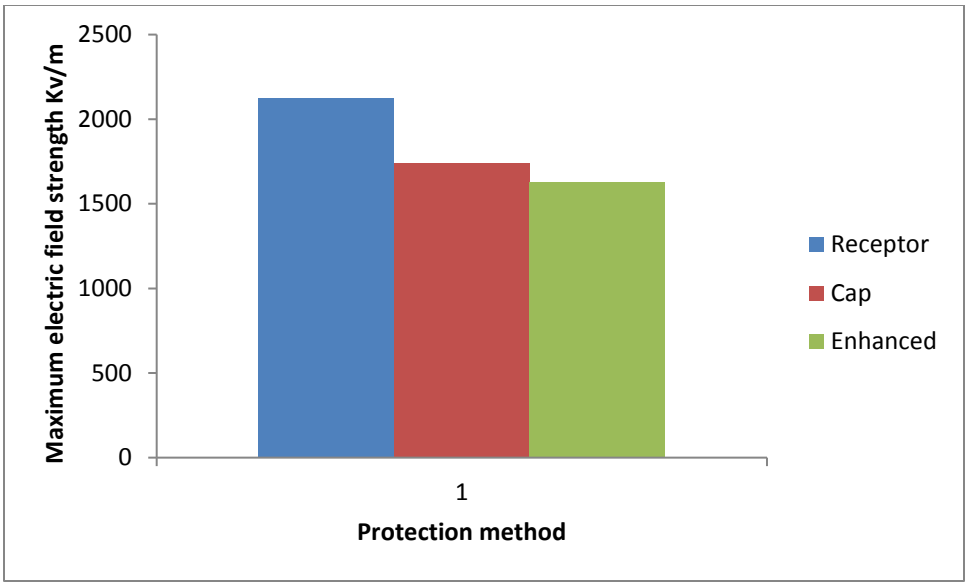


Figure 5-20. Maximum electric field strength distributions on the blade surface for horizontal (TEFC) position

From above plot, with blade A in the horizontal (TEFC) position, the maximum electric field strength for the receptor method is higher followed by the metallic cap method and lowest for the enhanced method. Since the enhanced method has the lowest value on the blade surface, it is more proficient at this position than other methods.

*(g) $45^0$ (LEFC) (Protection System)*

The plot for the maximum electric field strength on the protection system for the three protection systems while the blade is $45^0$ (LEFC) from vertical position is shown in Figure 5-21 below

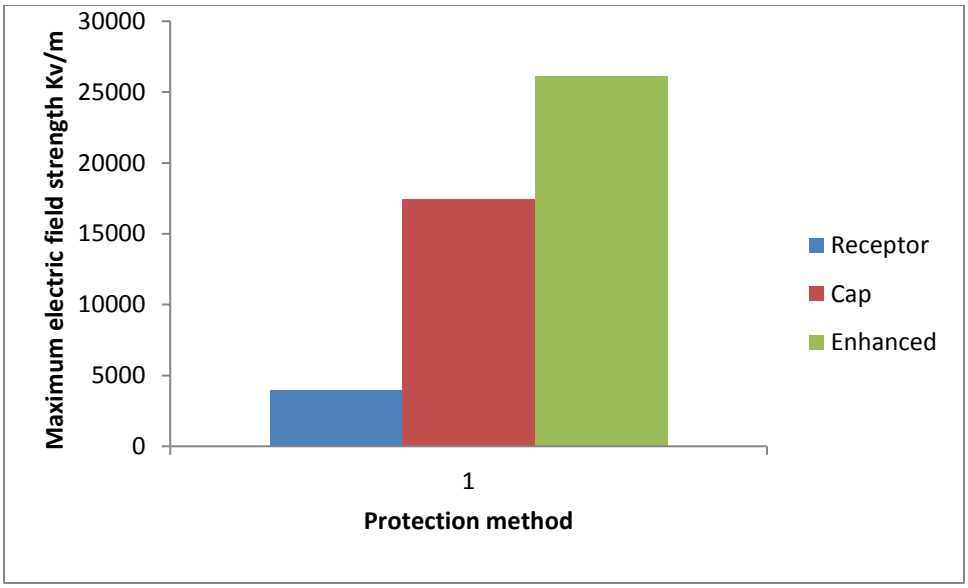


Figure 5-21. Maximum electric field strength distributions on the protection system for $45^0$ (LEFC) position

From the plot above, with blade A $45^0$ (LEFC) position, the maximum electric field strength for the enhanced method is higher followed by the metallic cap method and lowest for the receptor method. Since the enhanced method has the highest value on the cap, it is more proficient at this position than other methods

*(h) $45^0$ (LEFC) (Blade Surface)*

The plot for the maximum electric field strength on the blade surface for the three protection systems while the blade is $45^0$ (LEFC) from vertical position is shown in Figure 5-22 below

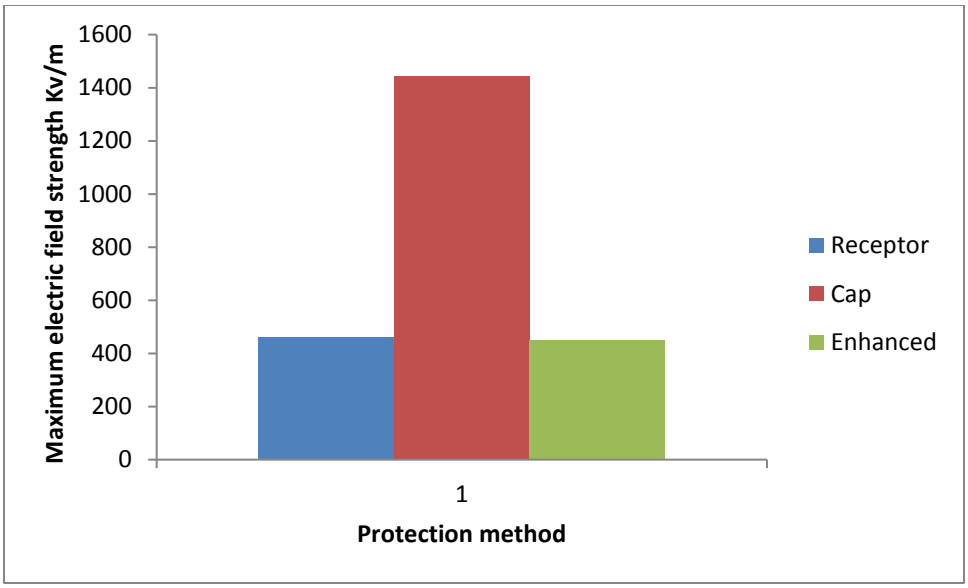


Figure 5-22. Maximum electric field strength distributions on the blade surface for $45^0$ (LEFC) position

As seen in the above plot, with blade A $45^0$ (LEFC) position, the maximum electric field strength for the metallic cap method is higher followed by the receptor method and lowest for the enhanced method. Since the enhanced method has the lowest value on the blade surface, it is more proficient at this position than other methods.

*(i) Horizontal (LEFC) (Protection System)*

The plot for the maximum electric field strength distribution on the protection system for the three protection systems while the blade is in the horizontal (LEFC) position is shown in Figure 5-23 below.

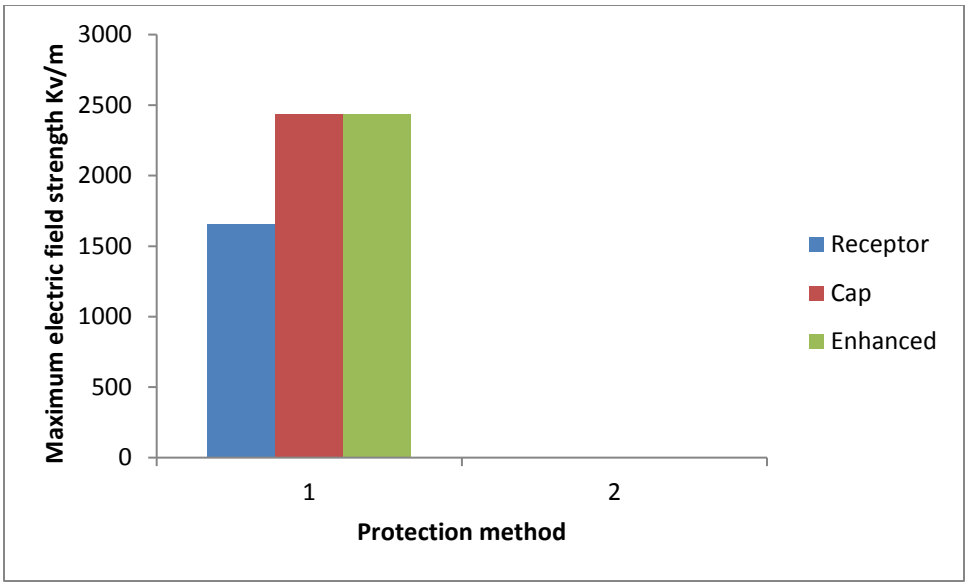


Figure 5-23. Maximum electric field strength distributions on the protection system for horizontal (LEFC) position

With blade A in horizontal (LEFC) position, the maximum electric field strength for both the metallic cap method and the enhanced method is the same and higher compared to the receptor method. Since the metallic cap and the enhanced both has the highest value on the cap, they are more proficient at this position than the receptor method.

*(j) Horizontal (LEFC) (Blade Surface)*

The plot for the maximum electric field strength distribution on the blade surface for the three protection systems while the blade is in the horizontal (LEFC) position is shown in Figure 5-24. below

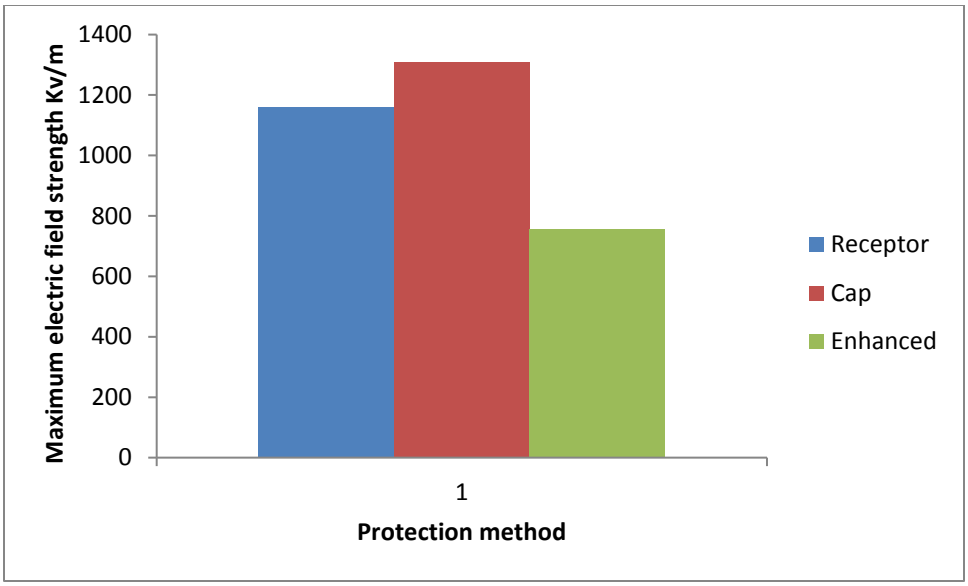


Figure 5-24 Maximum electric field strength distributions on the blade surface for horizontal (LEFC) position

From the plot, with blade A in horizontal (LEFC) position, the maximum electric field strength for the metallic cap method is higher followed by the receptor method and lowest for the enhanced method. Since the enhanced method has the lowest value on the blade surface, it is more proficient at this position than other methods.

Considering efficient lightning protection, the presence of the protection system should ensure that the electric field on the blade surface is kept minimum but maximum on protection system so that leader will incept from the protection system first. On the average, the new protection system (the enhanced method) has the highest maximum electric field on the protection system and lower on the blade surface. The electric field at the metallic cap of a blade protected with the enhanced method is found to be boosted when compared to other methods. Adding a receptor at the middle of a blade protected by the metallic cap method was found to influence the electric field distribution immensely.

In this section, two lightning protection systems (metallic cap and receptor methods) commonly in use have been applied on a full scale polluted offshore wind turbine and compared for efficiency in lightning protection. In the performance enhancement method, the performance of the metallic cap was improved by adding a receptor at the middle of the blade. This was found to influence the electric field distribution immensely. The new method was compared with the metallic cap method and the tip receptor method. The new method performed better. It can greatly improve the lightning protection performance for offshore wind turbines.

## 5.4 Conclusion

The extended vertical tri-pole model has been used to evaluate the maximum electric field strength required for the initiation of upward leader from the wind turbine. Initially, in this chapter, the effect of pollution on the performance of the receptor is evaluated and estimated on a full-scale offshore wind turbine. It is found that pollution dampens the performance of the receptor by 93% and on average, the general performance of the receptor in a polluted blade condition is found to be less than 10%. Secondly, two lightning protection systems (metallic cap and receptor methods) commonly in use have been applied on a full scale polluted offshore wind turbine and compared for efficiency in lightning protection. In the enhanced method, the performance of the metallic cap was improved by adding a receptor at the middle of the blade. This was found to influence the electric field distribution immensely. The new method was compared with the metallic cap method and the tip receptor method and it performed better. Considering efficient lightning protection, the presence of the protection system should ensure that the electric field on the blade

surface is kept minimum but maximum on protection system so that leader will incept from the protection system first. On the average, the new protection system (the enhanced method) has the highest maximum electric field on the protection system and lower on the blade surface. The electric field at the metallic cap of a blade protected with the enhanced method is found to be boosted when compared to other methods. It can greatly improve the lightning protection performance for offshore wind turbines.

# Chapter 6

# Experimental Validation

## 6.1 Introduction

This chapter describes the validation of the simulation model used in evaluating the maximum electric field strength required for the initiation of upward leader from wind turbine due to varying blade conditions as shown in previous chapters. In this chapter, High voltage test is carried out to study the development of streamers on different receptor sizes in a wind turbine blade made of fiberglass to validate the obtained simulation results. Apart from the size of the receptor, the conductivity of the blade samples is also considered. Obtained experimental results are compared with that of simulation and then discussed.

## 6.2 Experimental setup and Procedure for high voltage strike attachment test

Lightning attachment to wind turbines has gained attention, with many research works focused on downward propagating lightning. Nevertheless, a few work, done on upward propagating lightning (Particularly due to electric fields from winter clouds developed at lower altitudes) has shown that apart from the fact that tall wind turbine can increase the number of lightning strike, due to rotation, turbines are triggering their own lightning [91, 93, 128], indicating that large portion of the lightning that attach to a wind turbine are upward initiated. This type of lightning are majorly influenced by the slowly increasing electric field with a rise rate lower than 1 KV/m/s [183], and the formation is dominated by the electric field distribution and the wind turbine geometry. The stepped leader position

influence is removed. Therefore, the analysis in this work only involves upward lightning strike.

The high voltage strike attachment test is usually applied to determine specific lightning attachment points on a structure. The main idea is to know from where upward initiated leaders or answering leaders are emitted.

The test arrangement is intended to result in initiation of electrical activity, such as corona, streamers and leaders at a wind turbine blade just before a lightning strike attachment. Immediately ionization of the air at the wind turbine blade test specimen is initiated, the incepted streamer will progress towards the ground which has a large geometry and is intended to represent an electric field equipotential surface some distance from a blade extremity. In this manner, the influence of the external test electrode on test results is minimized. Figure (6-3) shows the setup of the test arrangement, this include; high voltage generator, blade test specimen and ground. This test setup is chosen because it usually allows a larger dimension external electrode (i.e. a conductive surface on the floor of the laboratory) and a more realistic electric field environment during the test around the blade specimen to be provided. The test is performed by elevating the specimen above a grounded test plane in a high voltage laboratory. This grounded plane simulates an equipotential plane of the electric field between the blade tip and an approaching lightning leader of a downward initiated lightning flash or the static background electric field present prior to an upward initiated lightning flash.

As has been shown in previous chapters, there are a number of lightning protection methods used on wind turbines, these includes; Receptors, Metallic Cap, Metallic Conductor on the Blade Tip, Mesh, Ring Electrode [10] and the Backside Electrode [11] methods, also the

combined cap and receptors method recommended in previous chapter for offshore wind turbines. However, modern onshore wind turbines are predominantly protected with the receptor method. More also, multiple receptors on the blade has been a focus of research but the single-receptor method has remained the preferred choice. Therefore, only the single-receptor method is considered in this experiment.

The receptor though effective [19], also failed in so many instances as mentioned in [28, 29]. The efficiency of the receptor is dependent on its interception proficiency which is its ability to intercept a lightning stroke. This strongly dependent on the size of the receptors [39]. In other words, the size of the receptor can greatly influence the electric field distribution, the point of leader inception as well as discharge attachment point.

The test aims at defining an efficient receptor size achieved by a pass or fail in their ability to influence electric field distribution and to determine to which point lightning discharge will attach on the wind turbine blade. The test environment experienced by the wind turbine blade is similar to real lightning situation and the entire blade is totally affected by the external field prior to a lightning strike.

The high voltage waveform used is a double exponential switching type impulse voltage with rise times in order of 50-250μs and decay times of 2000μs. This voltage waveform is selected since it is the most representative of the electric field in the vicinity of a structure during an initial leader attachment.

### 6.2.1 *Test Specimen*

In order to assess the normal distribution of the points of discharge attachment on the blade surface, a large sized wind turbine hit by natural lightning strike is experimentally required while it is rotating, this can only be done in the natural lightning laboratory such as in

Florida [14]. The protection evaluation is done using 3 m blade tip section that is a part of Vestas V100 wind turbine, with 2 MW rated power, 100 m rotor diameter and 49 m long blade made of glass fibers reinforced polyester, cut from an actual blade. This size is adopted because most of the lightning attachments are located in the tip area of the blade. As compared to full scale wind turbine, testing with small specimens like 3 m of a full-scale length, makes it is possible to perform many tests within a limited amount of time and the duration for the test in this experiment is within one week. The elevated blade specimen is connected to the output of a Marx generator injecting high voltage impulses into the lightning protection system (receptor) of the blade. Blade thickness is 10 cm, chamber length: 0.9 m, maximum chord 3.9 m. Six receptor sizes (10 mm, 15 mm, 20 mm, 25 mm, 30 mm and 35 mm receptor diameters) (Figure 6-1), are applied on the wind turbine model to investigate the effect of receptor size on initiation of upward leader. The receptor is placed 1.5 m from the blade tip.

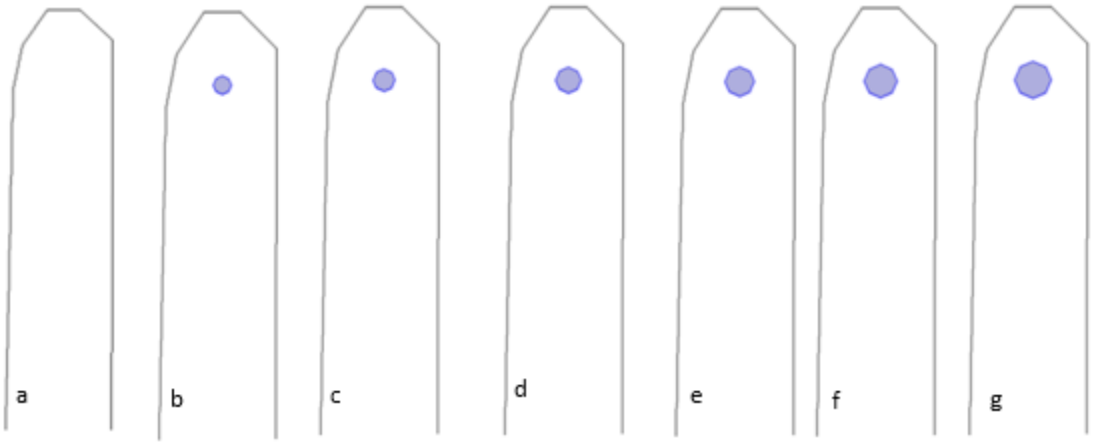


Figure 6-7 Different receptor sizes: (a) No receptor (b) 10 mm; (c) 15 mm; (d) 20 mm; (e) 25 mm; (f) 30 mm and (g) 35 mm diameters

At each instance, during the experiment, the applied size of receptor is connected to ground through a down conductor of 6 $mm^2$ cross section area embedded in the blade. A receptor fixed in a blade tip is shown in Figure 6-2 below.

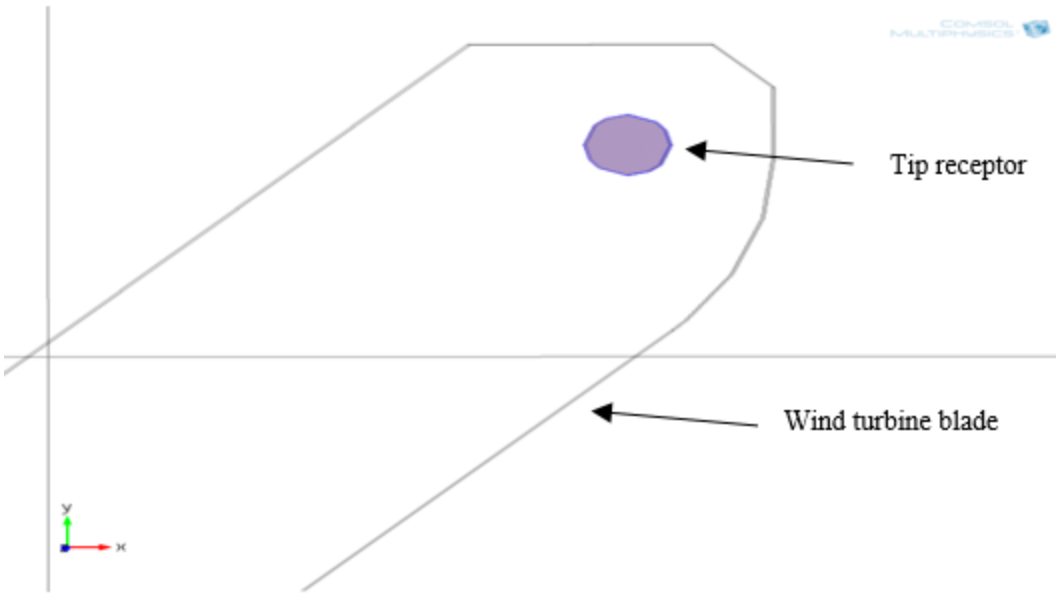


Figure 6-8. A receptor fixed in a blade tip

### 6.2.2 *Test Setup*

The tests are performed on the test setups illustrated in Figure 6-3 having the blade specimen elevated above a ground plane in the high voltage laboratory.

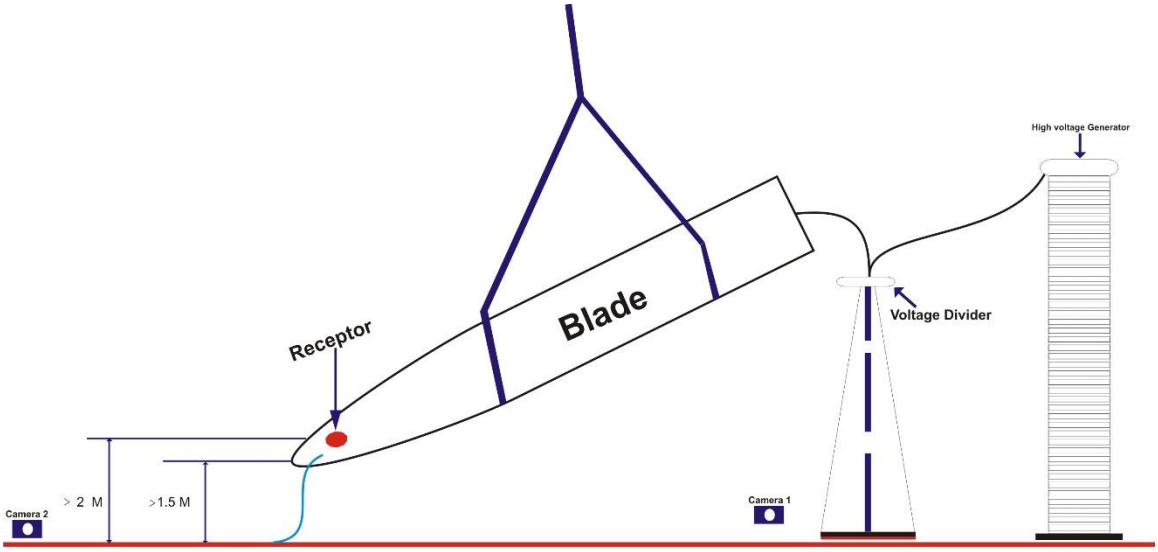


Figure 6-9 Initial leader attachment test setup

It includes the following:

1. The blade sample described above,
2. Marx generator with resistances and capacitances configured to generate desired voltage waveform.
3. Voltage divider and additional measuring system
4. Digital camera used to determine and show the discharge attachment point to the blade sample.

The size of the ground plane below the blade tip is large enough to avoid discharges from the blade to the edges of the ground plane.

### 6.2.3 *Test Procedure*

The Marx generator is adjusted to produce double exponential voltage waveforms D with positive and negative polarity. The blade is then suspended above the ground plane with all distances as shown in the figure. The output of the Max generator is connected to the down conductor inside the blade sample and the down conductor is then connected to the lightning receptor.

Five pulses are first applied to the model blade without receptor, then various configuration of receptor sizes and a picture is taken at each discharge. High voltage strike attachment test is performed with the test specimen blade positioned in different orientations as prescribed by IEC 61400-24. In each orientation, the size of the receptor is changed as well as the conductivity of the blade and the steps are repeated. Polluted blade surface was achieved with salt contamination 10 g/l solution of sodium chloride (NaCl) sprayed on the surface of the blade. The waveform for each discharge was recorded and, in each case, the

peak value and the time to flashover was determined. Determination of the attachment points was made possible by capturing images of the discharge with a digital camera.

As the blade rotates, it was tested in selected five positions to investigate the performance of wind turbine lightning protection systems on initiation of upward leader. The positions of the blade are chosen to determine the complete successes and failures of each receptor size. These positions are shown in Figure 6-4 (b). They are; (b) vertical, (c) $45^0$ (Trailing edge facing the cloud) (TEFC), (d) $45^0$ (Leading edge facing the cloud) (LEFC), (e) horizontal (Trailing edge facing the cloud) (TEFC), and (f) horizontal (Leading edge facing the cloud) (LEFC).

The model used for the rotation mode is shown in Figure 6-4 (a). In the experimental configuration, compared to the simulation, the blade in the vertical position referred to as facing the cloud is pointing directly downwards towards the ground plane, where after the tip was pitched in steps of 45°. Also referred to as 45°, Leading or Trailing edge facing the cloud.

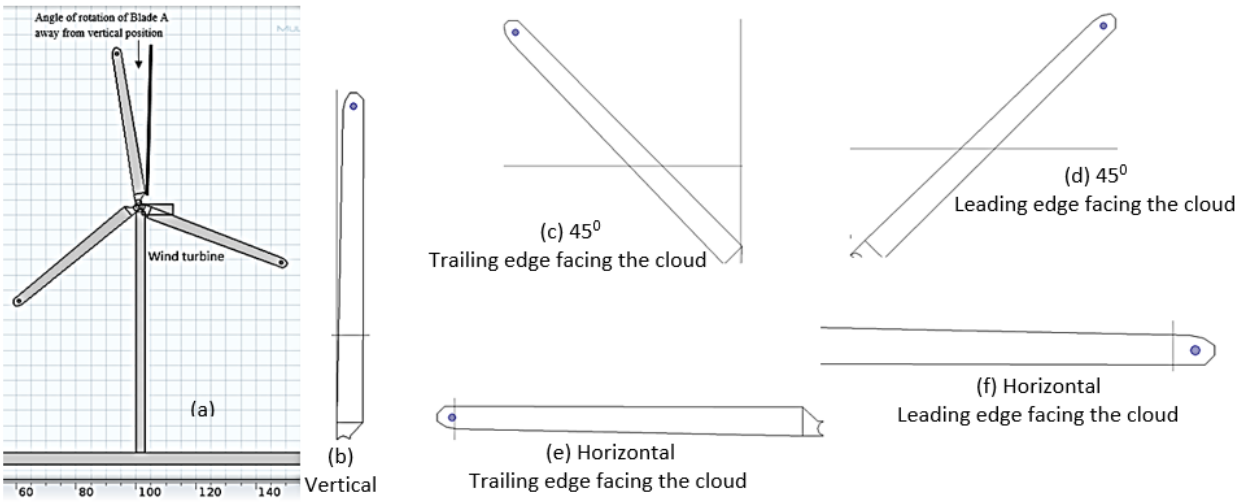


Figure 6-10 (a) Model for rotation mode, (b, c, d, e and f) Arrangement of blade sample

A 3m GFRP blade tip elevated above the ground electrode in a laboratory is shown Figure 6-5.

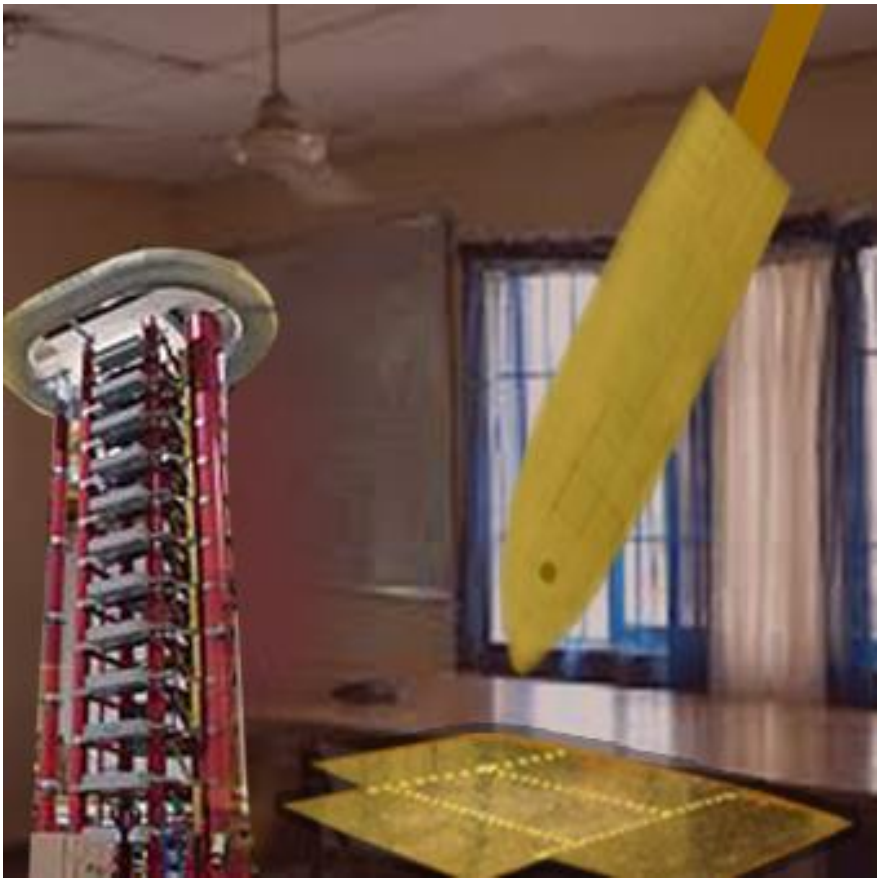

Figure 6-11. A 3m GFRP blade tip elevated above the ground electrode.

Six different configurations of receptor sizes (Figure 6-1) are applied on the wind turbine to investigate the effect of receptor sizes on initiation of upward leader. The six receptor sizes are 10 mm, 15 mm, 20 mm, 25 mm, 30 mm and 35 mm receptor diameters.

### 6.2.4 *experimental conditions*

The protected blade tip was tested as the size of the receptor was changed and the test conducted according to IEC 61400-24. The experiments were performed with the model blade set as a high-voltage electrode. The receptor is a disk-type with a metal disk of various sizes in mm diameter, it is covered with a flat metal braid set on the surface of the modal blade. The polarity of the applied voltage is positive and negative.

## 6.3 Results and Discussion

This section initially presents experimental results obtained from different receptor sizes, later discussion is on relating the developed model with experimental results, field experience and previous experimental data.

The most efficient receptor size is the one with highest number of discharge inception from the receptor and minimum at the tip, leading edge, trailing edges and the entire blade surface.

In evaluating the effect of receptor sizes on discharge inception, the experiment is conducted on the wind turbine, first without receptor and then as the blade is rotated, the receptor size is changed.

The polarity of the charge removed from the thundercloud can be used to sub-divide lightning into negative and positive flashes

A negative flash results in negative charge being transferred to the earth from the thundercloud. They are the dominant type of lightning flashes, around 90% of all cloud to ground, exhibiting the steepest current impulses (highest d$i$/d$t$).

A positive flash lowers positive charge from the thundercloud to the earth, around 10 % of all cloud to ground flashes, exhibiting the most powerful current parameters (higher $I$, $Q$ and $W/R$).

The experimental results follow a regular pattern for both positive and negative polarity and are similar to that in literature, however, since negative flashes are the dominant type of lightning and are more pertinent to the present experiment, only results for negative polarity are presented.

### 6.3.1 *Experiments with and without receptor on the model blade*

The test results are summarized as follows.

**(1) Experiments without receptor on the model blade**

Without the receptor, discharge to the model blade occurred at different points.

**(2) Experiments with receptor on the model blade**

The experimental results with various receptor sizes are shown in Table 2. The results are summarized as follows.

**a. Experiments with 10 mm receptor diameter**

(1) For blade tip facing the ground (Also referred to as vertical position in Figure 5), whether polluted or unpolluted, 100% of the discharge initiated from the receptor.

(2) In the case of $45^0$ (Trailing edge facing the cloud) (TEFC), 99% of the discharge initiated from the receptor, however, 1% of the discharge initiated from the blade trailing edge and was more for the polluted blade condition.

(3) In the case of $45^0$ (Leading edge facing the cloud) (LEFC), the observation was similar to 2 above, 99% of the discharge initiated from the receptor, and 1% of the discharge initiated from the blade leading edge and was also more for the polluted blade condition.

(4) In the case of horizontal (Trailing edge facing the cloud) (TEFC), the observation was similar to 2 above.

(5) In the case of horizontal (Leading edge facing the cloud) (LEFC), the receptor performance at this position was relatively better, 100% of the discharge initiated from the receptor.

**b. Experiments with 15 mm receptor diameter**

1. For blade tip facing the ground (Also referred to as vertical position in Figure 5), for unpolluted, 80% of the discharge initiated from the receptor, 10% from the blade tip, 5% from the leading edge and 5% from the trailing edge.
2. In the case of $45^0$ (Trailing edge facing the cloud) (TEFC), 85% of the discharge initiated from the receptor, 15% from the trailing edge, no discharge was observed from the blade tip as well as the leading edge and was more for the polluted blade condition.
3. In the case of $45^0$ (Leading edge facing the cloud) (LEFC), the observation was as follows, 80% of the discharge initiated from the receptor, and 15% of the discharge initiated from the blade leading edge while it was 5% on the blade tip and no discharge was initiated from the trailing edge and as usual, it was also more for the polluted blade condition.
4. In the case of horizontal (Trailing edge facing the cloud) (TEFC), the observation was that 75% of discharge was initiated from the receptor, 15% from the trailing edge, 10% from the blade tip and none at the leading edge.
5. In the case of horizontal (Leading edge facing the cloud) (LEFC), the receptor performance was also 75% as above, 5% at the blade tip, 20% at the leading edge and there was no discharge from the trailing edge.

**c. Experiments with 20 mm receptor diameter**

1. For blade tip facing the ground (Also referred to as vertical position in Figure 5), whether polluted or unpolluted, 75% of the discharge initiated from the receptor, 15% from

the blade tip, 5% from the leading edge and 5% from the trailing edge. The performance of this receptor size is relatively very poor.

2. In the case of $45^0$ (Trailing edge facing the cloud) (TEFC), 75% of the discharge initiated from the receptor, 15% from the trailing edge, 10% from the blade tip and no discharge was observed from the leading edge and was more for the polluted blade condition. This is because the electric field is enhanced at the trailing edge more than the leading blade edge.

3. In the case of $45^0$ (Leading edge facing the cloud) (LEFC), the observation was as follows, 80% of the discharge initiated from the receptor, 15% of the discharge initiated from the blade leading edge while it was 5% on the blade tip and no discharge was initiated from the trailing edge and as usual, it was also more for the polluted blade condition.

4. In the case of horizontal (Trailing edge facing the cloud) (TEFC), the observation was that 70% of discharge was initiated from the receptor, 15% from the trailing edge, 10% from the blade tip and none at the leading edge.

5. In the case of horizontal (Leading edge facing the cloud) (LEFC), the receptor performance was also 70% as above, 15% at the blade tip, 15% at the leading edge and there was no discharge from the trailing edge.

**d. Experiments with 25 mm receptor diameter**

1. For blade tip facing the ground (Also referred to as vertical position in Figure 5), for unpolluted, 90% of the discharge initiated from the receptor, 5% from the blade tip, 5% from the trailing edge and none from the trailing edge. The performance of this receptor size is relatively good.

2. In the case of $45^0$ (Trailing edge facing the cloud) (TEFC), 90% of the discharge initiated from the receptor, 10% from the leading edge and no discharge was observed from the trailing edge as well as the blade tip and was more for the polluted blade condition.

3. In the case of $45^0$ (Leading edge facing the cloud) (LEFC), the observation was as follows, 90% of the discharge initiated from the receptor, and 10% of the discharge initiated from the blade leading edge and no discharge was initiated from the trailing edge as well as the blade tip and as usual, it was also more for the polluted blade condition.

4. In the case of horizontal (Trailing edge facing the cloud) (TEFC), the observation was that 85% of discharge was initiated from the receptor, 10% from the trailing edge, 5% from the blade tip and none at the leading edge.

5. In the case of horizontal (Leading edge facing the cloud) (LEFC), the receptor performance was also 85%, 15% at the leading edge and there was no discharge from the trailing edge as well as the blade tip.

**e. Experiments with 30 mm receptor diameter**

1. For blade tip facing the ground (Also referred to as vertical position in Figure 5), whether polluted or unpolluted, 85% of the discharge initiated from the receptor, 15% from the blade tip and none from the trailing edge as well as the leading edges.

2. In the case of $45^0$ (Trailing edge facing the cloud) (TEFC), 85% of the discharge initiated from the receptor, 10% from the trailing edge, 5% from the blade tip and no discharge was observed from the leading edge and was more for the polluted blade condition.

3. In the case of $45^0$ (Leading edge facing the cloud) (LEFC), the observation was as follows, 85% of the discharge initiated from the receptor, and 10% of the discharge initiated from the blade leading edge, 5% from the blade tip and no discharge was initiated from the trailing edge, it was also more for the polluted blade condition.

4. In the case of horizontal (Trailing edge facing the cloud) (TEFC), the observation was that 85% of discharge was initiated from the receptor, 15% from the trailing edge, 5% from the blade tip and none at the leading edge.

5. In the case of horizontal (Leading edge facing the cloud) (LEFC), the receptor performance was also 80%, 15% at the leading edge, 5% from the blade tip and there was no discharge from the trailing edge.

**f. Experiments with 35 mm receptor diameter**

1. For blade tip facing the ground (Also referred to as vertical position in Figure 5), for unpolluted, 80% of the discharge initiated from the receptor, 10% from the blade tip, 5% from the leading edge and 5% from the trailing edge.
2. In the case of $45^0$ (Trailing edge facing the cloud) (TEFC), 75% of the discharge initiated from the receptor, 15% from the trailing edge, 10% from the blade tip and no discharge was observed from the leading edge and was more for the polluted blade condition.
3. In the case of $45^0$ (Leading edge facing the cloud) (LEFC), the observation was as follows, 80% of the discharge initiated from the receptor, and 15% of the discharge initiated from the blade leading edge while it was 5% on the blade tip and no

discharge was initiated from the trailing edge and as usual, it was also more for the polluted blade condition.

4. In the case of horizontal (Trailing edge facing the cloud) (TEFC), the observation was that 75% of discharge was initiated from the receptor, 20% from the trailing edge, 10% from the blade tip and none at the leading edge.
5. In the case of horizontal (Leading edge facing the cloud) (LEFC), the receptor performance was also 75% as above, 10% at the blade tip, 15% at the leading edge and there was no discharge from the trailing edge.

Other forms of discharge were also observed, puncture discharges from inside the blade sample to the ground occurred. In some cases, discharge incepted from a receptor progressed on the blade surface and then terminated to the ground.

Image of a negative discharge terminating on the ground is shown in Figure 6-6.


Figure 6-12 discharge from the blade tip towards the ground plane.

Table 13 No of discharge initiation for a blade-to-ground gap

| Blade tip angle from ground plane | Blade tip | Leading Edge | Trailing Edge | Receptor |
|---|---|---|---|---|
| Receptor 10mm diameter | | | | |
| $-90^0$ | 0 | 0 | 0 | 20 |
| $-45^0$ | 0 | 1 | 0 | 19 |
| $0^0$ | 0 | 0 | 0 | 20 |
| $45^0$ | 0 | 0 | 1 | 19 |
| $90^0$ | 0 | 0 | 1 | 19 |
| Receptor 15mm diameter | | | | |
| $-90^0$ | 1 | 4 | 0 | 15 |
| $-45^0$ | 1 | 3 | 0 | 16 |
| $0^0$ | 2 | 1 | 1 | 16 |
| $45^0$ | 0 | 0 | 3 | 17 |
| $90^0$ | 2 | 0 | 3 | 15 |
| Receptor 20mm diameter | | | | |
| $-90^0$ | 3 | 3 | 0 | 14 |
| $-45^0$ | 1 | 3 | 0 | 16 |
| $0^0$ | 3 | 1 | 1 | 15 |
| $45^0$ | 2 | 0 | 3 | 15 |
| $90^0$ | 2 | 0 | 4 | 14 |
| Receptor 25mm diameter | | | | |
| $-90^0$ | 0 | 3 | 0 | 17 |
| $-45^0$ | 0 | 2 | 0 | 18 |
| $0^0$ | 1 | 0 | 1 | 18 |
| $45^0$ | 0 | 0 | 2 | 18 |
| $90^0$ | 1 | 0 | 2 | 17 |
| Receptor 30mm diameter | | | | |
| $-90^0$ | 1 | 3 | 0 | 16 |
| $-45^0$ | 1 | 2 | 0 | 17 |
| $0^0$ | 3 | 0 | 0 | 17 |
| $45^0$ | 1 | 0 | 2 | 17 |
| $90^0$ | 1 | 0 | 3 | 16 |
| Receptor 35mm diameter | | | | |
| $-90^0$ | 2 | 3 | 0 | 15 |
| $-45^0$ | 1 | 3 | 0 | 16 |
| $0^0$ | 2 | 1 | 1 | 16 |
| $45^0$ | 2 | 0 | 3 | 15 |
| $90^0$ | 2 | 0 | 4 | 15 |

Six different receptor size configurations were tested. Depending on the receptor size, the discharge initiation behaved differently. The test reveals the best receptor size that can better influence initiation of discharge from the receptor rather than the blade surface. This is necessary for a more efficient lightning protection. Occasionally, discharge is initiated from the blade surface rather than the receptor, in this case, failure of receptor size is discussed and determined. The points of discharge initiation correlated very well with experience with wind turbine blades in service that have been struck by lightning.

To pass the test by a receptor size, all or majority of the discharge must initiate from the receptor. To fail, all or majority of the discharge have to initiate from the blade surface or other part of the wind turbine. From the experimental results, 10 mm receptor diameter has majority of the discharge initiated from the receptor compared to other receptor sizes. This is in agreement with simulation results. This indicates that 10 mm receptor diameter will allow leader to be initiated from the receptor before any other part of the blade or wind turbine and as a result prevent damage. This receptor size will therefore provide higher protection efficiency than other receptor sizes and is therefore recommended. 10 mm is the smallest amongst the sizes considered and would be thought least in withstanding high current, however, it has been shown in literature that this size is adequate for an average peak stroke current and if need be, this can be improved by increasing the diameter of the down conductors.

The maximum electric field strength on the model shown in Figure 6-7 with blade A at the vertical position is located between the receptor and the blade tip, which indicates that an upward leader will likely be initiated from that position. This agrees favorably well with the number of discharge initiation at this position in the experimental result indicating that

the tip is worst hit. In addition, the figure reveals that the maximum electric field strengths locations are changing as the wind turbine is rotating.

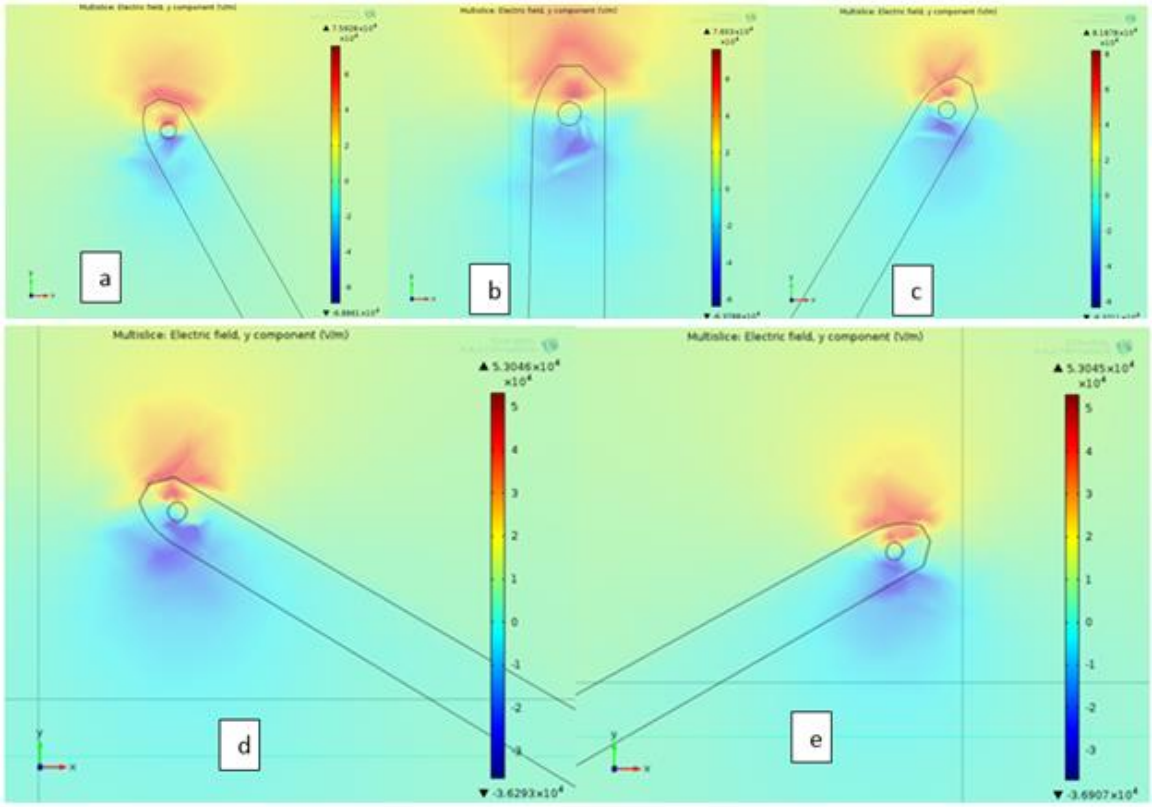


Figure 6-13. Arrangement of the blade sample in simulation. Blade A is rotated from -60 to +60 degrees from the vertical position: (a) 30; (b) vertical position; (c) -30; (d) 60; and (e) -60.

This is also in line with the number of discharge initiation and also corroborated result in [44], that the blade positions significantly affect the lightning attachment manner as well as the performance of the blade lightning protection systems. This result is also corroborated by the experimental result from the reduced size model in [42], that when the rotor of the reduced size wind turbine is rotating, a slight reduction in the number of direct strikes in the zone of the air-termination system on the blades was observed, as compared to the case when the rotor is stationary.

Another very important correlation of the simulation with experimental result is that in most cases in the simulation, the maximum electric field strength locations on the trailing

edge are higher than that of the leading edge which agrees with experimental result that the blade trailing edge attracts discharges more times than the blade leading edge. The implications of these two correlations are that as the blade is rotated, the points of leader inception changes and it is likely going to be more at the trailing edge than at the leading edge.

Obtained results of maximum electric field strength for both polluted and unpolluted blade conditions agree with the number of discharge initiation and upward leader initiation points in experimental results. It corroborated the experimental result in [44], that, In case of unpolluted surface, the air-termination system successfully captures surges more than in case of polluted surfaces. The level of damping on the polluted blade surface also supports the findings by Naka et al. [45], that, regarding non-conductive blade, creeping discharge occurred more frequently in the polluted condition, and sometimes penetrative destruction was also observed.

## 6.4 Conclusion

Experimental validation has been carried out for the simulation model used in evaluating the maximum electric field strength required for the initiation of upward leader from wind turbine due to varying blade conditions.

Initially, the experiment was conducted with varying receptor sizes and then, the implication of the developed model is discussed.

The protection evaluation is done using 3 m blade tip section that is a part of Vestas V100 wind turbine, with 2 MW rated power, 100 m rotor diameter and 49 m long blade made of glass fibers reinforced polyester, cut from an actual blade.

The simulation results of the present study were compared with that of experiment. Interestingly, the comparison has confirmed that the blade condition plays an important role in determining the maximum electric field strength required for the initiation of upward leader from wind turbine as well as discharge attachment points.

# Chapter 7

# Conclusions and Future Work

## 7.1 Introduction

This chapter deals with the conclusion and future work. The investigation done with the vertical tri-pole cloud charge distribution model to analyze the maximum electric field strength required for the initiation of upward leader from wind turbine considering various blade condition and the corresponding validation is summarized and future work are suggested.

## 7.2 Conclusions

When lightning attaches to the blade surface instead of the air-terminal, the blade and even the entire wind turbine can be destroyed resulting in downtimes, loss of wind turbine, expensive cost of repair and can cause some power company to shut down and dismantle. In the presence of a thundercloud, tall wind turbines are increasingly subjected to upward lightning attachment triggered by the wind turbine itself. In contrast to static objects, the maximum electric field strength required for the inception of upward leader from wind turbine changes due to varying blade conditions. To protect modern wind turbines from lightning strikes, the investigation of the maximum electric field strength required for the inception of upward leader from wind turbine due to varying blade conditions is carried out in this thesis.

The study extends the vertical tri-pole model made from two positive charges and a negative charge representing the idealized gross charge structure of a thundercloud to

create an ambient field representing uniform electric field due to cloud charge distribution at 200 m above ground. By applying the extended model to a 3D electrostatics model of a full-scale wind turbine; Vestas V100 with 2 MW rated power, 100 m rotor diameter and 49 m long blade, and a model of a 19.1 m blade length of 600 kW wind turbine, the maximum electric field strength is obtained.

Initially, the model is utilized to evaluate and compare various receptor sizes. The receptor size is evaluated and optimized by comparing the electric field strength as the receptor size is changed and the blade is rotated. Six receptor sizes (10 mm, 15 mm, 20 mm, 25 mm, 30 mm and 35 mm receptor diameters), encompassing adopted sizes in literature were investigated. The point of upward leader inception is predicted by the magnitude of the electric field strength. It was found that 10 mm receptor diameter presents the highest electric field strength on the receptor than other receptor sizes. Also, relatively, the electric field distribution at the blade tip, leading edge, trailing edge for 10 mm receptor diameter was lower than that of other sizes. This indicates that 10 mm receptor diameter will allow leader to be initiated from the receptor before any other part of the blade or wind turbine and as a result prevent damage. This receptor size will therefore provide higher protection efficiency than other receptor sizes and is therefore recommended.

Secondly, the model is utilized to evaluate and compare discrete receptor position from the blade tip. By comparing the electric field strength as the receptor position is changed and the blade is rotated, the receptor position was evaluated and optimized. Four different configurations of receptor positions were applied on the wind turbine to investigate the effect of receptor position on initiation of upward leader. In the configurations, the receptor was fixed at discrete positions from the blade tip. These positions are 2 m, 1.5 m, 1 m and

0.6 m respectively. It was found that locating the receptor 1.5 m away from the blade tip will allow the leader to be initiated from the receptor before any other part of the blade and as a result prevent damage. This configuration therefore provides higher protection efficiency than other configurations and is therefore recommended.

Again, the model is utilized to evaluate blade pollution in offshore wind turbines. By comparing the electric field strength as the blade surface conductivity is changed and the blade is rotated, the effect of pollution on lightning protection systems was evaluated. It was found that pollution dampens the performance of the receptor by 93% and on average, the general performance of the receptor in a polluted blade condition was found to be less than 10%. This indicates that offshore wind turbines are at higher risk of failure of its lightning protection systems and are prone to higher probability of damage.

Finally, two lightning protection systems (metallic cap and receptor methods) commonly in use was applied on a full scale polluted offshore wind turbine and compared. A new protection system with higher lightning protection efficiency was developed. This was found to influence the electric field distribution immensely. The new method was compared with the metallic cap method and the tip receptor method. The new method performed better. It can greatly improve the lightning protection performance for offshore wind turbines.

High voltage test was carried out to validate the developed model. The simulation results of the present study were compared with that of experiment. Interestingly, the comparison has confirmed that the blade condition plays an important role in determining the maximum electric field strength required for the initiation of upward leader from wind turbine.

By proper scaling of the receptor, the results and findings in this work could be extended to different wind turbine sizes.

## 7.3 Future Work

This thesis presents a detailed research evaluation of the maximum electric field strength required for the inception of upward leader from wind turbine due to varying blade conditions. The blade conditions that has been varied included; blade and receptor sizes, blade pollution, receptor position on blade and receptor types. In addition to these, for further research, the impact of wind would be considered also.

The extended vertical tri-pole model was studied with a single wind turbine in this thesis, in order to better model the maximum electric field strength required for the inception of upward leader from wind turbines in a wind farm, it should be further studied, considering two or more wind turbines.

Incidence of upward lightning inception from wind turbine is not well understood when compared with incidence of downward lightning. Further work is needed regarding experimental data, field observation etc.

This work and the overall results form a platform for further investigation on modern wind turbines with regard to protecting long blades from lightning. It is a viable substitute for the invalidated EGM which according to IEC 61400-24, must not be used on the rotor blades. The invalidated EGM as well as existing protection methods for downward initiated lightning has not been able to address key issues in wind turbine lightning protection such as receptor position on the blade, size of the receptor, the effect of pollution on the receptor's performance and evaluation of the performance of the protection systems. These

problems have been well addressed by this thesis. Manufacturers may look at the finding of this work when dealing with the design aspects of very large future wind turbine blades of practical importance.

# REFERENCES


1. Peesapati, V., et al., *Lightning protection of wind turbines–a comparison of measured data with required protection levels.* IET renewable power generation, 2011. **5**(1): p. 48-57.
2. Wilson, N., et al., *Lightning attachment to wind turbines in central Kansas: Video observations, correlation with the NLDN and in-situ peak current measurements.* EQEA, The European Wind Energy Association, Vienna, Austria, PO, 2013. **145**.
3. Garolera, A.C., et al., *Lightning Damage to Wind Turbine Blades From Wind Farms in the US.* IEEE Transactions on Power Delivery, 2016. **31**(3): p. 1043-1049.
4. Rachidi, F., M. Rubinstein, and A. Smorgonskiy, *Lightning protection of large wind-turbine blades*, *Wind Energy Conversion Systems*. 2012, Springer. p. 227-241.
5. Vestas. Available from: http://www.windpoweroffshore.com/article/1211179/vestas-begins-testing-first-v164-80-metre-blade.
6. Glushakow, B., *Effective lightning protection for wind turbine generators.* IEEE Transactions on Energy Conversion, 2007. **22**(1): p. 214-222.
7. Ma, P.-C. and Y. Zhang, *Perspectives of carbon nanotubes/polymer nanocomposites for wind blade materials.* Renewable and Sustainable Energy Reviews, 2014. **30**: p. 651-660.
8. Gwec. Available from: http://www.gwec.net/wp-content/uploads/2014/04/Market-Forecast-for-2016-2020-1.jpg.
9. Byrne, A. and M. Malkin, *Field Performance Assessment of Wind Turbine Lightning Protection Systems. 5th International Lightning Meteorological Conference 20-21 March 2014. Tucson, Arizona, USA.*
10. Zavareh, H.T. *Wind turbines protection against the lightning struck using a combined method*. *Renewable Energy and Distributed Generation (ICREDG), IEEE Second Iranian Conference*, 2012.
11. Minowa, M., et al. *A study of lightning protection for wind turbine blade by using creeping discharge characteristics, IEEE International Conference on Lightning Protection (ICLP)*, 2012. Vienna, Austria.
12. Ayub, A.S., W.H. Siew, and S. MacGregor. *Lightning protection of wind turbine blades—An alternative approach, IEEE 7th Asia-Pacific International Conference (APL)*. 2011. Chengdu, China.
13. Staszewski, Ł., *Lightning Phenomenon–Introduction and Basic Information to Understand the Power of Nature.* University of Technology, Wroclaw, Poland, 2001.
14. Yoh, Y., *A new lightning protection system for wind turbines using two ring-shaped electrodes.* IEEJ Transactions on Electrical and Electronic Engineering, 2006. **1**(3): p. 314-319.
15. Vishnyakov, L., L. Pereselentseva, and E. Vishnyakova, *Knitted Soldered Meshes and Nanostructured Carbon Particles for Lightning Protection of Composite Wind Turbine Blades.* Powder Metallurgy and Metal Ceramics, 2014. **53**(5-6): p. 368-374.
16. Danoon, L., A. El-Makadema, and A. Brown, *On the integration of lightning protection with stealth coated wind turbine blades.* Wind Energy, 2013.
17. Yokoyama, S., *Lightning protection of wind turbine blades.* Electric Power Systems Research, 2013. **94**: p. 3-9.
18. Madsen, S., et al., *Proposal of new zoning concept considering lightning protection of wind turbine blades.* Journal of Lightning Research, 2012. **4**(2): p. 108-117.
19. Shindo, T., A. Asakawa, and M. Miki, *Characteristics of lightning strikes on wind turbine blades. Experimental study of the effects of receptor configuration and other parameters.* Electrical Engineering in Japan, 2011. **176**(3): p. 8-18.

20. Plumer, J.A. *Laboratory Test Results and Natural Lightning Strike Effects: How Well do They Compare, 2012 International Conference on Lightning Protection (ICLP)*, 2012. IEEE, Vienna, Austria
21. Xiaohui, W., Z. Xiaoqing, and Y. Dasheng, *An efficient algorithm of transient responses on wind turbine towers struck by lightning.* COMPEL-The international journal for computation and mathematics in electrical and electronic engineering, 2009. **28**(2): p. 372-384.
22. Madsen, S.F., C.F. Mieritz, and A. Candela Garolera. *Numerical tools for lightning protection of wind turbines*. *International Conference on Lightning and Static Electricity, 2013.*
23. Sorensen, T.S., et al. *The update of IEC 61400-24 lightning protection of wind turbines*. *29th International Conference on Lightning Protection, 23rd–26th June, Sweden*. 2008.
24. Gromicko, N., *Tree Dangers-Int'l Association of Certified Home Inspectors (InterNACHI).* International Association of Certified Home Inspectors (InterNACHI).
25. Kalair, A., N. Abas, and N. Khan, *Lightning interactions with humans and lifelines.* Journal of Lightning Research, 2013. **5**(1).
26. Durstewitz, M., et al. *External conditions for wind turbine operation-results from the German'250MW wind'programme*. *European Union Wind Energy Conference*. 1996.
27. Griffin, D.A. and M.C. Malkin, *Lessons Learned from Recent Blade Failures: Primary Causes and Risk-Reducing Technologies.* 49th AIAA Aerospace Sciences Meeting including the New Horizons Forum and Aerospace Exposition 4 - 7 January 2011, Orlando, Florida.
28. Yoh, Y. and Y. Shigeru. *Proposal of lightning damage classification to wind turbine blades*. *7th Asia-Pacific International Conference on Lightning (APL)*, 2011. IEEE.
29. Yokoyama, S. *Lightning protection of wind turbine generation systems*. *7th Asia-Pacific International Conference on Lightning (APL)*. 2011. IEEE.
30. Candela Garolera, A., et al., *Multiple Lightning Discharges in Wind Turbines Associated With Nearby Cloud-to-Ground Lightning.* IEEE Transactions on Sustainable Energy, 2015. **6**(2): p. 526-533.
31. Long, M., M.B. Garcia, and R. Thottappillil. *On the interception of dart lightning leaders from wind turbine blades*. *2014 International Conference on Lightning Protection (ICLP)*, IEEE. Shanghai, China.
32. Malcolm, N. and R.K. Aggarwal. *Estimation of the failure rate of wind turbine electrical systems exposed to lightning strikes*. *Power & Energy Society General Meeting, 2015 IEEE*.
33. Madsen, S.F., C.F. Mieritz, and H. dk ApS, *Current distribution and magnetic fields in complex structures using Comsol Multiphysics.* The Proceedings of the 2011 COMSOL Conference, Stuttgart.
34. Simani, S., S. Farsoni, and P. Castaldi, *Fault diagnosis of a wind turbine benchmark via identified fuzzy models.* Industrial Electronics, IEEE Transactions on, 2015. **62**(6): p. 3775-3782.
35. Rodrigues, R.B., V.M. Mendes, and J.P. Catalão. *Direct lightning surge analysis in wind turbines using electromagnetic transients computer program*. *International Conference on Computer as a Tool (EUROCON), 2011 IEEE*.
36. Bagherian, H. and H.K. Karegar. *Effects of location, size and number of wind turbine receptors on blade lightning protection by voltage distribution analysis*. *International Conference on Advanced Power System Automation and Protection (APAP)*, 2011. IEEE.
37. Peesapati, V. and I. Cotton. *Lightning protection of wind turbines—A comparison of real lightning strike data and finite element lightning attachment analysis*. *International Conference on Sustainable Power Generation and Supply, SUPERGEN'09.* 2009. IEEE.

38. Alonso, M. and D. Irastorza. *Dynamic wind turbine lightning protection behaviour under stom conditions*. *29th International Conference on Lightning Protection*. 2008.
39. 61400-24, I., *Wind turbine - Part 24: Lightning protection*. 2010.
40. Wang, Y. and W. Hu, *Investigation of the Effects of Receptors on the Lightning Strike Protection of Wind Turbine Blades.* IEEE Transactions on Electromagnetic Compatibility, 2017.
41. Arinaga, S., K. Inoue, and T. Matsushita, *Experimental study for wind turbine blades lightning protection.* Renewable Energy, 2006. **4**: p. 5.
42. Radicevic, B.M. and M.S. Savic, *Experimental research on the influence of wind turbine blade rotation on the characteristics of atmospheric discharges*. IEEE Transactions on Energy Conversion, 2011. **26**(4): p. 1181-1190.
43. Madsen, S.F., et al., *Interaction between electrical discharges and materials for wind turbine blades-particularly related to lightning protection*. 2006, Technical University of Denmark Tekniske Universitet, Department of Electric Power Engineering Institut for Elteknik.
44. Abd-Elhady, A.M., N.A. Sabiha, and M.A. Izzularab, *Experimental evaluation of air-termination systems for wind turbine blades.* Electric Power Systems Research, 2014. **107**: p. 133-143.
45. Naka, T., et al., *Experimental studies on lightning protection design for wind turbine blades.* Proceedings of Euro-pean Wind Energy Association (EWEC), Athen, Greece, 2006.
46. Berger, K., *Novel observations on lightning discharges: Results of research on Mount San Salvatore.* Journal of the Franklin Institute, 1967. **283**(6): p. 478-525.
47. Golde, R. *Lightning currents and related parameters*. *Physics of Lightning, Volume 1 & 2*. 1977.
48. Horvath, T., *Standardization of lightning protection based on the physics or on the tradition?* Journal of electrostatics, 2004. **60**(2): p. 265-275.
49. Romero, C., et al. *Current waveforms associated with positive flashes recorded on the säntis tower in summer*. *2011 International Symposium on Lightning Protection (XI SIPDA)*, IEEE.Fortalezia Brazil.
50. Rakov, V.A. and M.A. Uman, *Lightning: physics and effects*. 2003: Cambridge University Press.
51. Wada, A., et al. *Lightning Damages of Wind Turbine Blades in Winter in Japan—Lightning Observation on the Nikaho-Kogen Wind Farm— 27th International Conference on LIGHTNING PROTECTION*. 2004.
52. Asakawa, A., et al., *Direct Lightning Hits on Wind Turbines in Winter Season: Lightning Observation Results for Wind Turbines at Nikaho Wind Park in Winter.* IEEJ Transactions on Electrical and Electronic Engineering, 2010. **5**(1): p. 14-20.
53. Gül, Ö., *Analysis of Wind Turbine Grounding Systems In Terms of Touch and Step Voltages.* IU-Journal of Electrical & Electronics Engineering, 2015. **15**(1): p. 1867-1872.
54. Guimarães, M., et al., *Assessing currents of upward lightning measured in tropical regions.* Atmospheric Research, 2014.
55. Dolan, D., C. Sao, and P. Lehn. *Lightning exposure of wind turbines*. *Canadian Conference on Electrical and Computer Engineering, 2006. CCECE'06.* 2006. IEEE.Ottawa Canada.
56. Gay-Lussac, F. and C. Pouillet, *Introduction sur les paratonneres, adoptee par L'Academie des Sciences.* French Academy of Sciences, 1823.
57. Lodge, O., *Lightning Conductors and Lightning Guards: A Treatise on the Protection of Buildings, of Telegraph Instruments and Submarine Cables, and of Electrical Installations Generally, from Damage by Atmospheric Discharges*. 2012: Cambridge University Press.
58. Golde, R., *Lightning, Vol 1'Physics of Lightning', Vol 2'Lightning Protection'*. 1977, Academic Press, London.

59. Preece, W.H., *XLVIII. On the space protected by a lightning-conductor.* The London, Edinburgh, and Dublin Philosophical Magazine and Journal of Science, 1880. **10**(64): p. 427-430.
60. Commission, I.E., *International Standard IEC 61024-1 Protection of structures against lightning–Part 1: General principles*. 1990, Geneva: IEC.
61. Szedenik, N., *Rolling sphere–method or theory?* Journal of electrostatics, 2001. **51**: p. 345-350.
62. durch Abschalten, Ä.d.F., *Fehlergrößen des Stromwandlers.*
63. Lee, R.H., *Protection Zone for Buildings Against Lighning Strokes Using Transmission Line Protection Practice.* IEEE transactions on industry applications, 1978(6): p. 465-469.
64. Lee, R.H., *Lightning protection of buildings.* IEEE Transactions on industry applications, 1979(3): p. 236-240.
65. Rodrigues, R., V. Mendes, and J. Catalão, *Estimation of lightning vulnerability points on wind power plants using the rolling sphere method.* Journal of Electrostatics, 2009. **67**(5): p. 774-780.
66. Anderson, J., *Monte Carlo computer calculation of transmission-line lightning performance.* Transactions of the American Institute of Electrical Engineers. Part III: Power Apparatus and Systems, 1961. **80**(3): p. 414-419.
67. Young, F., J. Clayton, and A. Hileman, *Shielding of transmission lines.* IEEE Trans. on PAS, 1963. **83**: p. 132.
68. Sargent, M., *Monte Carlo simulation of the lightning performance of overhead shielding networks of high voltage stations.* IEEE Transactions on Power Apparatus and Systems, 1972. **4**(PAS-91): p. 1651-1656.
69. Mousa, A.M., *Shielding of high-voltage and extra-high-voltage substations.* IEEE Transactions on Power Apparatus and Systems, 1976. **95**(4): p. 1303-1310.
70. Eriksson, A., *Lightning and tall structures.* Trans. South Afr. IEE, 1978. **69**(Pt 8): p. 238-252.
71. MOUSA, A. and K. Srivastava. *A revised electrogeometric model for the termination of lightning strokes on ground objects*. *NOAA, International Aerospace and Ground Conference on Lightning and Static Electricity p 342-352 (SEE N 89-10429 01-47)*. 1988.
72. Abdel-Gawad Mousa, A.-M., *A study of the engineering model of lightning strokes and its application to unshielded transmission lines*. 1986, University of British Columbia.
73. Cotton, I., N. Jenkins, and K. Pandiaraj, *Lightning protection for wind turbine blades and bearings.* Wind Energy, 2001. **4**(1): p. 23-37.
74. Bankaitis, H., *Lightning accommodation systems for wind turbine generator safety*. 1981.
75. Bankaitis, H., *Evaluation of lightning accommodation systems for wind-driven turbine rotors*. 1982.
76. Dodd, C.W., T. McCalla Jr, and J.G. Smith, *How to protect a wind turbine from lightning.* 1983.
77. Gewehr, H. *Lightning protection for composite rotor blades*. *American Wind Energy Association*. 1980.
78. Celi, O., A. Pigini, and E. Garbagnati, *Evaluation of the damages caused by lightning current flowing through bearings.* 1991.
79. TSUCHIYA, K., S. YAMADA, and T. MATSUZAKA, *A Study of Lightning Damages to WECs with Artificial Lightning Strokes.* Wind Energy: Technology and Implementation, 1991: p. 737-741.
80. Pols, E., *Bliksemschade aan windturbines is te beperken.* Energietechniek, 1995. **73**(12): p. 824-827.
81. Durstewitz, M., et al. *External conditions for wind turbine operation-results from the German'250MW wind'programme*. *European Union Wind Energy Conference*. 1996.

82. Erichsen, H.V. and K. Bertelsen. *Verification of the Safe Locations in a Wind Turbine during Thunderstorms*. *Proceedings of the International Conference on Lightning and Static Electricity, Pittsfield MA, USA*. 2009.
83. Canturk, R. and M. Inalpolat. *A computational acoustic interrogation of wind turbine blades with damage, Comsol Conference, Boston*. 2015.
84. Li, D., et al., *A review of damage detection methods for wind turbine blades.* Smart Materials and Structures, 2015. **24**(3): p. 033001.
85. Djalel, D., M. Mourad, and S. Ghoudelbourk. *Protection of wind turbine against the lightning damage*. *6th International Renewable Energy Congress (IREC)*, 2015. IEEE.
86. Wang, Y. and O. Zhupanska, *Lightning strike thermal damage model for glass fiber reinforced polymer matrix composites and its application to wind turbine blades.* Composite Structures, 2015. **132**: p. 1182-1191.
87. Yasuda, Y., et al., *Classification of lightning damage to wind turbine blades.* IEEJ Transactions on Electrical and Electronic Engineering, 2012. **7**(6): p. 559-566.
88. Yokoyama, S., et al. *Clarification of the mechanism of wind turbine blade damage taking lightning characteristics into consideration and relevant research project*. *International Conference on Lightning Protection (ICLP)*, 2012. IEEE, Vienna, Austria.
89. Yasuda, Y., et al. *Classification of wind turbine blade incidents regarding lightning risk management*. *International Conference on Lightning Protection (ICLP)*, 2014. IEEE Shanghai, China.
90. Wen, X., et al., *Effect of Wind Turbine Blade Rotation on Triggering Lightning: An Experimental Study.* Energies, 2016. **9**(12): p. 1029.
91. Rachidi, F., et al., *A review of current issues in lightning protection of new-generation wind-turbine blades.* IEEE Transactions on Industrial Electronics, 2008. **55**(6): p. 2489-2496.
92. Hernández, Y.M., et al., *A simulation approach on rotor blade electrostatic charging and its effect on the lightning overvoltages in wind parks.* Electric Power Systems Research, 2016. **139**: p. 22-31.
93. Montanyà, J., O. Velde, and E.R. Williams, *Lightning discharges produced by wind turbines.* Journal of Geophysical Research: Atmospheres, 2014.
94. Radičević, B.M., et al., *Impact of wind turbine blade rotation on the lightning strike incidence–A theoretical and experimental study using a reduced-size model.* Energy, 2012. **45**(1): p. 644-654.
95. Holbøll, J., et al. *Discharge phenomena in the tip area of wind turbine blades and their dependency on material and environmental parameters*. *International Conference on Lightning Protection. Ka-nazawa: ICLP*. 2006.
96. Schubel, P.J. and R.J. Crossley, *Wind turbine blade design.* Energies, 2012. **5**(9): p. 3425-3449.
97. Garolera, A.C., J. Holboell, and M. Henriksen. *Breakdown and tracking properties of rubber materials for wind turbine blades*. *Conference Record of the 2012 IEEE International Symposium on Electrical Insulation (ISEI)*,
98. Holbøll, J., M. Henriksen, and S. Krog-Pedersen. *Breakdown Tests of Composite Materials, and the Importance of the Volume Effect*. in *Nordic Insulation Symposium 2005*. 2005.
99. Madsen, S.F., et al. *Breakdown tests of glass fibre reinforced polymers (GFRP) as part of improved lightning protection of wind turbine blades, Conference Record of the 2004 IEEE International Symposium on* Electrical Insulation. IEEE.
100. Sorensen, T., et al. *Lightning protection for offshore wind turbines*. *Part 1: Contributions. CIRED. 16th International Conference and Exhibition on Electricity Distribution, (IEE Conf. Publ No. 482)*. 2001. IET.

101. Cavka, D., D. Poljak, and R. Goic. *Antenna model of wind turbine struck by lightning*. International Symposium on *Electromagnetic Compatibility (EMC EUROPE)*, 2012. IEEE.
102. Kern, A., C. Schelthoff, and M. Mathieu. *Calculation of interception efficiencies for air-terminations using a dynamic electro-geometrical model*. International Symposium on *Lightning Protection (XI SIPDA)*, 2011. IEEE. Fortaleza, Brazil.
103. Peesapati, V., et al., *Lightning protection of wind turbines-a comparison of measured data with required protection levels.* IET renewable power generation, 2011. **5**(1): p. 48-57.
104. Peesapati, V. and I. Cotton. *Lightning protection of wind turbines—A comparison of lightning data & IEC 61400-24*. International Conference on *Sustainable Power Generation and Supply. SUPERGEN'09 UK*. 2009. IEEE.
105. Lewke, B., et al., *Conductive surface layer on wind turbine blade as lightning protection system.* Proceedings of Windpower, Los Angeles, 2007: p. 3-6.
106. Zoro, R. and A. Purwadi. *The use of wind turbine structure for lightning protection system*. *International Conference on* Electrical Engineering and Informatics (ICEEI), 2011. IEEE. Bandung, Indonesia
107. Becerra, M. and V. Cooray, *A self-consistent upward leader propagation model Electrical Engineering and Informatics (ICEEI)*, Journal of Physics D: Applied Physics, 2006. **39**(16): p. 3708.
108. Becerra, M. and V. Cooray, *On the velocity of positive connecting leaders associated with negative downward lightning leaders.* Geophysical Research Letters, 2008. **35**(2).
109. Madsen, S., et al. *New test method for evaluating the lightning protection system on wind turbine blades. Proceedings of the 28th International Conference on Lightning Protection, Kanazawa, Japan*. 2006.
110. Bertelsen, K., H. Erichsen, and S. Madsen. *New high current test principle for wind turbine blades simulating the life time impact from lightning discharges*. *Proceedings of International Conference on Lightning and Static Electricity, Paris, France*. 2007.
111. Cummins, K.L., et al., *Overview of the Kansas Windfarm 2013 Field Program.*
112. Romero, D., J. Montanyà, and J. Vinck. *Test and simulation of lightning current distribution on a wind turbine blade*. *International Conference on Lightning Protection (ICLP)*. 2014. IEEE. Shanghai, China.
113. Naghipour, P., E. Pineda, and S. Arnold, *Simulation of Lightning-Induced Delamination in Un-protected CFRP Laminates.* Applied Composite Materials, 2016. **23**(4): p. 523-535.
114. Nath, S. and S. Rana, *The modeling and simulation of wind energy based power system using MATLAB.* International Journal of Power System Operation and Energy Management, 2011. **1**(2): p. 12.
115. Yamamoto, K., S. Yanagawa, and T. Ueda. *Verifications of transient grounding impedance measurements of a wind turbine generator system using the FDTD method*. *International Symposium on Lightning Protection (XI SIPDA)*. 2011. IEEE. Fortaleza, Brazil
116. Paolone, M., et al. *Models of wind-turbine main shaft bearings for the development of specific lightning protection systems*. in *Power Tech, 2007 IEEE Lausanne*.
117. Lewke, B., et al. *EMC Analysis of a Wind Turbine Blade's Lightning Protection System. IEEE International Symposium on Electromagnetic Compatibility*. 2007. IEEE.
118. Bertelsen, K., et al. *Application of numerical models to determine lightning attachment points on wind turbines*. in *Proceedings of the International Conference on Lightning and Static Electricity, Paris, France*. 2007.
119. Madsen, S. and H. Erichsen. *Numerical model to determine lightning attachment point distributions on wind turbines according to the revised IEC 61400-24* in *Proceedings of the international conference on lightning and static electricity*. 2009.
120. Madsen, S., A. Garolera, and K. Bertelsen, *Lightning Protection Zoning and Risk Exposure Assessment of Wind Turbines. 2015 EWEA Offshore, Copenhagen, Denmark*

121. Fisher, F.A. and J.A. Plumer, *Lightning protection for aircraft.* 1980.
122. Hernandez, Y., et al. *An experimental approach of the effects of lightning currents on rotor blade tips of wind turbines*. *International Conference on Lightning Protection (ICLP)*, 2012. IEEE. Vienna, Austria
123. Glushakow, B. *10/350 lightning test waveform in focus*. *International Symposium on Lightning Protection (XI SIPDA)*, 2011. IEEE, Fortaleza, Brazil.
124. D'Alessandro, F. and J. Gumley, *A modern perspective on direct strike lightning protection.* Proceedings of 25th ICLP, Rhodes, Greece, 2000: p. 362.
125. Zhou, H., et al., *A review of full-scale structural testing of wind turbine blades.* Renewable and Sustainable Energy Reviews, 2014. **33**: p. 177-187.
126. Yang, R., Y. He, and H. Zhang, *Progress and trends in nondestructive testing and evaluation for wind turbine composite blade.* Renewable and Sustainable Energy Reviews, 2016. **60**: p. 1225-1250.
127. Diendorfer, G. *Lightning initiated from tall structures—A review*. *International Symposium on Lightning Protection (XI SIPDA)*. 2011. IEEE,Fortaleza Brazil.
128. Wang, D., et al., *Observed characteristics of upward leaders that are initiated from a windmill and its lightning protection tower.* Geophysical Research Letters, 2008. **35**(2).
129. Lu, W., et al., *Two associated upward lightning flashes that produced opposite polarity electric field changes.* Geophysical Research Letters, 2009. **36**(5).
130. Zhou, H., et al., *Measured current and close electric field changes associated with the initiation of upward lightning from a tall tower.* Journal of Geophysical Research: Atmospheres, 2012. **117**(D8).
131. Miki, M., et al., *Initial stage in lightning initiated from tall objects and in rocket-triggered lightning.* Journal of Geophysical Research: Atmospheres, 2005. **110**(D2).
132. Diendorfer, G., H. Pichler, and M. Mair, *Some parameters of negative upward-initiated lightning to the Gaisberg tower (2000–2007).* IEEE Transactions on Electromagnetic Compatibility, 2009. **51**(3): p. 443-452.
133. Lyons, W.A., et al., *Meteorological Aspects of Two Modes of Lightning-Triggered Upward Lightning (LTUL) Events in Sprite-Producing MCS.*
134. Diendorfer, G. *On the risk of upward lightning initiated from wind turbines*. *IEEE 15th International Conference on Environment and Electrical Engineering (EEEIC)*, 2015. IEEE.
135. Diendorfer, G., *LLS performance validation using lightning to towers.* Impulse, 2010. **1**(7.5): p. 11.
136. Diendorfer, G., H. Zhou, and H. Pichler. *Review of 10 years of lightning measurement at the Gaisberg Tower in Austria*. in *Proc. 3rd International Symposium on Winter Lightning, Sapporo, Japan*. 2011.
137. Saito, M., et al., *Frequency of Upward Lightning Hits to Wind Turbines in Winter.* Electrical Engineering in Japan, 2015. **190**(1): p. 37-44.
138. Vogel, S., et al. *Lightning Attachment Estimation to Wind Turbines by Utilizing Lightning Location Systems*. in *24th International Lightning Detection Conference & 6th International Lightning Meteorology Conference, San Diego, California*. 2016.
139. Smorgonskiy, A., et al. *On the Estimation of the Number of Upward Flashes From Wind Turbines in Mountainous Areas*. in *24th International Lightning Detection Conference (ILDC)*. 2016. San Diego, California, USA
140. Smorgonskiy, A., et al. *A new method for the estimation of the number of upward flashes from tall structures*. *International Symposium on Lightning Protection (XI SIPDA)*. 2011. IEEE.Fortaleza Brazil.
141. Rodrigues, R., et al. *An investigation over the lightning location system in Portugal for wind turbine protection development*. in *Power and Energy Society General Meeting-Conversion and Delivery of Electrical Energy in the 21st Century, 2008 IEEE*. 2008. IEEE.

142. Romero, C., et al. *Preliminary comparison of data from the Säntis Tower and the EUCLID lightning location system*. *International Symposium on Lightning Protection (XI SIPDA)*, 2011. IEEE, Fortaleza, Brazil.
143. Ishii, M., et al. *Frequency of upward lightning from tall structures in winter in Japan*. *7th Asia-Pacific International Conference on Lightning (APL)*, 2011. IEEE. Chengdu, China.
144. Saito, M., et al. *Lightning strokes forming hot spots observed by LLS in winter in Japan*. *International Conference on Lightning Protection (ICLP)*, 2012. IEEE. Vienna, Austria.
145. Sarajcev, P. and R. Goic, *Estimation of lightning current amplitudes incident to wind turbines in exposed locations.* Wind Energy, 2015. **18**(9): p. 1515-1530.
146. Zhou, H., et al. *The influence of meteorological conditions on upward lightning initiation at the Gaisberg Tower*. *International Conference on Lightning Protection (ICLP), 2014*. IEEE.
147. Cooray, V., *Mechanism of electrical discharges.* The Lightning Flash, V. Cooray, Ed, 2003: p. 45-126.
148. Becerra, M., *Glow corona generation and streamer inception at the tip of grounded objects during thunderstorms: revisited.* Journal of Physics D: Applied Physics, 2013. **46**(13): p. 135205.
149. Madsen, S. *A new principle of measuring static electric fields using two floating electrodes*. *International Conference on Lightning and static electricity (ICOLSE)*. 2007.
150. Rubinstein, M., et al. *A physical derivation of the horizontal electric field under the ground associated with lightning return strokes*. *International Symposium on Lightning Protection (XI SIPDA), 2011*. IEEE Fortaleza Brazil.
151. Barbosa, C.F., J.O.S. Paulino, and W.C. Boaventura. *Horizontal electric field at the surface of layered earth due to lightning*. *International Symposium on Lightning Protection (XI SIPDA), 2011*. IEEE. Fortaleza Brazil.
152. Yu, Z., et al., *Calculation of surface electric field on UHV transmission lines under lightning stroke.* Electric Power Systems Research, 2013. **94**: p. 79-85.
153. Xiaoqing, Z., *Calculation of transient potential rise on the wind turbine struck by lightning.* The Scientific World Journal, **2014**.
154. Wang, X. and X. Zhang. *Electric field distribution inside wind turbine towers struck by lightning*. *ISAPE 2008. 8th International Symposium on Antennas, Propagation and EM Theory (ISAPE)*,2008. IEEE.
155. Rizk, M.E., et al., *Investigation of lightning electromagnetic fields on underground cables in wind farms.* IEEE Transactions on Electromagnetic Compatibility, 2016. **58**(1): p. 143-152.
156. Malinga, G. and J. Niedzwecki, *Modeling lightning strike behavior in the near field of elevated systems.* Journal of Engineering Mathematics, 2016. **97**(1): p. 195-221.
157. Eriksson, A.J., *The lightning ground flash: an engineering study*. 1979: CSIR= WNNR.
158. Soula, S. and S. Chauzy, *Multilevel measurement of the electric field underneath a thundercloud: 2. Dynamical evolution of a ground space charge layer.* Journal of Geophysical Research: Atmospheres (1984–2012), 1991. **96**(D12): p. 22327-22336.
159. Willett, J., D. Davis, and P. Laroche, *An experimental study of positive leaders initiating rocket-triggered lightning.* Atmospheric research, 1999. **51**(3): p. 189-219.
160. Golde, R., *The frequency of occurrence and the distribution of lightning flashes to transmission lines.* Electrical Engineering, 1945. **64**(12): p. 902-910.
161. Eriksson, A., *Lightning and tall structures.* Trans. SAIEE, 1978. **69**(pt 8): p. 238-252.
162. Cooray, V., *Mechanism of electrical discharges.* The Lightning Flash, 2003. **34**: p. 45.
163. Garolera, A.C., J. Holbøll, and C.F. Mieritz. *Modelling of lightning streamer formation and propagation in wind turbine blades*. *International Conference on Lightning and Static Electricity*. 2013.

164. Carrara, G. and L. Thione, *Switching surge strength of large air gaps: a physical approach.* IEEE Transactions on power apparatus and systems, 1976. **95**(2): p. 512-524.
165. Gary, C., et al., *Laboratory aspects regarding the upward positive discharge due to negative lightning.* Revue roumaine des sciences techniques. Electrotechnique et énergétique, 1989. **34**(3): p. 363-377.
166. Bernardi, M., et al., *Leader progression model of lightning: updating of the model on the basis of recent test results.* Proc. 23rd ICLP, Florence, Italy, 1996: p. 399-407.
167. D'alessandro, F., et al., *Experimental study of lightning rods using long sparks in air.* IEEE transactions on dielectrics and electrical insulation, 2004. **11**(4): p. 638-648.
168. Dellera, L. and E. Garbagnati, *Lightning stroke simulation by means of the leader progression model. I. Description of the model and evaluation of exposure of free-standing structures.* IEEE Transactions on Power Delivery, 1990. **5**(4): p. 2009-2022.
169. Eriksson, A., *An improved electrogeometric model for transmission line shielding analysis.* IEEE Transactions on Power Delivery, 1987. **2**(3): p. 871-886.
170. Eriksson, A., *The incidence of lightning strikes to power lines.* IEEE Transactions on Power Delivery, 1987. **2**(3): p. 859-870.
171. D'Alessandro, F., *The use of 'field intensification factors' in calculations for lightning protection of structures.* Journal of electrostatics, 2003. **58**(1): p. 17-43.
172. Rizk, F.A., *A model for switching impulse leader inception and breakdown of long air-gaps.* IEEE Transactions on Power Delivery, 1989. **4**(1): p. 596-606.
173. Petrov, N. and R. Waters. *Determination of the striking distance of lightning to earthed structures*. in *Proceedings of the Royal Society of London A: Mathematical, Physical and Engineering Sciences*. 1995. The Royal Society.
174. Petrov, N. and F. D'alessandro, *Theoretical analysis of the processes involved in lightning attachment to earthed structures.* Journal of Physics D: Applied Physics, 2002. **35**(14): p. 1788.
175. Akyuz, M. and V. Cooray, *The Franklin lightning conductor: conditions necessary for the initiation of a connecting leader.* Journal of Electrostatics, 2001. **51**: p. 319-325.
176. Bazelyan, E.M. and Y.P. Raizer, *Lightning physics and lightning protection*. 2000: CRC Press.
177. Lalande, P., *Study of the lightning stroke conditions on a grounded structure*. 1996, Doctoral Thesis.
178. Goelian, N., et al., *A simplified model for the simulation of positive-spark development in long air gaps.* Journal of Physics D: Applied Physics, 1997. **30**(17): p. 2441.
179. Gallimberti, I., *The mechanism of the long spark formation.* Le Journal de Physique Colloques, 1979. **40**(C7): p. C7-193-C7-250.
180. Becerra, M. and V. Cooray, *A simplified physical model to determine the lightning upward connecting leader inception.* IEEE Transactions on Power Delivery, 2006. **21**(2): p. 897-908.
181. Becerra, M. and V. Cooray, *Time dependent evaluation of the lightning upward connecting leader inception.* Journal of Physics D: Applied Physics, 2006. **39**(21): p. 4695.
182. Warner, T.A., T.J. Lang, and W.A. Lyons, *Synoptic scale outbreak of self-initiated upward lightning (SIUL) from tall structures during the central US blizzard of 1–2 February 2011.* Journal of Geophysical Research: Atmospheres, 2014. **119**(15): p. 9530-9548.
183. Cooray, V., *Lightning protection. The Institution of engineering and technology*. London: The Institution of Engineering and Technology, 2010.
184. Ancona, D. and J. McVeigh, *Wind turbine-materials and manufacturing fact sheet.* Princeton Energy Resources International, LLC, 2001. **19**.
185. Imyanitov, I., E. Chubarina, and Y.M. Shvarts, *Cloud Electricity*. Gidrometeoizdat, Moscow, 1971.

186. Rodrigues, R., et al., *Analysis of the thunderstorm activity in Portugal for its application in the lightning protection of wind turbines.* IEEE Latin America Transactions, 2009. **7**(5).
187. MacGorman, D.R. and W.D. Rust, *The electrical nature of storms*. 1998: Oxford University Press on Demand.
188. Sadiku, M.N., *Elements of electromagnetics*. 2014: Oxford university press.
189. Zhou, H., et al. *Close electric field changes associated with upward-initiated lightning at the Gaisberg Tower*. *International Symposium on Lightning Protection (XI SIPDA)*, 2011. IEEE.Fortaleza Brazil.
190. Godson, I., et al., *Optimum receptor location for efficient lightning protection of modern wind turbines.* International Journal of Simulation Systems, Science & Technology, 2017. **18**.
191. Wada, A., et al. *Lightning Damages of wind turbine blades in winter in Japan–lightning observation on the Nikaho-Kogen wind farm*. *Proceedings of the 27th International Conference on Lightning Protection (ICLP),(Avignon, France)*. 2004.
192. Ishii, M., et al. *Lightning incidence on wind turbines in winter*. *International Conference on Lightning Protection (ICLP)*, 2014. IEEE. Shanghai, China.
193. Fujii, F., et al., *Characteristics of winter lightning threatening wind turbines in coastal area of the Sea of Japan.* IEEJ Transactions on Power and Energy, 2011. **131**: p. 973-978.
194. Sinha, Y. and J.A. Steel, *A progressive study into offshore wind farm maintenance optimisation using risk based failure analysis.* Renewable and Sustainable Energy Reviews, 2015. **42**: p. 735-742.
195. Malinga, G.A. and J.M. Niedzwecki, *Nearshore regional behavior of lightning interaction with wind turbines.* Journal of Ocean Engineering and Science, 2016. **1**(1): p. 66-76.
196. Soloot, A., H.K. Hoidalen, and B. Gustavsen. *A Study of switching overvoltages in offshore wind farm*. *Proc. of XVII International Symposium on High Voltage Engineering*. 2011.
197. Kumar, V.S., et al. *LIBS combined with temporal and spatial measurements for detecting a salt deposit on a GFRP material*. *Conference on Lasers and Electro-Optics/Pacific Rim*. 2013. Optical Society of America.
198. Garolera, A.C., J. Holboell, and S.F. Madsen. *Lightning attachment to wind turbine surfaces affected by internal blade conditions*. *International Conference on Lightning Protection (ICLP)*, 2012. IEEE. Vienna, Austria.
199. Kumar, V.S., N.J. Vasa, and R. Sarathi, *Remote surface pollutant measurement by adopting a variable stand-off distance based laser induced spectroscopy technique*. Journal of Physics D: Applied Physics, 2015. **48**(43): p. 435504.